A COMMUNICATION METHOD USING MULTI-RING AND DARK SOLITON

CHAROEN VONGCHUMYEN

A THESIS SUBMITTED IN PARTIAL FULFILLMENT

OF THE REQUIREMENT FOR THE DEGREE OF

DOCTOR OF ENGINEERING IN ELECTRICAL ENGINEERING

FACULTY OF ENGINEERING

KING MONGKUT'S INSTITUTE OF TECHNOLOGY LADKRABANG

2016

KMITL-2016-EN-D-018-203

THESIS CERTIFICATION
FACULTY OF ENGINEERING
KING MONGKUT'S INSTITUTE OF TECHNOLOGY LADKRABANG

Thesis Title	A Communication Method using Multi-Ring and Dark Soliton
Student	Mr. Charoen Vongchumyen
Student Id.	52610109
Degree	Doctor of Engineering
Program	Electrical Engineering
Thesis Advisor	Assoc. Prof. Dr. Somsak Mitatha
Thesis Reference Number	KMITL-2016-EN-D-018-203

EXAMINERS	SIGNATURES
Prof. Dr. Kosin Chamnongthai	
Dr. Pakorn Watanachaturaporn	
Dr. Amnach Khawne	
Dr. Chompoonuch Jinjakam	
Assoc. Prof. Dr. Somsak Mitatha	

Date 6th December 2016 **Time** 3:00-5:00 PM.
Place Building A , Conference room no.1

(Assoc. Prof. Dr. Komsan Maleesee)
Dean, Faculty of Engineering
6th December 2016

หัวข้อวิทยานิพนธ์	กระบวนการสื่อสารโดยใช้หลายวงแหวนและโซลิตอนแบบมืด
นักศึกษา	นายเจริญ วงษ์ชุ่มเย็น
รหัสประจำตัว	52610109
ปริญญา	วิศวกรรมศาสตรดุษฎีบัณฑิต
สาขาวิชา	วิศวกรรมไฟฟ้า
พ.ศ.	2559
อาจารย์ที่ปรึกษาวิทยานิพนธ์	รศ.ดร.สมศักดิ์ มิตะถา

บทคัดย่อ

การสื่อสารทางแสงในสายไฟเบอร์ออฟติกโดยทั่วไปจะใช้สัญญาณโซลิตอนซึ่งมีคุณสมบัติที่ดีในการสื่อสารทางไกลเนื่องจากไม่มีผลกระทบจากการกระจายตัวของสัญญาณ และใช้อุปกรณ์วงแหวนสั่นพ้องและตัวกรองแอดดรอปในการเลือกสัญญาณที่ต้องการมาใช้งาน แต่การใช้งานสัญญาณโซลิตอนโดยทั่วไป จะเป็นสัญญาณโซลิตอนแบบสว่างเพื่อให้สามารถใช้ตัวตรวจจับสัญญาณที่ปลายทางได้ ทำให้เกิดปัญหาเรื่องความปลอดภัยเนื่องจากหากมีผู้ไม่ประสงค์ดีทำการลักลอบดักจับสัญญาณระหว่างทางก็จะสามารถดักจับข้อมูลในสายสัญญาณไปได้

วิทยานิพนธ์ฉบับนี้จึงได้นำเสนอการเพิ่มความปลอดภัยในการสื่อสารข้อมูลภายในสายไฟเบอร์ออฟติกโดยการใช้สัญญาณโซลิตอนแบบมืด ซึ่งจะทำให้ผู้ที่ลักลอบดักจับสัญญาณระหว่างทางไม่สามารถดักตรวจจับสัญญาณโดยใช้ตัวตรวจจับสัญญาณทั่วไปได้ อันจะเป็นการเพิ่มความปลอดภัยในการสื่อสารให้มากขึ้น อีกทั้งยังได้มีการนำเสนออุปกรณ์วงแหวนสั่นพ้องและตัวกรองแอดดรอปที่ใช้ในการแปลงสัญญาณโซลิตอนแบบสว่างให้เป็นแบบมืดเพื่อส่งสัญญาณ และการแปลงกลับที่ปลายทางเพื่อให้ผู้รับยังคงสามารถใช้ตัวตรวจจับสัญญาณปกติในการรับข้อมูลได้ รวมถึงได้นำเสนอถึงวิธีการและการทดลองในการสร้างสัญญาณโซลิตอนแบบมืดและสัญญาณโซลิตอนแบบมืดที่เป็นชุดเพื่อเพิ่มความจุในการสื่อสารข้อมูลให้มากยิ่งขึ้น

Thesis	A communication method using multi-ring and dark soliton
Student	Mr. Charoen Vongchumyen
Student ID.	52610109
Degree	Doctor of Engineering
Program	Electrical Engineering
Year	2016
Thesis Advisor	Assoc. Prof. Dr. Somsak Mitatha

ABSTRACT

Normal optical communication in fiber optic used soliton which has a good characteristic in long range communication because it doesn't effect by signal dispersion, and used ring resonator device and add-drop filter to filter the desire signal. But the commonly used of soliton is bright soliton for ensuring the ability to detect the signal by the detector at the end of the communication link. It has a security problem that if any hacker can tap the link, they can detect and get the data from the signal link.

This signal proposed the way to increase the security in fiber optic communication using dark-soliton, which not allows the hacker that tap the link to detect the data using normally detector. Then, we shown the ring resonator device and add-drop filter used to convert bright soliton to the dark one and vice versa to ensure the used of normal detector for the receiver at the end of communication link. Furthermore, we shown the way to create the multiplexed dark soliton to increase the bandwidth of communication within a link and even actually setup the experiment to create it.

ACKNOWLEDGEMENT

Firstly, I would like to express my sincere gratitude to my advisor Assoc.Prof.Dr.Somsak Mitatha for the continuous support me during all this years of research, for his patience, actively encourage, motivation and usefully experience. His guidance helped me in all the time of research and writing of this thesis. Working with him has been a great opportunity in my research period of time.

Besides my advisor, I would like to thank the rest of my thesis committee: Prof.Dr.Kosin Chamnongthai, Dr.Pakorn Watanachaturaporn, Dr.Amnach Khawne and Dr.Chompoonuch Jinjakam for their insightful comments and encouragement, but also for the hard question which incented me to widen my research from various perspectives.

Finally, my greatest thanks are to my beloved family whose caring, understand, and possible attitude have encouraged me to go forward during difficult times. Whose never-ending love and support made the completion of this work completed and my dream of a graduate education come true.

Charoen Vongchumyen

Table of Contents

Table of Figures

CHAPTER 1

INTRODUCTION

This chapter includes of several parts of the thesis. Start with motivation of this thesis then explain the aims of this work to clarify what is the focus of the research. Next, the scopes of the thesis, which is the part that describe about the boundaries of the work in this research, which is investigate and propose and which is not. The final part of this chapter is to make clear of that what are in the rest chapters in this work.

1.1 Motivation

The invention of the laser in 1960 is the most advance technology in digital communication, it become the main source of carrier in high speed and high security of optic communication today. The advantages of this kind of communication compare to the original, radio frequency are,

- There is low loss in optic medium (fiber optic).
- No interference by electromagnetic nor electricity.
- High bandwidth in carrier, which mean high-capacity and –throughput of data to be transfer
- Small size and light weight.
- Hard to tapping and steeling data.

In the most optic communication, the linear effect which have some drawbacks in linear effect that hold down the speed of data, Such as loss and Group Velocity Dispersion (GVD). To overcome this problem, non-linear effect and soliton have been use in fiber optic. Soliton has dispersion compensation that allow it to propagate through fiber far more than the linear one. There are two types of solitons, Bright and Dark soliton. Most of the communication today that uses the detector to detect the signal within a fiber optic is using bright soliton. Bright soliton has a main drawback that if the receiver can get the data by using the detector, so the hacker

that can tap onto the medium too. The question is how to increase the security in the fiber optic that widely uses soliton and the detector.

1.2 Aims of this work

This research aims to study, investigate and propose a way to increase the security within fiber optic communication using soliton. To complete that task, Dark soliton has been selected as a problem solver on this thesis. Therefore, the aims and objectives of this work were:

(a) To investigates and simulate the microring resonator, theory and application.

(b) To investigates and distinct the difference between Bright and Dark soliton, the way to converse bright to dark soliton and vice versa.

(c) To propose a way to generate bright and dark soliton, with an experiment in generate its.

(d) To propose a way to improve security and bandwidth in optic communication using dark solitons.

1.3 Organization of the thesis

This thesis consists of 5 parts, which are as follow.

(a) Chapter 1 gave an introduction of this thesis which contain many topics such as the motivation, aims of this work to organization of the thesis.

(b) Chapter 2 gave information of the literature review of the related work. Then explain the improvement opportunity of the previous work.

(c) Chapter 3 proposed a system to improve the other work to make it more secure using multi-ring and dark soliton method both theory and experiment.

(d) Chapter 4 proposed a way to improve the bandwidth in optical communication using multiplexed dark soliton's technique.

(e) Finally, chapter 5 presented the conclusion of the result and experiment of this thesis. It also give a roughly idea on PANDA ring resonator and the possible way to use it in optical communication.

According to the motivation of this thesis, the old system has some drawback in using bright soliton as a carrier. The bright soliton did not give an advantage in the attack prevention. If someone attacks the communication by tapping technique, they can easily detect the carrier and the data using normal photo detector. In case of that, dark soliton has been proposed to overcome this problem.

CHAPTER 2

LITERATURE REVIEW AND IMPROVEMENT OPPORTUNITY

In this chapter, we will investigate the other work that related to the generation of soliton using pumping system. Then, we will analyze the old work to find a point to improvement it in both security and capacity criteria's. Final, we will summarize the potential improvement opportunity of the old work and it'll become the main work of this thesis.

2.1 Literature review

In optical communication, Soliton is the most suitable signal for using as a carrier in optical fiber, according to its advantage such as dispersion compensation in the fiber optic. Many research were focus on the generation of soliton signal such as S. Li and their team shown a way to generation triple-soliton in the paper named "Reported the generation of triple-wavelength picosecond mode locked pulses using a self-seeded Fabry-Perot laser diode with fiber Bragg gratings" or J. Yao and his members were generated multiple soliton using fiber Bragg grating in the paper name "Multiwavelength actively mode-locked fiber lasers incorporating either a single sampled fiber Bragg grating or biased semiconductor optical amplifier in cavity". Even S. Pan and the team on paper name "Simultaneous dual- and five-wavelength actively mode-locked erbium-doped fiber lasers at 10 GHz by virtue of the nonlinear polarization rotation (NPR) effect". All of this paper shown the way to create soliton signal using pumping system.

The other paper that shown a good example of the way to generated the multiple soliton signal was the research named "Multi-wavelength dissipative soliton operation of an erbium-doped fiber laser" by H. Zhang, D. Y. Tang, X. Wu and L. M. Zhao from School of Electrical and Electronic Engineering, Nanyang Technological

University, Singapore. This research setup the experiment as in Figure 2.1 base on this following parameters.

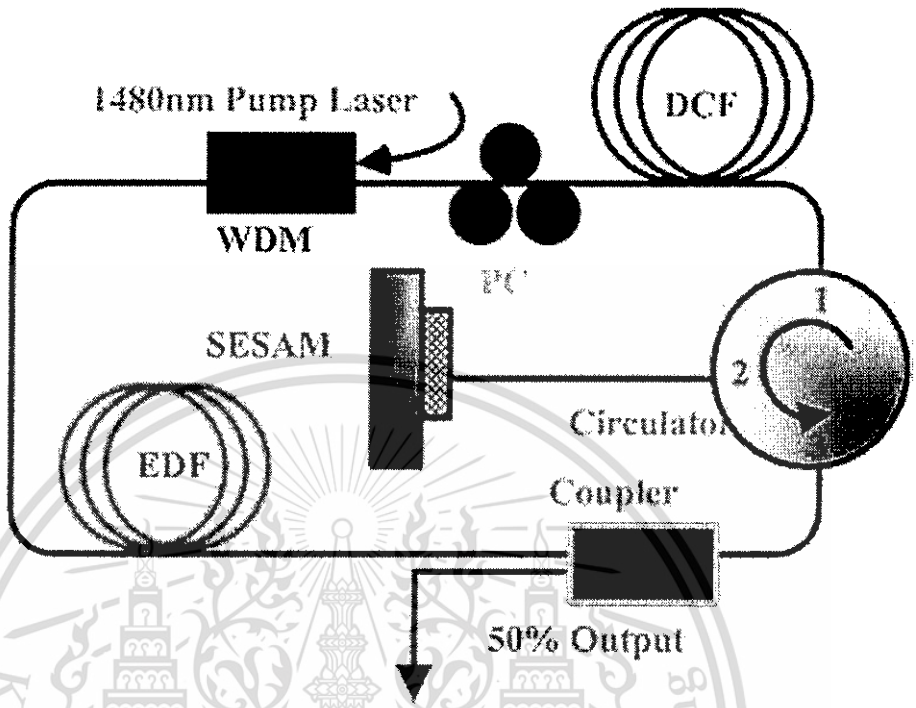

Figure 2.1 Schematic of the experimental setup. EDF: Erbium doped fiber. WDM: wavelength division multiplexer. DCF: dispersion compensation fiber. PC: polarization controllers.

The fiber cavity was long 13.5 M using normal dispersion fiber. The EDF-fiber(Erbium-doped fiber) was 5 M long with 2,880 ppm erbium doped and -32(ps/nm)/km of Group Velocity Dispersion(GVD). The DCF fiber(Dispersion compensation fiber) has -4(ps/nm)km of Group Velocity Dispersion(GVD). The mode-locking laser is Semiconductor Saturable Absorber Mirror(SESAM). The laser source was using high power Raman pump model KPS-BT2-FRL-1480-60-FA with 1480 nm center wavelength and 5W of maximum power. Polarization independent circulator was use to force unidirectional operation of the ring.

The SESAM was made based on GaInNAs(Gallium Indium Nitrogen Arsenic) quantum wells with 30% saturable absorption modulation depth. It has 90 uJ/cm^2 saturation fluency and 10 ps recovery time with 0.5 DCF pigtailed. The output of the experiment was monitor by Optical spectrum analyzer(Ando AQ-6315B). The mode

locked pulse train were monitor by 350 MH_z oscilloscope(Agilen 5461A) with a 2 GH_z photo-detector.

The result of the experiment may conclude on this following information. Mode locking laser has been self-started only when the pump power is over the mode locking threshold. The multiple soliton pulses were formed in the cavity. When carefully decreased the pump power, the number of soliton pulses could be reduced. Eventually a single soliton operation state can be produced.

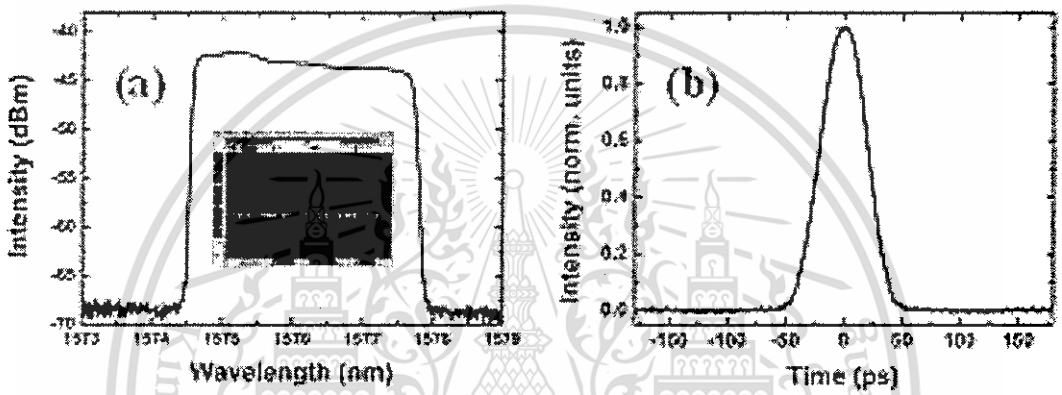

Figure 2.2 (a) Optical spectra of single wavelength GGS. Insert: the oscilloscope trace. (b) The corresponding autocorrelation trace.

In Figure 2.2 is the typical single soliton operation state of the laser. In figure (a) the generated soliton has a steep spectral edge (Dissipative soliton) with a center wave length of 1576.2 nm. In figure (b) the autocorrelation trace has 28.8 ps soliton pulse width in a $sech^2$ shape.

The experimental result was confirmed that soliton pulse was linearly polarized. When adjusting the orientations of the polarize controller (PC), Changing the linear birefringence of the cavity. The center wavelength has varied from 1570 to 1590 nm. When the center wavelength was closed to 1570 or 1590 nm, the soliton were less stabled.

A new soliton was formed in the cavity by given a stronger pumping power to the system. The features of the new soliton were sensitively depended on the cavity birefringence. In Figure 2.3 has shown the optical spectrum of dual wavelength GGS(Gain-guided soliton). In figure (a), there were two steep-edge shaped spectrums with different central wavelength. The two soliton have the central wavelength 1576.2 and 1579.6 nm respectively. Each soliton have different pulse energies, propagated with different group velocities and in orthogonal polarizations.

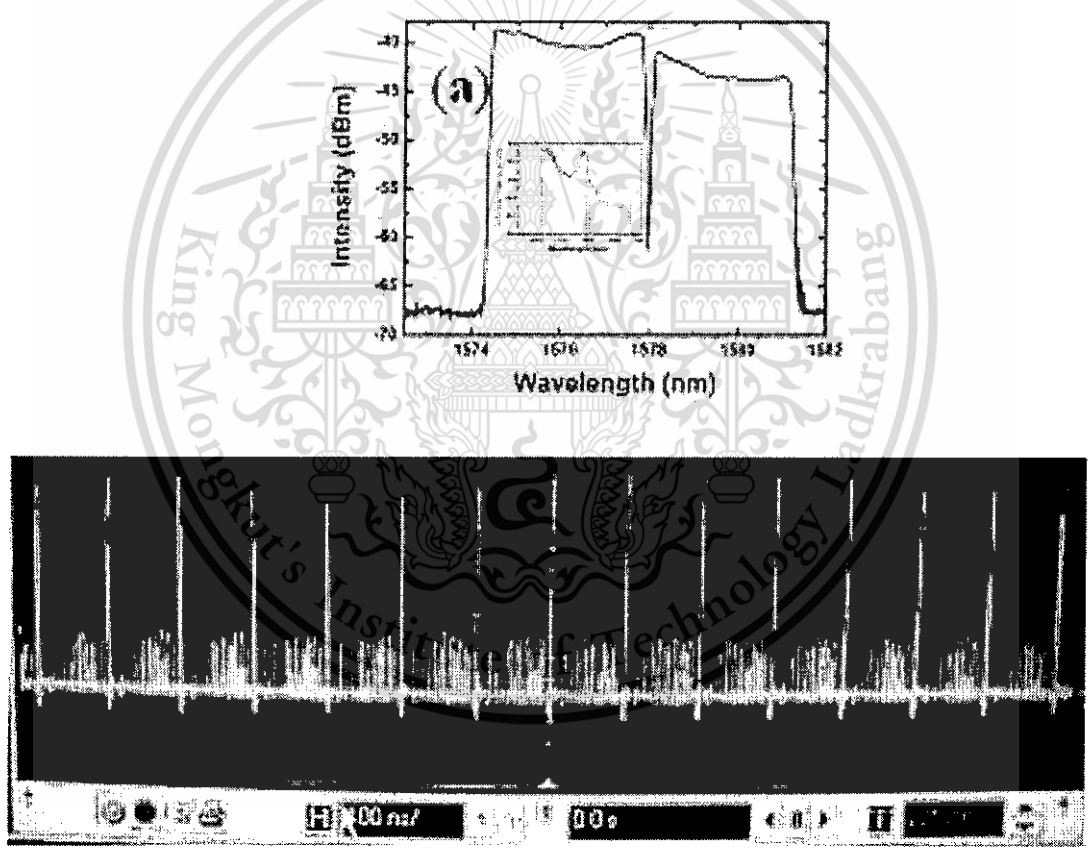

Figure 2.3 (a) Optical spectrum of dual wavelength GGSs. Insert: the normalized optical spectrum; (b) Oscilloscope trace of dual wavelength GGSs.

In Figure 2.4 shown the oscilloscope trace of synchronized dual wave length GGS. They have relative strength varied with the cavity birefringence. By slightly tuning the PC, continuously changed the relative soliton pulse energy can be achieved. The two solitons could even have the same group velocity, different central wavelength.

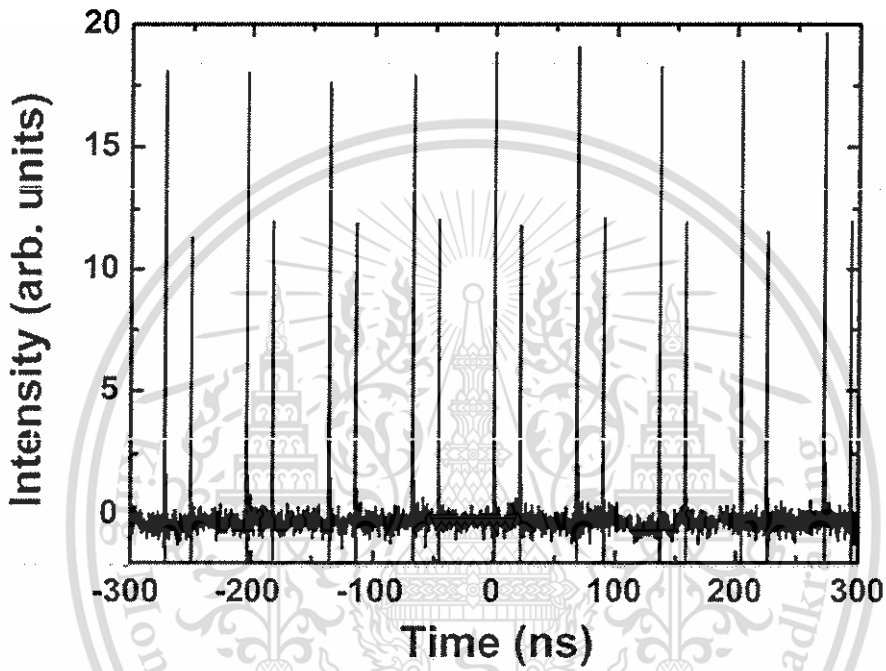

Figure 2.4 Oscilloscope trace of synchronized dual wavelength GGS.

Figure 2.5 (a) has shown the two soliton transformed into a vector soliton by kept the fixed the pump strength and significantly changed the orientation of the PC.

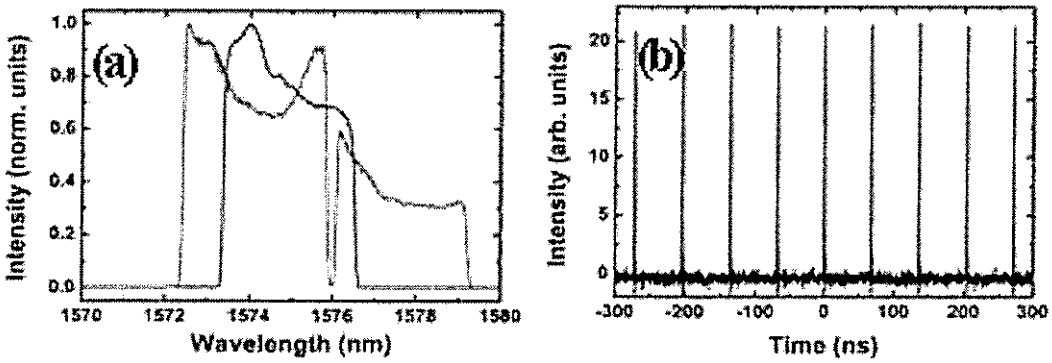

Figure 2.5 (a) Optical spectra of polarization locked gain guided vector soliton and dual wavelength spectrum obtained through rotating PCs but kept the pump strength fixed: normalized unit. (b) Oscilloscope trace of polarization locked gain guided vector soliton after passing through a polarizer.

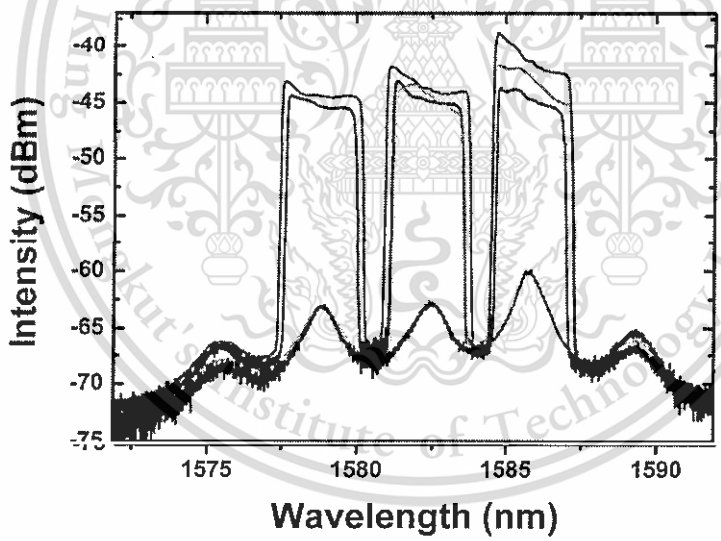

Figure 2.6 Single/dual/triple wavelength spectra obtained through rotating PCs but kept the pump strength fixed.

The result of kept the pump strength fixed and rotated the PCs show the single/dual and triple soliton with linearly polarized.

2.2 The conclusion of the literature review

The conclusions on the literature review were, they have shown the way to create multiple-soliton (up to triple soliton) by using the technique of pumping power and rotate the PCs. All of the papers were

1. Focus on the layer 1 of OSI model, Physical layer.
2. The used of bright soliton as a carrier which is not secure.
3. Bright soliton was generated using pumping system was too big and cost so much money.
4. Only three carriers were generated, Low capacity of the bandwidth of the communication.

2.3 Improvement opportunity

From the conclusion on the literature review, we saw the opportunity to improve the previous system which lead to more secure and more bandwidth than the shown model. All of the improvement opportunities were

1. Still focus on the layer 1 of OSI model, Physical layer (No need to change to upper layer of the system).
2. The used of dark soliton as a carrier which is More secure than bright.
3. Dark soliton was generated using Microring resonator was smaller and cost effective way.
4. Multiplexed dark soliton were generated, higher capacity of the bandwidth of the communication.

The improvement opportunity that proposed in this thesis has an advantage to overcome the attacker problem, the tapping one. By using the dark soliton as a carrier instead of bright soliton will give a better security parameter when the communication line has been tap. This thesis will show a way to generate dark soliton and convert it back to bright in the following chapter.

CHAPTER 3

HIGHER SECURITY USING DARK-SOLITON

The disadvantage of the old system are security and costly, in order to overcome this two problems this thesis proposed a way to make the communication system more secure and more cost effective. In every communication, they always have two parts, Transmitter (TX) and Receiver (RX). The transmitter is the one who send out the information and the receiver is the one who use that information. In typical optical communication system, the transmitter's carrier is the bright soliton which have a weak again the tapping type attack in fiber communication.

Tapping, one of four major attack types of the optical communication in physical layer is the hardest type to overcome. The most system cannot detect the tapping nor secure the communication data. Most of them did the security in the upper laser by using encryption method. This thesis proposed a way to give more security in physical layer by using Dark-soliton technique.

The idea to use dark soliton in this thesis is use it as a carrier instead of bright soliton. The advantage of dark soliton is even the attacker can tap the cable, they cannot use normal detector to detect the carrier and the data of that fiber. The dark soliton as a carrier make the carrier disappear for curtain center wavelength. In order to restore the carrier and the data, the receiver has to convert to dark soliton to bright soliton using dark-bright soliton conversion which will describe later in this thesis.

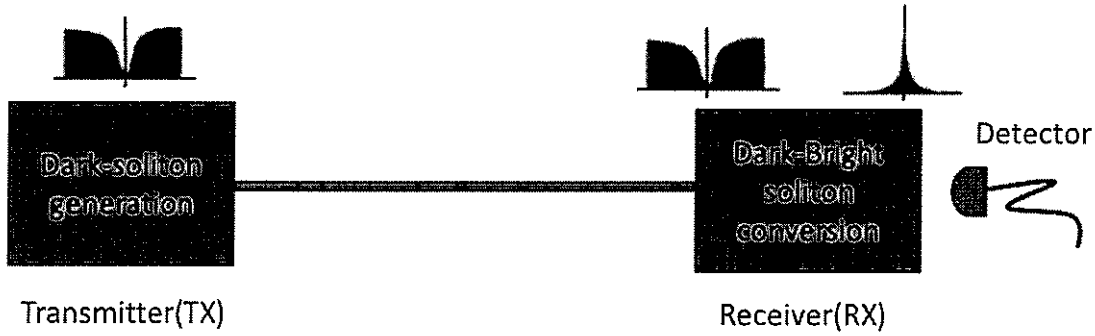

Figure 3.1 Proposed system that using dark soliton technique

3.1 Proposed system, TX

In mostly optical communication, bright soliton was used to be the carrier of the signal. The soliton can be easily detected at the end of the communication line using detector. If the communication line has been trapped, the hacker can get the soliton signal using normally detector. In order to increase the security of the communication link, we proposed the use of dark soliton instead of bright. Dark solitons are hardly detect by normally detect or even impossible to detect because it's lack of the signal in that frequency.

In this chapter, we proposed the way to increase security of the general optic communication using microring resonator by using dark solitons. We explained the theory of the generation of the dark soliton and yet setup the experiment to actually generate to dark soliton as above.

3.2 Dark Soliton Generation

The experimental configuration for the dual Brillouin fiber laser (DBFL) is shown in Figure 3.2 The laser consists of a 7.7 km length Dispersion Compensate Fiber (DCF) as the non-linear gain medium that produces the first Stokes, a Brillouin pump (BP) that pumps a narrow signal with a power of 1.96 dBm and a wavelength of 1500 nm into the cavity. The two optical circulators used are labeled as C1 and C2. The signal from BP is injected into the cavity from port 3 of CI and detected at port 1 of CI by

the optical spectrum analyzer (OSA) with a resolution of 0.02nm. Port 3 and port 1 of C2 which is placed at the end side of the configuration, is connected to form the double pass configuration inside the linear cavity. This double pass configuration allows the signal from BP and the first Stokes to re-circulate into the DCF and hence producing a significant amplification with stable dual Brillouin peaks. The enhanced DBFL is obtained after the insertion of Raman pump (RP) with a pump power of 296 mW at a wavelength of 1420 nm into the linear cavity (Figure 3.3). RP will pump the DCF thus enhancing the non-linear interaction of BP signal. A 1420/1500nm wavelength selective coupler (WSC) is used to combine the pump and laser wavelength.

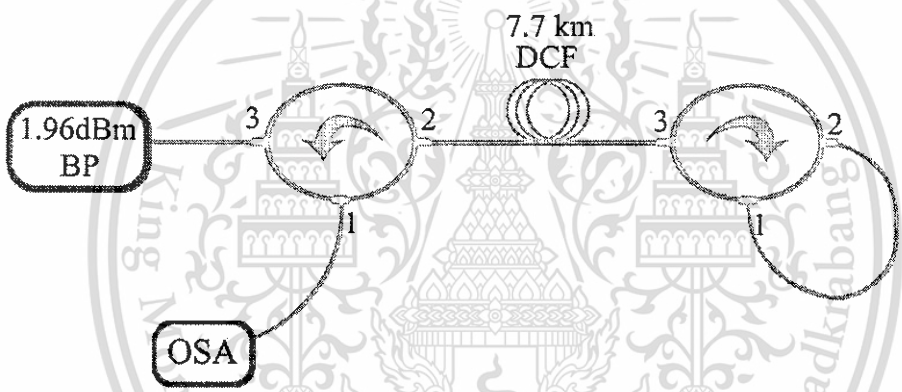

Figure 3.2 DBFL configuration

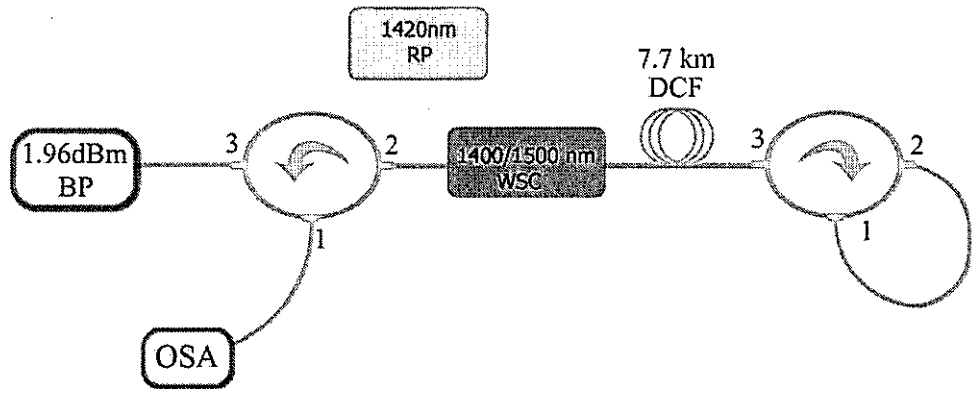

Figure 3.3 Enhanced DBFL configuration

The stability of the dual Brillouin is shown in Figure 3.4 and Figure 3.5 shows the stability of the enhanced dual Brillouin spectrum obtained by repeating the experiments. The dark soliton valley depth, i.e. potential well, is changed when it was modulated by the trapping energy as shown in Figure 3.5 The trapping of photon within the dark well is occurred and seen, the recovery photon can be obtained by using the dark-bright soliton conversion, which is well analyzed by reference [1], where the trapped photon or molecule can be released an seen separately from the dark soliton pulse, in practice, in this case the bright soliton is become alive and seen.

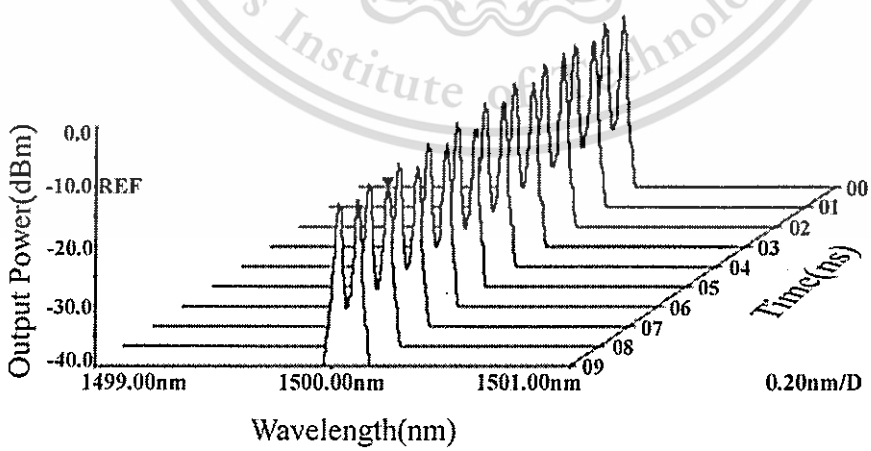

Figure 3.4 DBFL spectrum train

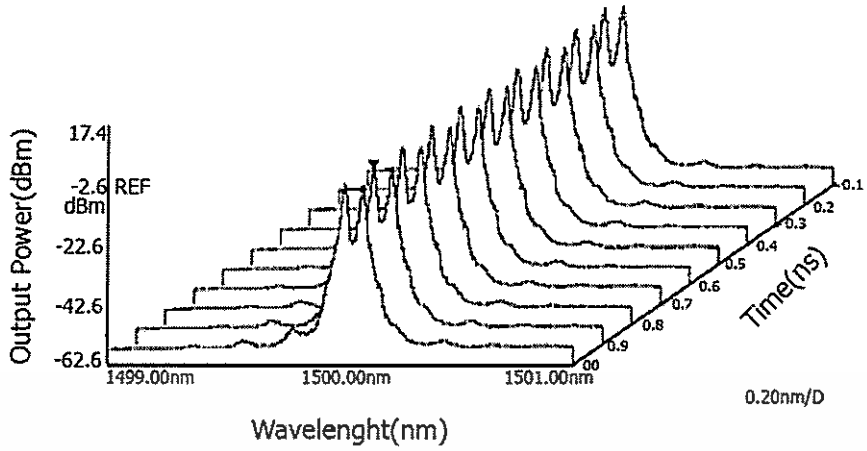

Figure 3.5 Enhanced DBFL spectrum train with Raman pumping

3.3 Dark soliton generation theory and experimental result

To describe the multiplexed dark soliton pulses which is introduced the dark soliton array generation, a stationary dark soliton pulse that is introduced into the nonlinear micro-ring resonator system as shown in

Figure 3.6 each of input optical fields (E_{in}) of the dark soliton pulses input is given by [2]

$$E_{in}(t) = A \tanh\left[\frac{T}{T_0}\right] \exp\left[\left(\frac{z}{2L_D}\right) - i\omega_0 t\right] \quad (3.1)$$

Where A and z are the optical field amplitude and propagation distance, respectively. T is a soliton pulse propagation time in a frame moving at the group velocity, $T = t - \beta_1 * z$, where β_1 and β_2 are the coefficients of the linear and second-order terms of Taylor expansion of the propagation constant. $L_D = T_0^2/|\beta_2|$ is the dispersion length of the soliton pulse. T_0 in equation is a soliton pulse propagation time at initial input (or soliton pulse width), where t is the soliton phase shift time, and the frequency shift of the soliton is ω_0. This solution describes a pulse that keeps its temporal width invariance as it propagates, and thus is called a temporal

soliton. When a soliton peak intensity ($|\beta_2/\Gamma \times T_0^2|$) is given, then T_0 is known. For the soliton pulse in the microring device, a balance should be achieved between the dispersion length (L_D) and the nonlinear length ($L_{NL} = 1/\Gamma\phi_{NL}$), where $\Gamma = n_2 * k_0$, is the length scale over which dispersive or nonlinear effects makes the beam become wider or narrower. For a soliton pulse, there is a balance between dispersion and nonlinear lengths, hence $L_D = L_{NL}$.

When light propagates within the nonlinear material (medium), the refractive index (n) of light within the medium is given by

$$E_{in}(t) = A \tanh\left[\frac{T}{T_0}\right]\exp\left[\left(\frac{z}{2L_D}\right) - i\omega_0 t\right] \tag{3.2}$$

where n_0 and n_2 are the linear and nonlinear refractive indexes, respectively. I and P are the optical intensity and optical power, respectively. The effective mode core area of the device is given by A_{eff}. For the series microring resonator (MRRs), the effective mode core areas range from 0.50 to 0.10 μm^2 [3]. When a soliton pulse is input and propagated within a MRR, as shown in

Figure 3.6, which consists of a series MRRs. The resonant output is formed, thus, the normalized output of the light field is the ratio between the output and input fields [$E_{out}(t)$ and $E_{in}(t)$] in each roundtrip, which is given by [4]

$$\left|\frac{E_{out}(t)}{E_{in}(t)}\right|^2 = (1-\gamma)\left[1 - \frac{(1-(1-\gamma)x^2)\kappa}{(1-x\sqrt{1-\gamma}\sqrt{1-\kappa})^2 + 4x\sqrt{1-\gamma}\sqrt{1-\kappa}\sin^2(\frac{\varphi}{2})}\right] \tag{3.3}$$

The close form of Eq. (3.3) indicates that a ring resonator in this particular case is very similar to a Fabry–Perot cavity, which has an input and output mirror with a field reflectivity, $(1-\kappa)$, and a fully reflecting mirror. κ is the coupling coefficient, and $x=\exp(-\alpha L/2)$ represents a roundtrip loss coefficient, $\phi_0 = kLn_0$ and $\phi_{NL} = kLn_2|E_{in}|^2$ are the linear and nonlinear phase shifts, $k=2\pi/\lambda$ is the wave propagation number in a vacuum, where L and α are waveguide length and linear absorption coefficient,

respectively. In this work, the iterative method is introduced to obtain the results as shown in Eq. (3.3), and similarly, when the output field is connected and input into the other ring resonators.

The input optical field as shown in Eq. (3.1), i.e. a dark soliton pulse, is input into a nonlinear series microring resonator. By using the appropriate parameters, we propose to use the add/drop device with the appropriate parameters. This is given in details as followings. The optical outputs of a ring resonator add/drop filter can be given by the Eqs. (3.4) and (3.5), respectively [5].

$$\left|\frac{E_{out}(t)}{E_{in}(t)}\right|^2 = (1-\gamma)\left[1-\frac{(1-(1-\gamma)x^2)\kappa}{(1-x\sqrt{1-\gamma}\sqrt{1-\kappa})^2+4x\sqrt{1-\gamma}\sqrt{1-\kappa}\sin^2(\frac{\varphi}{2})}\right] \tag{3.4}$$

$$\left|\frac{E_d}{E_{in}}\right|^2 = \frac{\kappa_1\kappa_2 e^{-\frac{\alpha}{2}L}}{1+(1-\kappa_1)(1-\kappa_2)e^{-\alpha L}-2\sqrt{1-\kappa_1}\cdot\sqrt{1-\kappa_2}e^{-\frac{\alpha}{2}L}\cos(k_n L)} \tag{3.5}$$

where E_t and E_d represent the optical fields of the throughput and drop ports, respectively. $\beta = kn_{eff}$ is the propagation constant, n_{eff} is the effective refractive index of the waveguide, and the circumference of the ring is $L=2\pi R$, with R as the radius of the ring. In the following, new parameters is used for simplification with $\phi = \beta L$ as the phase constant. The chaotic noise cancellation can be managed by using the specific parameters of the add/drop device, and the required signals can be retrieved by the specific users. κ_1 and κ_2 are the coupling coefficient of the add/drop filters, $k_n=2\pi/\lambda$ is the wave propagation number for in a vacuum, and where the waveguide (ring resonator) loss is α = 0.5 dBmm^{-1}. The fractional coupler intensity loss is γ = 0.1. In the case of the add/drop device, the nonlinear refractive index is neglected.

In simulation, the generated dark soliton pulse, for instance, with 50-ns pulse width, and a maximum power of 0.5W is input into each of ring resonator systems with different center wavelengths, as shown in

Figure 3.6 The suitable ring parameters are used, such as ring radii and ring coupling coefficients, where R_1=15.0μm and R_2=10.0μm. In order to make the system associate with the practical device [17], n_0=3.34 (InGaAsP/InP). The effective core areas are A_{eff} =0.50 and 0.25 μm^2 for MRRs. The waveguide and coupling loses are α =0.5 $dBmm^{-1}$ and γ =0.1, respectively, and the coupling coefficients κ_s of the MRRs are ranged from 0.03 to 0.1. The nonlinear refractive index is $n_2=2.2\times10^{-13}$ m^2/W. In this case, the waveguide loss used is 0.5 $dBmm^{-1}$. However, more parameters are used as shown in

Figure 3.6 The input dark soliton pulse is chopped (sliced) into the smaller signals R_1, R_2, and the filtering signals within add/drop ring R_d are seen. We find that the output signals from R_2 is larger than from R_1 due to the different core effective areas of the rings in the system, however, the effective areas can be transferred from 0.50 and 0.25μm^2 with some losses. The soliton signals in R_d is entered in the add/drop filter, where the dark soliton conversion can be performed by using Eqs. (3.4) and (3.5). In application, the different dark soliton wavelength is input into the series microring resonators system, wheres the parameters of system are set the same. For instance, the dark solitons are input into the system at the center wavelengths λ_1 = 1.5, λ_2 = 1.52 and λ_3 = 1.54 μm, respectively. When a dark soliton propagates into the MRRs system, the occurrence of dark soliton collision (modulation) in multiplexer system and the filtering signals within add/drop ring (Rd) is as shown in

Figure 3.6 The dark soliton generated by multi-light sources at the center wavelength λ_1 = 1.5 μm. Simulation results obtained have shown that the band of bright solitons is seen, whereas there is no signal at λ_1 = 1.50 μm. The free spectrum range (FSR) and the amplified power of 2.1 nm and 20 W of the dark soliton are obtained, where in this case, the spectral width(Full width at half maximum, FWHM) of 0.1 nm is achieved.

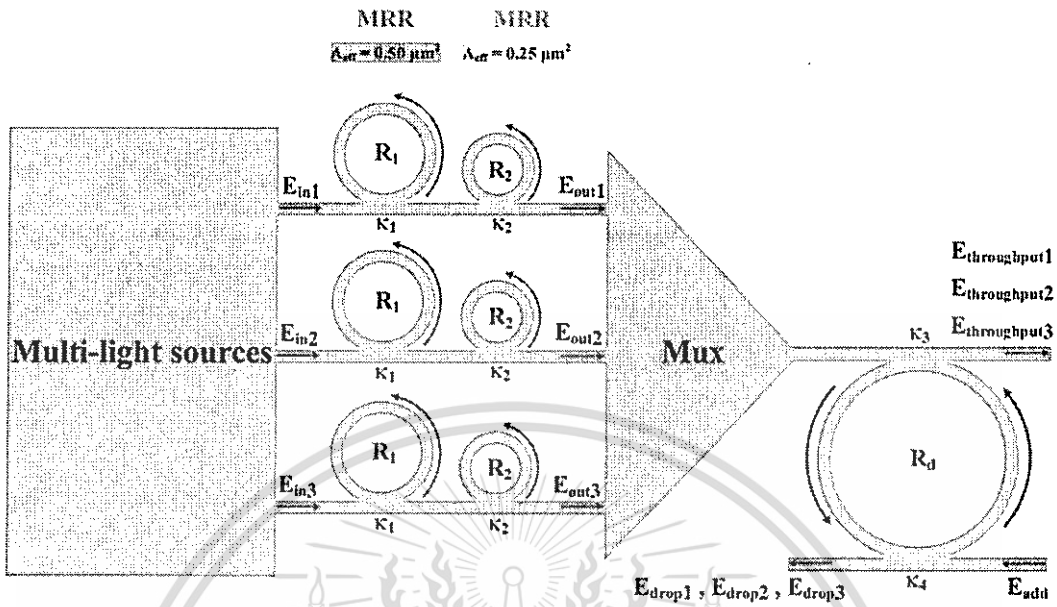

Figure 3.6 Schematic of generation trapping tool system, where Eins: Soliton inputs, Rs: ring radii, **K**s: coupling coefficients, MUX: Optical multiplexer, Rd: Add/drop radius.

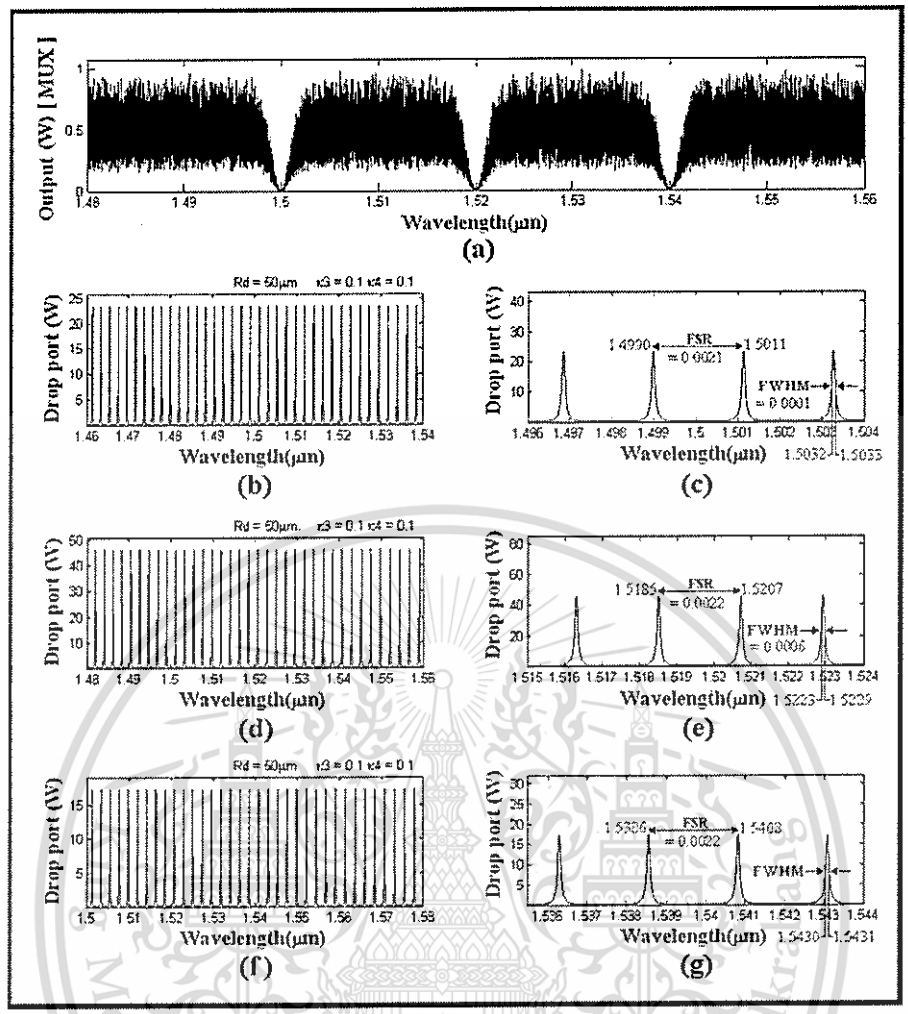

Figure 3.7 Simulation result of the dark soliton array when the dark soliton input wavelengths are 1.50, 1.52 and 1.54 μm, where (a) dark soliton array, (b) and (c), (d) and (e), (f) and (g) are the drop port signals, respectively.

Figure 3.8 shows the experimental setup for multi-wavelength Brillouin Enhanced Fiber Laser (BEFL) in the forward pumping configuration, which can be used to performed the dark soliton array by using nonlinear fiber optic setup system. The setup consists of a Brillouin pump (BP) with a 9.4 dBm output power, a Raman pump (RP) with a 296 mW output power that pumps the 7.7 km dispersion compensated fiber (DCF) and two laser diodes (LD) with an output power of 48 mW and 121 mW respectively. These LD's was bi-directionally pumped a 30m length depressed cladding fiber with a spooling diameter of 7cm. A linear resonator consists of two optical circulators (OC), where both ends of the setup were used. These two optical circulators also created a double pass configuration inside the cavity. Three

wavelength division multiplexers (WSC) were used to combine the different wavelength inside the cavity. A 3dB OC1 couples the signal from the BP into the cavity. A 90:10 output coupler that is replaced at different locations as shown in Figure 3.8 will tap 10% of this signal. This signal is directly observed using an optical spectrum analyzer (OSA) with a resolution of 0.02 nm.

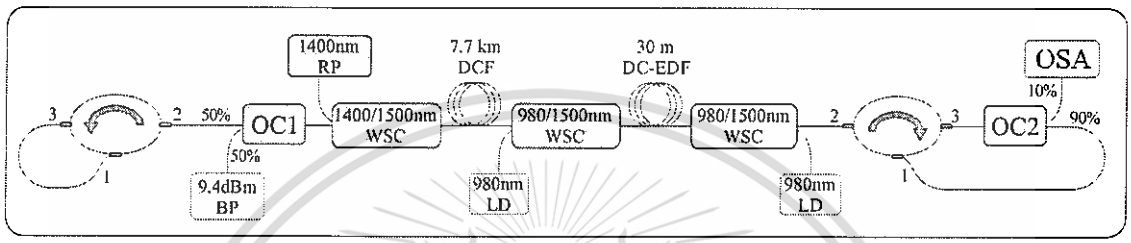

Figure 3.8 Experimental set up for forward pumping, where OSA: Optical Spectrum Analyzer, OCs: Optical Circulators, BP: Brillouin pumping, RP: Raman pumping, WSC: Wavelength division multiplexing, DCF: Dispersion compensated fiber, LDs: Laser diodes. DC-EDF: Depressed Cladding Erbium Doped Fiber.

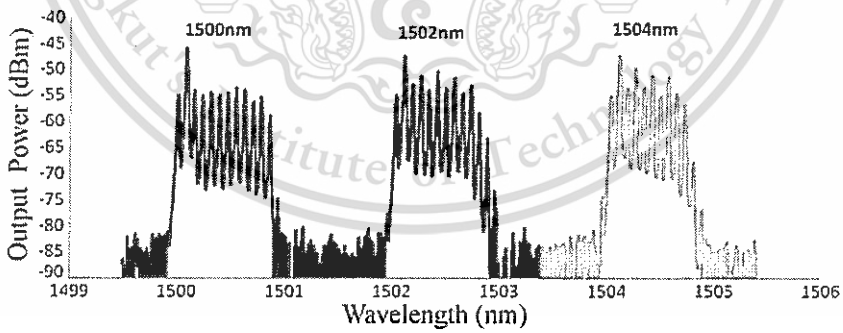

Figure 3.9 Tunable multiple-Brillouin lasing at different wavelengths of Brillouin pumping.

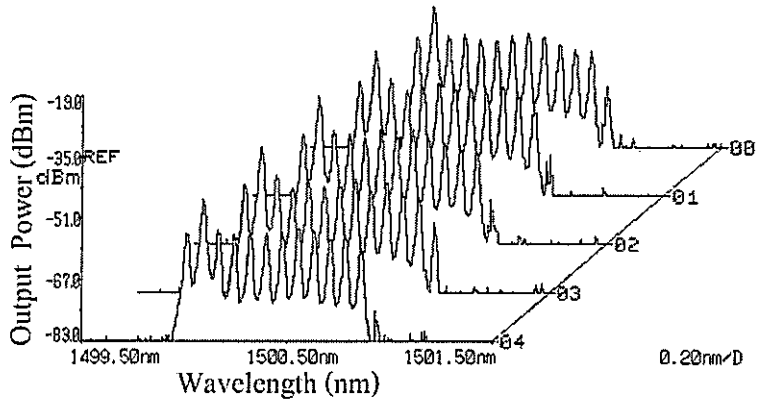

Figure 3.10 Shows the multi-dark-bright soliton train at 1,500 nm from 0 to 4.0 ns.

Figure 3.9 shows the tunable multiple-Brillouin lasing at different settings of wavelengths at BP. Note that this multi-wavelength Brillouin lasing are obtained from the experimental setup in Figure 3.8 The power setting of the BP is kept constant at 9.4 dBm but the wavelength of the signal is varied at 1,500 nm, 1,502 nm and 1,504 nm. From the spectrum obtained, 13, 12 and 11 peaks are obtained at 1,500 nm, 1,502 nm and 1,504 nm respectively. The lasing peaks at 1,500 nm are more stable and fluctuates less as compared to 1,502nm and 1,504nm lasing. Due to the less numbers of fluctuations of the lasing spectrum and the highest number of peaks obtained at 1,500 nm, the multi-Brillouin lasing at this wavelength is chosen for close scrutiny. Figure 3.10 shows the stability and evolution of the lasing spectrum of the dark-bright soliton conversion pulses. It can be seen that the same spectrum is almost reproducible. The time interval between two spectrums is 60 seconds. The generation of multi-Brillouin lasing is much dependent on the pumping power that interacts with the acoustic wave.

To increase the security of the channel, the dark soliton has been used instead of bright. In previous parts, we have shown the way to generate multiplex dark soliton as carrier signals of the data. The dark soliton as a carrier has travel to the fiber cavity to the destination. In case of the ability of receiver detector to detect the signal, dark soliton have to be converted back into the bright. Therefore, The dark-bright soliton conversion circuit have to be used and described as followed part.

3.4 Conclusion on dark soliton generation using pumping system

When using the pumping system to create the dark soliton, we can summarize the benefit of the system compare to the old one as follow.

1. Still focus on the layer 1 of OSI model, Physical layer (No need to change to upper layer of the system).
2. The used of dark soliton as a carrier which is More secure than bright.
3. Dark soliton was generated using pumping system was still too big and much more money.
4. Multi-dark soliton were generated, more capacity of the bandwidth of the communication.

3.5 The Micro Ring Resonator

Optical ring resonator has widely use in signal processing, laser application, sensor, optical communication, etc. They can be constructed using many optical elements such as mirror and beam splitter, fiber optic component or integrated optics technology. Regarding their geometry there are not only in circular shape. Integrated optical technologies are extreme miniaturization, for the fabrication of rings with very perimeters, the dimensions related with the wavelengths used in hi-speed communication systems.

In the past, smoke and fire are uses to communicate a piece of information, such as a victory message in a war. But all of that method has many setbacks such as speed or throughput. Electrons are the next media of transmitting a message. But it still has some problem to use electrons such as noise and bandwidth to use. Photons are more advantage and more popular in recently period. Photons are better than electrons by virtue of their special properties. They has a very large bandwidth, ~10^{15} Hz, gives optics a potential speed of a signal far beyond any electric method. Indeed, the shortest optical wavelength of <10fs give light three order of magnitude advantage over the shortest electrical pulse [6]. When it comes to interconnect on a chip, the wiring capacitance will set the speed limits of

integrated circuits. Besides, photons can pass through each other's unperturbed in the absence of a nonlinear interaction, whereas electrons interact with each other even at a distance.

In modern world, data-traffic volume is dramatically increased due to the demand on the internet connectivity. Therefore, all-optical switching devices have been looked at as key components for future high-speed optical communication systems. Such devices would enable highly parallel logic operations as well as ultrafast switching because of the instantaneous nature of virtual optical transitions [7]. With the recent advances in semiconductor fabrication, there has been a noticeable effort to bring those devices on semiconductor platforms to the real world. An ideal all-optical switch is the one that poses the following characteristics. It would only require as little as sub Pico joule of energy to switch with at least 20dB switching contrast. Beside compactness, it is desirable to integrate such a device with already established optoelectronics devices on a planar integrated photonic circuit. One category of devices that has a great potential to meet those requirements is *microring resonators*.

A ring resonator is simply a waveguide shaped into a ring structure. When an input electric field, E_i, is coupled to the ring waveguide through an external bus waveguide, a positive feedback is induced and the field inside the ring resonator E_r, starts to build up. Coupling between the straight and the ring waveguide is achieved through the evanescent wave. Therefore, the gap and coupling length between them determine how much power is coupled from the straight waveguide to the ring waveguide and vice versa. The feedback mechanism is simply induced by the ring waveguide and therefore there is no need for any Bragg gratings, mirrors, or distributed feedback waveguides which are more difficult to fabricate. In such configuration, only certain wavelengths will be allowed to resonate inside the ring waveguide, thus frequency selectivity is obtained.

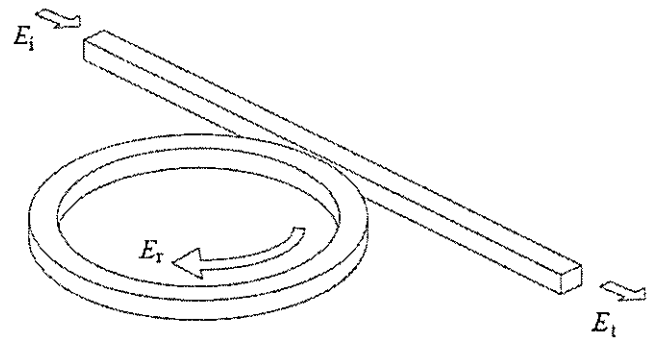

Figure 3.11 Schematic diagram for a ring resonator coupled to a single waveguide.

The proposal to use an integrated ring resonator for a band pass filter has been made in 1969 by E. A. Marcatili [8]. The transmission properties of the used guide consisting of a dielectric rod with rectangular cross section, surrounded by several dielectrics of smaller refractive indices have been described by E. A. Marcatili [9].

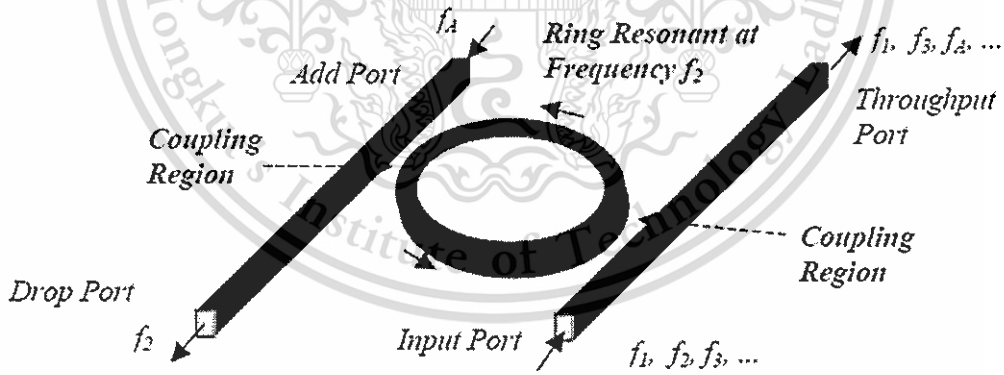

Figure 3.12 Ring resonator channel dropping filter.

A general architecture for an autoregressive planar waveguide optical filter was demonstrated for the first time in 1996 [10]. The autoregressive lattice filters which were designed and fabricated consisted of one and two stages using Ge-doped silica waveguides.

A signal flow chart transformation for evaluating the filter transfer functions was demonstrated. Purely passive single ring resonator filters have been realized in the material system AlGaAs-GaAs [11, 12] and Si-SiO_2 [13] and Si_3N_4- SiO_2 [14]. The radius of the used ring resonators is between 5 μm and 30 μm and the free spectral range (FSR) achieved is between 20 nm and 30 nm. Passive ring resonators in the form of a racetrack have been realized in the material system GaInAsP [15] and AlGaAs-GaAs [16]. The filter performance is limited by bending and scattering losses in the resonator. These losses could be compensated for by using or adding an active.

3.6 Optical Add/Drop Ring Resonator Filter

A ring resonator consists of a waveguide in a closed loop. The loop can be any closed shape, such as a circle, ellipse, or racetrack. The ring is placed near one or two bus waveguides. Typically, the input signal consists of one or more WDM channels. Signals on the input bus couple evanescently to the resonator. If a channel wavelength is resonant in the resonator, i.e., it encounters an integral multiple of 2π in phase over a round-trip, the signal intensity builds up in the ring, it couples to the output bus, and is "dropped." At the same time, a signal on the same wavelength can be added via the add port. The resonator thus functions as an add/drop multiplexer.

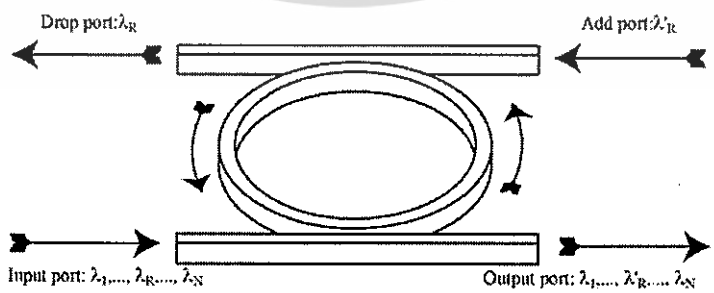

Figure 3.13 Schematic diagram for a ring resonator coupled to two waveguides as an add/drop filter.

An incident optical signal composed of multiple wavelengths ($\lambda_1,\ldots,\lambda_R,\ldots,\lambda_N$) at the input port coupled into the ring and for a resonant wavelength (λ_R), the energy builds up in the resonator despite the small coupling and eventually the signal is coupled into the drop port. Symmetrically, a new signal at resonant wavelength (λ_R') at the add port couples to the output port through the ring. As a result, such a configuration constitutes a very compact add/drop filter where a channel can be dropped from the WDM spectrum and replaced by a new signal on the same channel. Note that waves with a wavelength away from resonance will not repeat themselves in the ring and the coupled field interferes destructively with the wave in the resonator leading to little energy in the resonator and little dropped power. Residual dropped power at non-resonant wavelengths is possible due to imperfections and can induce inter-band crosstalk that is detrimental to WDM applications. Moreover, if the input channel at λ_R is not completely extinguished, intra-band crosstalk. These issues will be studied and can be theoretically overcome by varying coupling parameters, inducing loss/gain in the ring and inserting additional rings between the two waveguides.

3.7 The Z-Transform Description

The filter functions arise from the interference of two or more waves that are delayed relative to each other. The incoming signal is split into multiple paths by a division of the wave front or the amplitude. Diffraction gratings are an example of wave front division, while directional couplers and partial reflectors are examples of amplitude division. After traveling along different paths, the fields are combined and interference occurs. For interference, the optical waves must have the same polarization, the same frequency and be temporally coherent over the longest delay length. When signals are recombined, their relative phases determine whether they interfere constructively or destructively. The phase Φ for each path is the product of the distance traveled, L and the propagation constant, β i.e., $\Phi = \beta L$ where $\beta = 2\pi n_e / \lambda$, which is expressed in terms of the refractive index n for a diffraction-based delay line or an effective index n_e for a waveguide delay line [10].

The individual optical path lengths are typically integer multiples of the smallest path length difference. The unit delay is defined as $T = L_u n/c$ where L_u is the smallest path length and is called the unit delay length. The refractive index is assumed to be independent of wavelength. The key to analyzing optical filters using Z-transforms is that each delay be an integer multiple of a unit delay length L_u. The phase for each path is then expressed as a multiple of βL_u, so $\Phi_p = p\beta L_u$, where p is an integer. The total transverse electric field for N paths is the sum over each optical path length given by

$$E_{out} = E_o e^{-j\Phi_0} + E_1 e^{-j\Phi_1} + E_2 e^{-j\Phi_2} + \ldots + E_{N-1} e^{-j\Phi_{N-1}} \tag{3.6}$$

To obtain a Z-transform of E_{out}, we express the phase as a multiple of the unit delay T. Using $\Omega = 2\pi\nu$ where $c = \nu\lambda$

$$\beta L_u = \frac{2\pi n L_u}{\lambda} = \frac{2\pi\nu n L_u}{c} = \frac{\Omega L_u n}{c} = \Omega T \tag{3.7}$$

This gives $\Phi_p = p\beta L_u = p\Omega T$. Therefore Eq. (3.7) becomes,

$$E_{out} = E_o e^{-j0} + E_1 e^{-j\Omega T} + E_2 e^{-j2\Omega T} + \ldots + E_{N-1} e^{-j(N-1)\Omega T} \tag{3.8}$$

For a dispersion-less line, unit delay T is a constant and using $z = e^{j\Omega T}$ in Eq. (3.8), we get

$$E_{out} = E_o + E_1 z^{-1} + E_2 z^{-2} + \ldots + E_{N-1} z^{-(N-1)} \tag{3.9}$$

Because the delays are discrete multiples of the unit delay, the frequency response is periodic. One period is defined as the Free Spectral Range (FSR) and is given by $FSR = 1/T$. The normalized frequency $f = \omega/2\pi$ is related to the optical frequency by $f = (\nu - \nu_c)T$ or $f = (\Omega - \Omega_c)T/2\pi$. The center frequency $\nu_c = c/\lambda_c$ is

defined so that the product of refractive index and unit length is equal to an integer number of center wavelengths, i.e., $m\lambda_c = nL_u$ where m is an integer. Propagation loss of a delay line is accounted for by multiplying z^{-1} by $x = e^{-\alpha L/2}$ where α is the average loss per unit length and L is the delay path length.

For a more realistic case for a delay line with dispersion, the FSR is given as:

$$FSR = 1/T = \frac{c}{n_g L_u} \tag{3.10}$$

where $n_g = n_{eff} + f_o\left(dn_{eff}/df\right)_{f_o} = n_{eff} + \lambda_o\left(dn_{eff}/d\lambda\right)_{\lambda_o}$ is called as the *group refractive index* evaluated at either center frequency f_o or center wavelength λ_o.

The optical circuits are assumed to be linear and time invariant. They can be analyzed with Z-transforms using waveguide delays and directional couplers for splitting and combining signals. A schematic diagram of a directional coupler. The lines in the figure indicate waveguides of finite width and height. Two waveguides are brought close together so that their evanescent fields overlap. A power coupling ratio κ is associated with each directional coupler. For an input on one port, the power coupled to the cross-port is κ times the input power. The length of the region where the waveguides are coupled determines the coupling ratio. The input output relation can be expressed using a 2x2 transfer matrix $\Phi_{cplr}(\kappa)$ as shown in Eq. (3.11). where κ is the power coupling ratio, and E_n^i and E_n^o, for n = 1, 2 represent the coupler input and output fields respectively.

The coupling ratio is assumed to be wavelength independent and hence the matrix elements are constants. The through and the cross-port transmission terms are given by $c = \cos\theta = \sqrt{(1-\gamma)(1-\kappa)}$ and $-js = -j\sin\theta = -j\sqrt{(1-\gamma)\kappa}$, respectively, where γ is the coupling loss and θ is equal to the coupling strength integrated over the coupling length. A complex number $-j$ represents a $-(\pi/2)$ phase shift for the cross coupled light fields.

$$\begin{bmatrix} E_1^o \\ E_2^o \end{bmatrix} = \Phi_{cplr}(\kappa) \begin{bmatrix} E_1^i \\ E_2^i \end{bmatrix}, \quad \Phi_{cplr}(\kappa) = \begin{bmatrix} c & -js \\ -js & c \end{bmatrix} \tag{3.11}$$

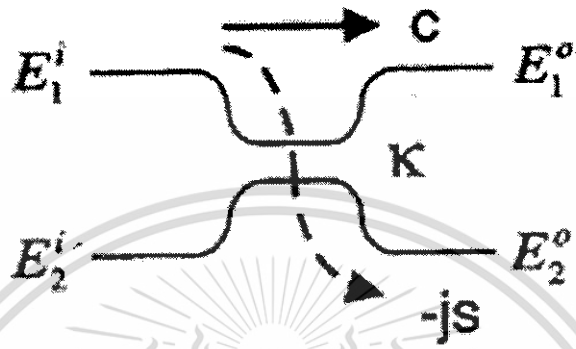

Figure 3.14 Directional coupler and I/O relations.

The basic filter structures require at least two paths for interference. The output is then the sum of each optical path. The transfer function from any input port to any output port can be written by inspection using the transmission of each path segment. The directional coupler transmission is given by $-js$ for the cross port and c for the through port. The transmission for each delay path is expressed in terms of the unit delay. A filter's transmission is then written by summing all paths between a particular input and output port.

3.8 Single Coupler Ring Resonator Filter (SCRR)

A ring resonator is simply a waveguide shaped into a ring structure as shown in Figure 3.15 To determine optical filter transfer function in Z-domain, the requirements of optical filters are considered to be satisfied are:

1) Linearity of all optical components.

2) Time invariance of all optical components.

3) Optical components must be lumped (i.e. not distributed).

The effects such as backscatter of light along the length of an optical fiber or waveguide, or saturation of an optical amplifier are therefore not considered here (the former is a distributed phenomenon; the latter is a nonlinear effect).

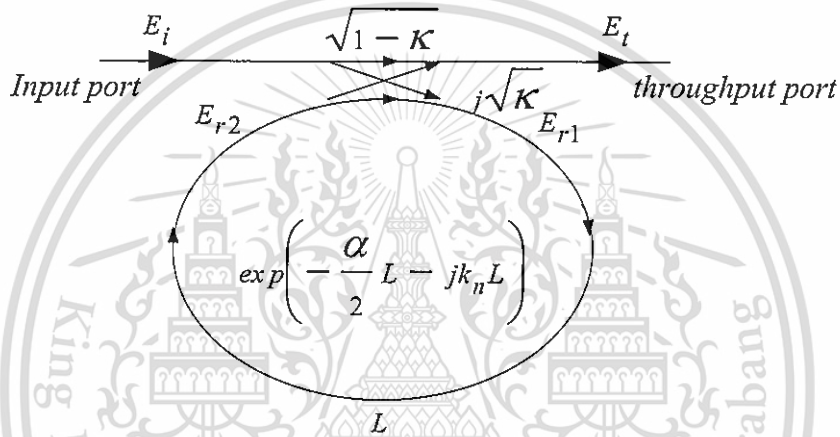

Figure 3.15 Schematic diagram for SCRR filter.

The transfer function of this configuration is derived using Z-transform analysis. The circumference of the ring is L ($L=2\pi R$, the radius is R), the coupling coefficient of the coupler is κ. The Z-transform parameter is represented by $z^{-1}=\exp^{-jk_nL}$ where $k_n=\frac{2\pi}{\lambda}n_{eff}$ is the propagation constant and n_{eff} is the effective index of the waveguide. The one round trip loss is $a=\exp^{-\alpha L/2}$, α is the intensity attenuation coefficient inside the waveguide [unit $length^{-1}$]. The transmitted or throughput field at the output of the straight waveguide, E_t and inserted electric field, E_i relations can be derived as followed:

$$E_t = (1-\gamma)^{1/2} \times \left[E_i \cdot \sqrt{1-\kappa} + j \cdot E_{r2} \sqrt{\kappa} \right] \tag{3.12}$$

$$E_{r1} = (1-\gamma)^{1/2} \times \left[j \cdot E_i \cdot \sqrt{\kappa} + E_{r2} \cdot \sqrt{1-\kappa} \right] \tag{3.13}$$

$$E_{r2} = E_{r1} \cdot a\, z^{-1} \tag{3.14}$$

Using three equations E_t / E_i can be calculated:

$$\frac{E_t}{E_i} = (1-\gamma)^{1/2} \times \left[\frac{\sqrt{1-\kappa} - (1-\gamma)^{1/2} \cdot a z^{-1}}{1 - (1-\gamma)^{1/2} \cdot \sqrt{1-\kappa} \cdot a\, z^{-1}} \right] \tag{3.15}$$

The transfer function in Eq. (3.15) indicates that a ring resonator is very similar to a Fabry-Perot cavity. In the particular case shown in (3.17), the corresponding Fabry-Perot cavity would have an input mirror with a field reflectivity and a fully reflecting output mirror. However, the field propagating inside the ring cavity is a traveling wave in contrast to the Fabry-Perot cavity which resonates a standing wave.

In the following, new parameter will be used for simplification:

$$\begin{aligned} D &= (1-\gamma)^{1/2} \\ x &= D \cdot \exp^{-\alpha L/2} \\ c &= \sqrt{1-\kappa} \\ \phi &= k_n \cdot L \end{aligned} \tag{3.16}$$

The intensity relation for the output port is given by:

$$T = \frac{I_t}{I_i}(\phi) = \left|\frac{E_t}{E_i}\right|^2 = D^2 \cdot \left[1 - \frac{\left(1-x^2\right)\cdot\left(1-c^2\right)}{\left(1-x\cdot c\right)^2 + 4\cdot x\cdot c\cdot sin^2\left(\frac{\phi}{2}\right)}\right] \quad (3.17)$$

3.9 Double Coupler Ring Resonator Filter (DCRR)

Consider the architectures of double coupler ring resonator which sometime called add/drop filters as illustrated in Figure 3.16, which are constructed by 2×2 optical couplers.

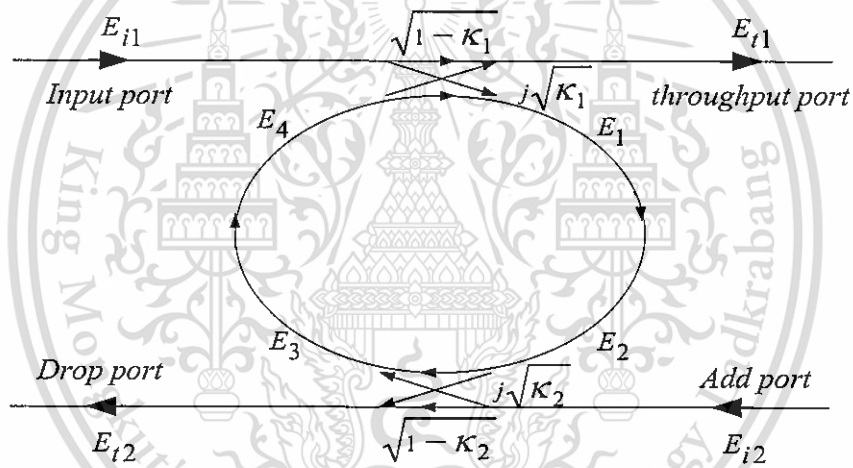

Figure 3.16 The architecture of DCRR or add/drop filter.

Similarly, the optical transfer functions of the ring resonator filters at the throughput port and drop port for an input port E_{i1} can be derived as followed. For the first coupler (κ_1), we have

$$E_{t1} = \sqrt{1-\gamma_1}\left[j\sqrt{\kappa_1}E_4 + \sqrt{1-\kappa_1}E_{i1}\right] \quad (3.18)$$

$$E_1 = \sqrt{1-\gamma_1}\left[j\sqrt{\kappa_1}E_{i1} + \sqrt{1-\kappa_1}E_4 \right] \tag{3.19}$$

where γ and κ_1 are the loss and the coupling coefficients, respectively. The incoming light of E_{i1} and E_4 are coupled through the first coupler to the output light E_{t1} and E_1 and the output light E_1 is transmitted through the ring becomes output light E_2. According to light transmission theory in linear optical systems, we obtain the following relation between E_1 and E_2

$$E_2 = E_1 e^{-\frac{\alpha L}{2}\frac{1}{2} - jk_n\frac{L}{2}} \tag{3.20}$$

where the transmission line length is $\frac{L}{2}$. The second coupler (κ_2) have the following relations:

$$E_{t2} = E_1 e^{-\frac{\alpha L}{2}\frac{1}{2} - jk_n\frac{L}{2}} \cdot j\sqrt{1-\gamma_2}\sqrt{\kappa_2} \quad \text{at} \quad E_{i2} = 0 \tag{3.21}$$

$$E_3 = E_1 e^{-\frac{\alpha L}{2}\frac{1}{2} - jk_n\frac{L}{2}} \sqrt{1-\gamma_2}\sqrt{1-\kappa_2} \tag{3.22}$$

Using the transmission theory, we obtain E_4 in terms of E_3

$$E_4 = E_3 e^{-\frac{\alpha L}{2}\frac{1}{2} - jk_n\frac{L}{2}} \tag{3.23}$$

$$E_1 = \frac{E_{i1}\, j\sqrt{1-\gamma_1}\sqrt{\kappa_1}}{1-\sqrt{1-\gamma_1}\sqrt{1-\kappa_1}\sqrt{1-\gamma_2}\sqrt{1-\kappa_2}\, e^{-\frac{\alpha}{2}L-jk_nL}} \tag{3.24}$$

$$E_4 = \frac{E_{i1} j\sqrt{1-\gamma_1}\sqrt{\kappa_1}}{1-\sqrt{1-\gamma_1}\sqrt{1-\kappa_1}\sqrt{1-\gamma_2}\sqrt{1-\kappa_2}\, e^{-\frac{\alpha}{2}L-jk_nL}} \sqrt{1-\gamma_2}\sqrt{1-\kappa_2}\, e^{-\frac{\alpha}{2}L-jk_nL} \tag{3.25}$$

By using the upper equations, the transfer function for throughput port and drop port in Eq. (3.24) can thus be expressed as

Throughput port:

$$\frac{E_{t1}}{E_{i1}} = \frac{-(1-\gamma_1)\kappa_1\sqrt{1-\kappa_2}\, e^{-\frac{\alpha}{2}L-jk_nL} + \sqrt{1-\gamma_1}\sqrt{1-\kappa_1}}{1-\sqrt{1-\gamma_1}\sqrt{1-\kappa_1}\sqrt{1-\gamma_2}\sqrt{1-\kappa_2}\, e^{-\frac{\alpha}{2}L-jk_nL}} \tag{3.26}$$

$$= \frac{-(1-\gamma_1)(1-\kappa_1)\sqrt{1-\gamma_2}\sqrt{1-\kappa_2}\, e^{-\frac{\alpha}{2}L-jk_nL}}{1-\sqrt{1-\gamma_1}\sqrt{1-\kappa_1}\sqrt{1-\gamma_2}\sqrt{1-\kappa_2}\, e^{-\frac{\alpha}{2}L-jk_nL}}$$

$$= \frac{-\sqrt{1-\gamma_2}\sqrt{1-\kappa_2}\, e^{-\frac{\alpha}{2}L-jk_nL} + \sqrt{1-\gamma_1}\sqrt{1-\kappa_1}}{1-\sqrt{1-\gamma_1}\sqrt{1-\kappa_1}\sqrt{1-\gamma_2}\sqrt{1-\kappa_2}\, e^{-\frac{\alpha}{2}L-jk_nL}}$$

Drop port:

$$\frac{E_{t2}}{E_{i1}}=\frac{-\sqrt{1-\gamma_1}\sqrt{1-\gamma_2}\sqrt{\kappa_1\cdot\kappa_2}\,e^{-\frac{\alpha}{2}\frac{L}{2}-jk_n\frac{L}{2}}}{1-\sqrt{1-\gamma_1}\sqrt{1-\kappa_1}\sqrt{1-\gamma_2}\sqrt{1-\kappa_2}\,e^{-\frac{\alpha}{2}L-jk_nL}} \tag{3.27}$$

The intensity relations for the throughput and drop port can be obtained by normalizing the transfer functions in Eqs. (3.26) and (3.27) which are given by

$$\frac{I_{t1}}{I_{i1}}=\left|\frac{E_{t1}}{E_{i1}}\right|^2=\frac{\begin{array}{c}1-(1-\gamma_1)\kappa_1-2\sqrt{1-\gamma_1}\sqrt{1-\kappa_1}\cdot\sqrt{1-\gamma_2}\sqrt{1-\kappa_2}\,e^{-\frac{\alpha}{2}L}\cos(k_nL)\\+(1-\gamma_2)(1-\kappa_2)e^{-\alpha L}\end{array}}{\begin{array}{c}1+(1-\gamma_1)(1-\kappa_1)\cdot(1-\gamma_2)(1-\kappa_2)e^{-\alpha L}\\-2\sqrt{1-\gamma_1}\sqrt{1-\kappa_1}\cdot\sqrt{1-\gamma_2}\sqrt{1-\kappa_2}\,e^{-\frac{\alpha}{2}L}\cos(k_nL)\end{array}} \tag{3.28}$$

$$\frac{I_{t2}}{I_{i1}}=\left|\frac{E_{t2}}{E_{i1}}\right|^2=\frac{(1-\gamma_1)(1-\gamma_2)\cdot\kappa_1\kappa_2e^{-\frac{\alpha}{2}L}}{\begin{array}{c}1+(1-\gamma_1)(1-\kappa_1)\cdot(1-\gamma_2)(1-\kappa_2)e^{-\alpha L}\\-2\sqrt{1-\gamma_1}\sqrt{1-\kappa_1}\cdot\sqrt{1-\gamma_2}\sqrt{1-\kappa_2}\,e^{-\frac{\alpha}{2}L}\cos(k_nL)\end{array}} \tag{3.29}$$

For simplification, the calculation of the intensity relation does not take into account coupling losses ($\gamma=0$) and the following parameters:

$$\begin{aligned}x&=exp\left(-\frac{\alpha}{2}L\right)\\c_1&=\sqrt{1-\kappa_1}\\c_2&=\sqrt{1-\kappa_2}\end{aligned} \tag{3.30}$$

The intensity relations Eqs. (3.28) and (3.29) are then given by

$$\frac{I_{t1}}{I_{i1}}(\phi)=\left|\frac{E_{t1}}{E_{i1}}\right|^2=1-\frac{\left(1-c_1^2\right)\cdot\left(1-c_2^2x^2\right)}{\left(1-c_1c_2x\right)^2+4c_1c_2xsin^2\left(\frac{\phi}{2}\right)} \tag{3.31}$$

$$\frac{I_{t2}}{I_{i1}}(\phi)=\left|\frac{E_{t2}}{E_{i1}}\right|^2=\frac{\left(1-c_1^2\right)\cdot\left(1-c_2^2\right)\cdot x}{\left(1-c_1c_2x\right)^2+4c_1c_2xsin^2\left(\frac{\phi}{2}\right)} \tag{3.32}$$

3.10 Enhanced Nonlinearity in Single Ring Resonator

This section will carefully study such enhancement and its projection on the dynamic performance of the micro ring resonator for all-optical switching applications. We will concentrate on the reduction achievable in the switching power of a micro ring due to the resonant condition.

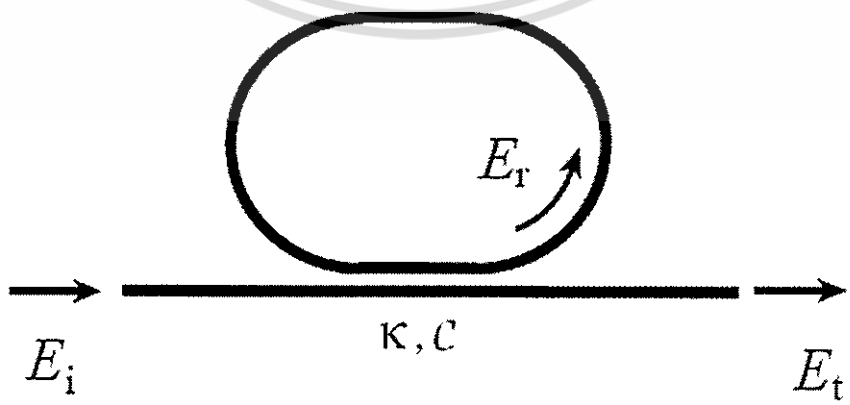

Figure 3.17 The waveguide layout of SCRR.

For a small range of detuning, i.e., much smaller than the 3-dB bandwidth of the micro ring resonance, a small signal analysis approach is enough to understand the dynamic behavior of the resonator and to determine its switching enhancement. In such analysis, we will assume that the linear parameters of the micro ring resonator are constants with respect to time. Without loss of generality, we will consider the SCRR filter case that we have introduced. At steady state, the field transmittance of the filter is given by

$$\frac{E_t}{E_i} = \frac{c - a e^{j\phi_0}}{1 - ca\, e^{j\phi_0}} \tag{3.33}$$

where $a = \exp(-\alpha L/2)$ is the round trip field attenuation of the microring, c is the field transmittance coefficient, and $\phi_0 = \beta L$ is linear phase shift in the ring. β is the wave propagation constant associated with the fundamental mode supported by the ring waveguide, and L is the circumference of the ring. One useful feature of a ring resonator is that the original power gets to build up in the ring and keeps circulating inside the ring. The buildup factor B, which is defined as the ratio of the power circulating inside the ring to the input power, is given by [17]

$$B = \frac{P_r}{P_i} = \frac{1 - c^2}{1 + c^2 a^2 - 2ca\cos\phi_0} \tag{3.34}$$

where P_i is the input power, P_r is the average power inside the ring. Under conditions that the incident light is on resonance with the ring and the loss is negligible ($a = 1$), the maximum value of the buildup factor $B_{\max} = (1+c)/(1-c)$.

Thus, when c is very close to unity, the power circulating inside the fiber ring becomes very high. This power buildup can induce nonlinear effects if the ring possesses an intensity-dependent nonlinear refractive index n_2 that results from the third-order susceptibility ($\chi^{(3)}$) of the waveguide material [17]. The nonlinear refractive index n_2 can be included in the single-pass phase shift as

$$\phi = \phi_0 + \phi_{NL} \cong \beta L + \gamma L_{eff} P_r \tag{3.35}$$

where $L_{eff} = [1 - \exp(-\alpha L)]/\alpha$, is the effective interaction length due to the loss and γ is the nonlinearity coefficient (related to n_2 by $\gamma = 2\pi n_2 / \lambda A_{eff}$, where λ is the input wavelength and A_{eff} is the effective core area of the waveguide). ϕ_0 and ϕ_{NL} are the single-pass linear and nonlinear phase shifts, respectively. In such a nonlinear case, ϕ_0 in Eq. (3.35) should now be replaced by ϕ. Thus, by substituting Eq. (3.35) into Eq. (3.36), we get a transcendental equation for the single-pass phase shift as

$$\phi(P_i, \phi_L) = \phi_L + \gamma L_{eff} \frac{1 - c^2}{1 + c^2 a^2 - 2ca \cos \phi(P_i, \phi_L)} P_i \tag{3.36}$$

The nonlinear response of switching device can be evaluated by the derivative of phase shift ϕ with respect to input power P_i. This derivative can be expressed as

$$\frac{d\phi}{dP_r} = \frac{d\phi}{d\phi_0} \frac{d\phi_0}{dP_r} \frac{dP_r}{dP_i} \approx \frac{8Ln_2}{\pi \lambda A_{eff}} F^2 \tag{3.37}$$

where F is resonator finesse [17].

3.11 Enhanced Nonlinearity in Add/Drop Ring Resonator

The transmission equation from input port to drop port for the DCRR is given by

$$\frac{E_{t2}}{E_{i1}} = \frac{s_1 s_2 \sqrt{\gamma} e^{j\phi_0}}{1 - c_1 c_2 \gamma e^{j\phi_0}} \tag{3.38}$$

where c_1, s_1 and c_2, s_2 are the coupling coefficients for the two couplers respectively. Critical coupling condition for the DCRR is defined to be $\left|E_{t2}/E_{i1}\right|^2 = 1$, i.e. all light goes through the drop port, which gives $s_{2c} = \sqrt{1 - c_1^2 e^{-\alpha L}}$. Since $s_{2c} = s_1$, symmetric DCRR (with two identical couplers) will operate at noncritical coupling. The phase shift of the drop port field (E_{t2}) is

$$\phi = \pi + \phi_0 + \arctan\left[\frac{c^2 \gamma \sin\phi_0}{1 - c^2 \gamma \cos\phi_0}\right] \tag{3.39}$$

Similar to SCRR, the nonlinear effect can be included by applying Eq. (3.38) to the computation of ϕ as follow.

$$\phi = \phi_0 + \frac{2\pi n_2 \frac{L}{2} P_2}{\lambda A_{eff}} + \frac{2\pi n_2 \frac{L}{2} P_4}{\lambda A_{eff}} \tag{3.40}$$

Where P_2 and P_4 are circulating powers, respectively.

The dark soliton generation system has an advantage than the bright soliton in order to secure the transmission link. But the generation system using pumping system is too big and highly cost. In order to maintain the advantage of this system but use less cost, the Gaussian pulse input will be better. In the next section, will propose a way to generate dark soliton using Gaussian pulse input.

3.12 Dark Soliton Generation using Gaussian pulse input

Optical soliton is recognized as the powerful light source for long distance link in optical communication. However, the pumping system is required before the soliton being generated. For simplicity, a Gaussian soliton is recommended to form the soliton instead of the pumping soliton. Moreover, one interesting aspect of the Gaussian soliton is that the non-dispersive soliton can be realized by using the 1,300 nm light source, which can be obtained by using the Gaussian soliton. Many research works have reported in use of a Gaussian pulse in both theoretical and experimental works [18, 19, 20, 21]. Recently, the interesting aspect of light pulse propagating within a nonlinear microring device has been reported [22], where the transfer function of the output at resonant condition is derived and studied. They found that the broad spectrum of light pulse can be transformed to the discrete pulses. An optical soliton is recognized as a powerful laser pulse, which can be used to enlarge the optical bandwidth when propagating within the nonlinear microring resonator [23, 24]. Moreover, the superposition of self-phase modulation (SPM) soliton pulses, where either bright or dark [25] solitons can generate the large output power. Therefore, in this work we are using a common laser source that can be used to generate dark soliton, with the broad center wavelengths within the range from 400-1,500 nm are used. One of the results has shown that by using the center wavelength at 1,300 nm with suitable parameters, the Gaussian soliton generation is plausible. By using the suitable microring parameters, most of the results have shown that the optical signals, i.e. Gaussian pulse can be amplified within the nonlinear ring resonator system.

Light from a monochromatic light source is launched into a ring resonator with constant light field amplitude (E_0) and random phase modulation, which is the combination of terms in attenuation (α) and phase(ϕ_0) constants, which results in temporal coherence degradation. Hence, the time dependent input light field (E_{in}), without pumping term, can be expressed as

$$E_{in}(t) = E_0 \exp^{-\alpha L + j\phi_0(t)} \tag{3.41}$$

where L is a propagation distance(waveguide length).

We assume that the nonlinearity of the optical ring resonator is of the Kerr-type, i.e., the refractive index is given by

$$n = n_0 + n_2 I = n_0 + (\frac{n_2}{A_{eff}})P, \tag{3.42}$$

where n_0 and n_2 are the linear and nonlinear refractive indexes, respectively. I and P are the optical intensity and optical power, respectively. The effective mode core area of the device is given by A_{eff}. For the microring and nanoring resonators, the effective mode core areas range from 0.10 to 0.50 μm^2 [26]

When a Gaussian pulse is input and propagated within a fiber ring resonator, the resonant output is formed, thus, the normalized output of the light field is the ratio between the output and input fields ($E_{out}(t)$ and $E_{in}(t)$) in each roundtrip, which can be expressed as [27]

$$\left|\frac{E_{out}(t)}{E_{in}(t)}\right|^2 = (1-\gamma)\left[1 - \frac{(1-(1-\gamma)x^2)\kappa}{(1-x\sqrt{1-\gamma}\sqrt{1-\kappa})^2 + 4x\sqrt{1-\gamma}\sqrt{1-\kappa}\sin^2(\frac{\phi}{2})}\right] \tag{3.43}$$

Eq. (3.43) indicates that a ring resonator in the particular case is very similar to a Fabry-Perot cavity, which has an input and output mirror with a field reflectivity, (1-

κ), and a fully reflecting mirror. κ is the coupling coefficient, and $x = \exp(-\alpha L/2)$ represents a roundtrip loss coefficient, $\phi_0 = kLn_0$ and $\phi_{NL} = kL(\frac{n_2}{A_{eff}})P$ are the linear and nonlinear phase shifts, $k = 2\pi/\lambda$ is the wave propagation number in a vacuum. Where L and α are a waveguide length and linear absorption coefficient, respectively. In this work, the iterative method is introduced to obtain the results as shown in Eq. (3.43), similarly, when the output field is connected and input into the other ring resonators.

The input optical field as shown in Eq. (3.41), i.e. a Gaussian pulse, is input into a nonlinear microring resonator. By using the appropriate parameters, the chaotic signal is obtained by using Eq. (3.43) To retrieve the signals from the chaotic noise, we propose to use the add/drop device with the appropriate parameters. This is given in details as followings. The optical outputs of a ring resonator add/drop filter can be given by the Eqs (3.44) and (3.45)

$$\left|\frac{E_t}{E_{in}}\right|^2 = \frac{(1-\kappa_1) - 2\sqrt{1-\kappa_1}\cdot\sqrt{1-\kappa_2}\,e^{-\frac{\alpha}{2}L}\cos(k_n L) + (1-\kappa_2)e^{-\alpha L}}{1 + (1-\kappa_1)(1-\kappa_2)e^{-\alpha L} - 2\sqrt{1-\kappa_1}\cdot\sqrt{1-\kappa_2}\,e^{-\frac{\alpha}{2}L}\cos(k_n L)} \tag{3.44}$$

and

$$\left|\frac{E_d}{E_{in}}\right|^2 = \frac{\kappa_1\kappa_2 e^{-\frac{\alpha}{2}L}}{1 + (1-\kappa_1)(1-\kappa_2)e^{-\alpha L} - 2\sqrt{1-\kappa_1}\cdot\sqrt{1-\kappa_2}\,e^{-\frac{\alpha}{2}L}\cos(k_n L)} \tag{3.45}$$

where E_t and E_d represents the optical fields of the throughput and drop ports respectively. The transmitted output can be controlled and obtained by choosing the suitable coupling ratio of the ring resonator, which is well derived and described by reference. [28] Where $\beta = kn_{eff}$ represents the propagation constant, n_{eff} is the effective refractive index of the waveguide, and the circumference of the ring is $L = 2\pi R$, here R is the radius of the ring. In the following, new parameters will be used for simplification, where $\phi = \beta L$ is the phase constant. The chaotic noise cancellation can be managed by using the specific parameters of the add/drop

device, which the required signals at the specific wavelength band can be filtered and retrieved. $K_1$and K_2 are coupling coefficient of add/drop filters, $k_n = 2\pi/\lambda$ is the wave propagation number for in a vacuum, and the waveguide (ring resonator) loss is α = 0.5 dBmm^{-1}. The fractional coupler intensity loss is γ = 0.1. In the case of add/drop device, the nonlinear refractive index is neglected.

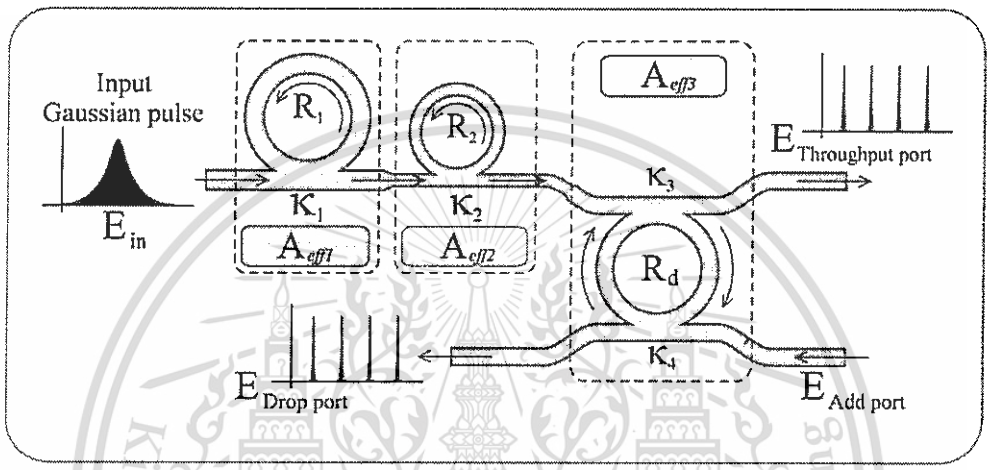

Figure 3.18 A schematic of a Gaussian soliton generation system, where Rs: ring radii, κ s: coupling coefficients, Rd: an add/drop ring radius, Aeffs: Effective areas.

From Figure 3.18, in principle, light pulse is sliced to be the discrete signal and amplified within the first ring, where more signal amplification can be obtained by using the smaller ring device (second ring).Finally, the required signals can be obtained via a drop port of the add/drop filter. In operation, an optical field in the form of Gaussian pulse from a laser source at the specified center wavelength is input into the system.

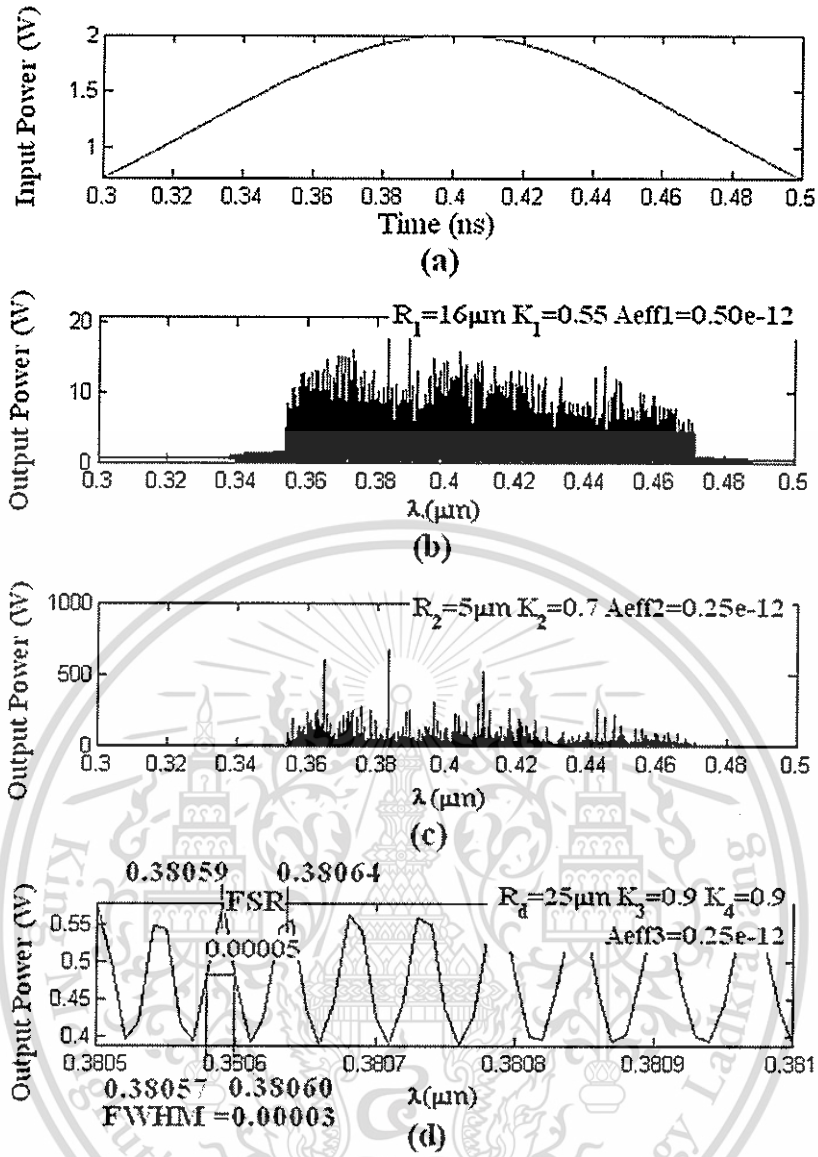

Figure 3.19 Result of the spatial pulses with center wavelength at 0.40 μm, where (a) the Gaussian pulse, (b) large bandwidth signals, (c) large amplified signals, (d) filtering and amplifying signals from the drop port.

From Figure 3.19, the Gaussian pulse with center wavelength (ϕ_0) at 0.40 μm, pulse width (Full Width at Half Maximum, FWHM) of 20 ns, peak power at 2 W is input into the system as shown in Figure 3.19(a). The large bandwidth signals can be seen within the first microring device, and shown in Figure 3.19(b). The suitable ring parameters are used, for instance, ring radii R_1= 16.0 μm, R_2= 5.0 μm, and R_d= 25.0 μm. In order to make the system associate with the practical device[13],

the selected parameters of the system are fixed to n_0 = 3.34 (InGaAsP/InP), A_{eff} = 0.50 μm^2 and 0.25 μm^2 for a microring and add/drop ring resonator, respectively, α = 0.5 $dBmm^{-1}$, γ = 0.1. In this investigation, the coupling coefficient (kappa, κ) of the microring resonator is ranged from 0.55 to 0.90. The nonlinear refractive index of the microring used is $n_2=2.2 \times 10^{-17}$ m^2/W. In this case, the attenuation of light propagates within the system (i.e. wave guided) used is $0.5dBmm^{-1}$. After light is input into the system, the Gaussian pulse is chopped (sliced) into a smaller signal spreading over the spectrum due to the nonlinear effects[8], which is shown in Figure 3.19(a). The large bandwidth signal is generated within the first ring device. In applications,

the specific input or out wavelengths can be used and generated. However, the amplified power is required to control to keep the device being realistic

The dark soliton can be used in optical communication in order to fulfill a higher security of it carrier signal, however a dark soliton can be used as a carrier of one channel in light communication. If we wish to increase the throughput of data, the multiplexed dark solitons have to be used as carriers of multiple channels of the communication. In the next part, we described the theory and experimental result of multiplexed dark solitons generation.

CHAPTER 4

HIGHER BANDWIDTH USING MULTIPLEXED DARK SOLITON

In chapter 3, we have described the way to increase security of fiber communication using dark soliton. We even showed the theory and the experiment of the dark soliton generation system. Next in this chapter, we showed the way to generate multiplexed dark soliton and the result of multiplexed dark soliton generation using Matlab by simulation using the math model. We showed the result of multiplex dark soliton generation to ensure the higher bandwidth of the link using multiplex dark soliton as proposed.

4.1 Generation of multiplexed dark soliton

To create a system by which multiplexed dark soliton pulses can be used to generate a dark soliton array, stationary dark soliton pulses are introduced into the microring resonator system shown in Figure 4.1 Each of input optical fields (E_{in}) of the dark soliton pulses is given by [29]

$$E_{in}(t) = A \tanh\left[\frac{T}{T_0}\right] \exp\left[\left(\frac{z}{2L_D}\right) - i\omega_0 t\right] \tag{4.1}$$

Where A and z are the optical field amplitude and propagation distance, respectively; T is a soliton pulse propagation time in a frame moving at the group velocity, $T = t - \beta_1 z$, where β_1 and β_2 are the coefficients of the linear and second-order terms of Taylor expansion of the propagation constant; $L_D = T_0^2/|\beta_2|$ is the dispersion length of the soliton pulse; T_0 is the soliton pulse propagation time at initial input (or soliton pulse width); t is the soliton phase shift time; and the frequency shift of the soliton is ω_0. This solution describes a pulse that keeps its

temporal width invariant as it propagates, and thus is called a temporal soliton. When the soliton peak intensity ($|\beta_2/\Gamma \times T_0^2|$) is given, then T_0 is known. For the soliton pulse in the microring device, a balance should be achieved between the dispersion length (L_D) and the nonlinear length ($L_{NL} = 1/\Gamma\phi_{NL}$), where $\Gamma = n_2 k_0$, is the length scale over which dispersive or nonlinear effects makes the beam become wider or narrower. For a soliton pulse, there is a balance between dispersion and nonlinear lengths; hence $L_D = L_{NL}$.

When light propagates within the nonlinear material (medium), the refractive index (n) of light within the medium is given by

$$n = n_0 + n_2 I = n_0 + \frac{n_2}{A_{eff}} P \tag{4.2}$$

where n_0 and n_2 are the linear and nonlinear refractive indices, respectively, and I and P are the optical intensity and optical power, respectively. The effective mode core area of the device is given by A_{eff}. For the series microring resonator (MRRs), the effective mode core areas range from 0.50 to 0.10 μm^2 [30]. When a soliton pulse is input and propagated within a MRR, (as shown in Figure 4.1, which consists of a series MRRs), a resonant output is formed. Thus, the normalized output light field is the ratio between the output and input fields [$E_{out}(t)$ and $E_{in}(t)$] in each roundtrip, which is given by [22]

$$\left|\frac{E_{out}(t)}{E_{in}(t)}\right|^2 = (1-\gamma)\left[1 - \frac{(1-(1-\gamma)x^2)\kappa}{(1-x\sqrt{1-\gamma}\sqrt{1-\kappa})^2 + 4x\sqrt{1-\gamma}\sqrt{1-\kappa}\sin^2(\frac{\varphi}{2})}\right] \tag{4.3}$$

The close form of Eq. (4.3) indicates that a ring resonator in this particular case is very similar to a Fabry–Perot cavity, which has an input and output mirror with a field reflectivity $1-\kappa$, and a fully reflecting mirror. Here κ is the coupling coefficient, $x=\exp(-\alpha L/2)$ represents a round-trip loss coefficient, $\phi_0=kLn_0$ and $\phi_{NL}=kLn_2|E_{in}|^2$ are the linear and nonlinear phase shifts, and $k=2\pi/\lambda$ is the wave propagation number in a vacuum, where L and α are waveguide length and linear absorption coefficient,

respectively. In this work, the iterative method is introduced to obtain the results as shown in Eq. (4.3), and similarly when the output field is connected and input into the other ring resonators.

The input optical field as shown in Eq. (4.1), i.e., a dark soliton pulse, is input into a nonlinear series microring resonator. We propose to use and add-drop device with the appropriate parameters. This is given in details as follows. The optical outputs of a ring- resonator add-drop filter can be given by [27].

$$\left|\frac{E_t}{E_{in}}\right|^2 = \frac{(1-\kappa_1)-2\sqrt{1-\kappa_1}\cdot\sqrt{1-\kappa_2}\,e^{-\frac{\alpha}{2}L}\cos(k_nL)+(1-\kappa_2)e^{-\alpha L}}{1+(1-\kappa_1)(1-\kappa_2)e^{-\alpha L}-2\sqrt{1-\kappa_1}\cdot\sqrt{1-\kappa_2}\,e^{-\frac{\alpha}{2}L}\cos(k_nL)} \tag{4.4}$$

And

$$\left|\frac{E_d}{E_{in}}\right|^2 = \frac{\kappa_1\kappa_2 e^{-\frac{\alpha}{2}L}}{1+(1-\kappa_1)(1-\kappa_2)e^{-\alpha L}-2\sqrt{1-\kappa_1}\cdot\sqrt{1-\kappa_2}\,e^{-\frac{\alpha}{2}L}\cos(k_nL)} \tag{4.5}$$

where E_t and E_d represent the optical fields of the throughput and drop ports, respectively, $\beta = kn_{eff}$ is the propagation constant, n_{eff} is the effective refractive index of the waveguide, and the circumference of the ring is $L=2\pi R$, with R the radius of the ring. In the following, new parameters are used for simplification, with $\phi = \beta L$ as the phase constant. The chaotic noise cancellation can be managed by using the specific parameters of the add-drop device, and the required signals can be retrieved by the specific users. In Eqs. (4.4) and (4.5), κ_1 and κ_2 are the coupling coefficient of the add-drop filters, $k_n=2\pi/\lambda$ is the wave propagation number in a vacuum, and the waveguide (ring resonator) loss is α = 0.5 dBmm^{-1}. The fractional coupler intensity loss is γ = 0.1. In the case of the add-drop device, the nonlinear refractive index is neglected.

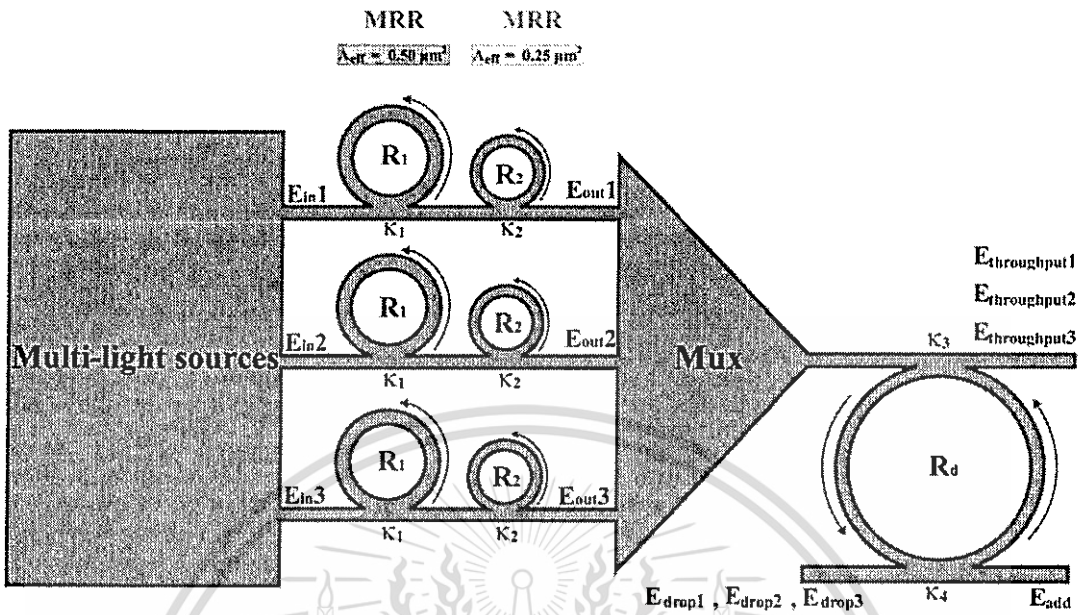

Figure 4.1 Schematic of generation trapping tool system, where Eins, soliton inputs; Rs, ring radii; **K**s, coupling coefficients; MUX, optical multiplexer; Rd, add-drop radius.

In simulation, the generated dark soliton pulse, for instance, with 50-ns pulse width and a maximum power of 0.5W, is input into each of ring resonator systems with different center wavelengths, as shown in Figure 4.1 Suitable ring parameters are used, such as ring radii (R_1=15.0μm and R_2=10.0μm) and ring coupling coefficients. In order to make the system correspond to a practical device [20], we set n_0=3.34 (InGaAsP/InP). The effective core areas are A_{eff} =0.50 and 0.25 μm^2 for MRRs. The waveguide and coupling loses are α =0.5 dB mm^{-1} and γ =0.1, respectively, and the coupling coefficients κ_s of the MRRs ranged from 0.03 to 0.1. The nonlinear refractive index is $n_2=2.2\times10^{-13}$ m^2/W. In this case, the waveguide loss used is 0.5 $dBmm^{-1}$. Other parameters used are shown in Figure 4.1 The input dark-soliton pulse is chopped (sliced) into the smaller signals R_1, R_2, and the filtering signals within add-drop ring R_d are seen. We find that the output signals from R_2 is larger than from R_1, due to the different effective core areas (0.50 and 0.25μm^2)of the rings in the system; however, the effective areas can be change with some losses. The soliton signals in

R_d are fed to the add-drop filter, where the dark-soliton conversion can be performed according to Eqs. (4) and (5).

In application, the different dark-soliton wavelengths are input into the series microring resonators system, whereas the parameters of the system are set the same. For instance, the dark solitons are input into the system at the center wavelengths λ_1 = 1.5 μm, λ_2 = 1.52 μm, and λ_3 = 1.54 μm. When a dark soliton propagates into the MRRs system, the occurrence of dark-soliton collision (modulation) in the multiplexer system and the filtering signals within add-drop ring (Rd) is as shown in Figure 4.1 The dark solitons are generated by multiple light sources at the center wavelength λ_1 = 1.5 μm; the filtering signals are as shown in Figure 4.2

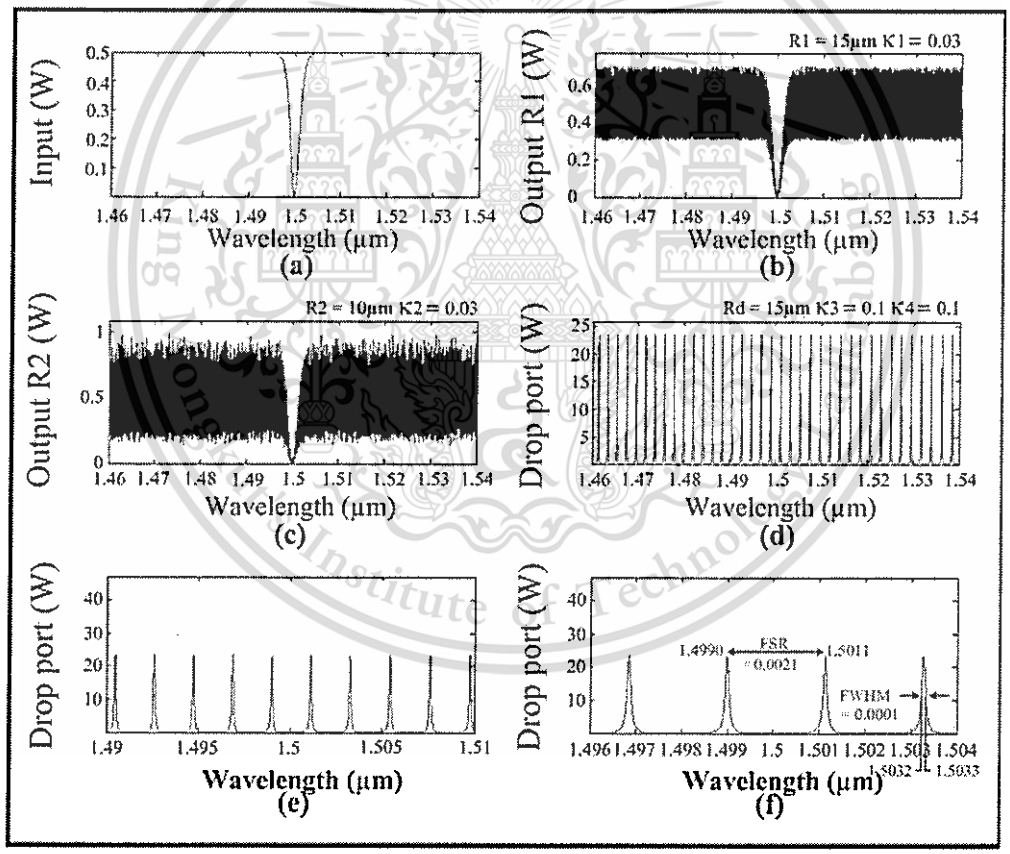

Figure 4.2 Simulation results for the dark solitons within the series microring resonators when the dark-soliton input wavelength is 1.5 μm: (a) dark-soliton input; (b), (c), dark solitons in rings R_1 and R_2; (d), (e), (f), are drop-port signals.

Simulation results have shown that a band of bright solitons is seen, whereas there is no signal at λ_1 = 1.5μm. A free spectrum range (FSR) of 2.1 nm and amplified power of and 20 W for the dark solitons are obtained, where in this case a spectral width (Full width at half maximum, FWHM) of 0.1 nm is achieved. In Figure 4.3, the dark-soliton array generated by multiple light sources at the center wavelength λ_1 = 1.5 μm, λ_2 = 1.52 μm, and λ_3 = 1.54 μm and the corresponding filtered signals are shown. Similarly, the dark-soliton array generated by multiple light sources at the center wavelength λ_1 = 1.56 μm, λ_2 = 1.58 μm , and λ_3 = 1.60 μm, and the corresponding filtered signals are shown in Figure 4.4, where the optical-ring radii used are 15, 10 μm and R_d = 50 μm.

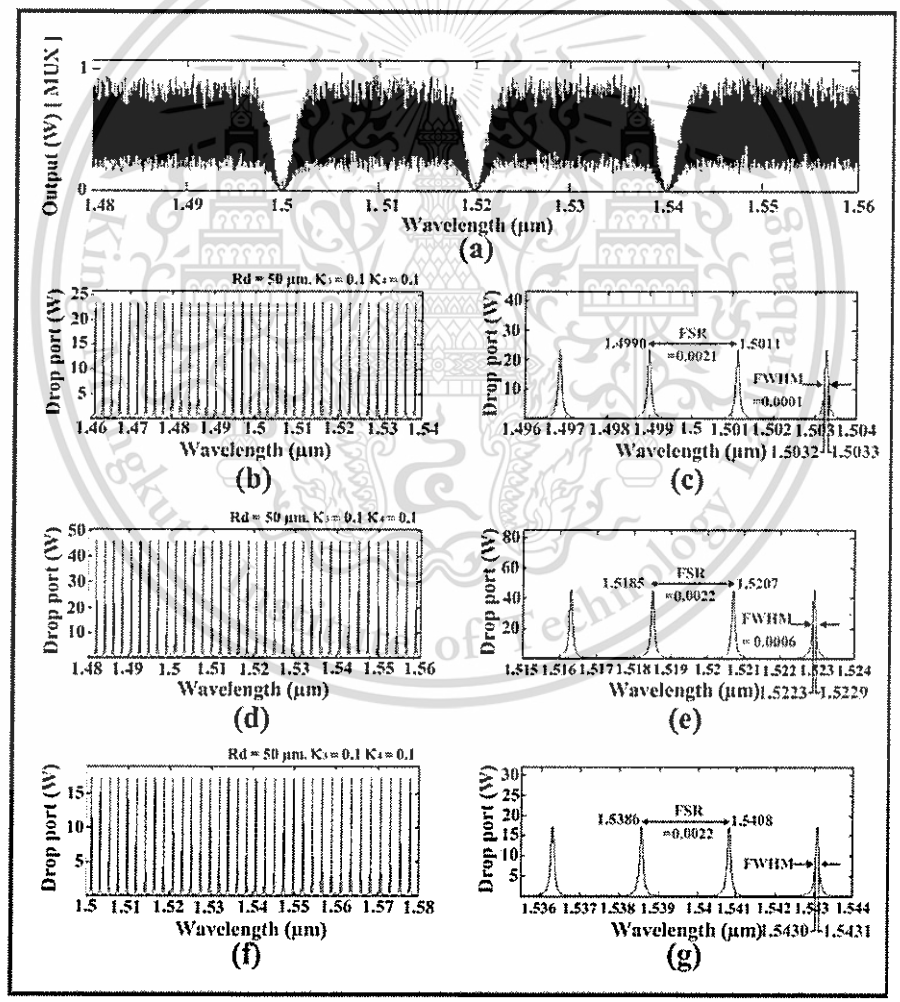

Figure 4.3 Simulation result on the dark-soliton array when the dark soliton input wavelengths are 1.5, 1.52, and 1.54 μm: (a) dark-soliton array; (b) through (g), drop-port signals.

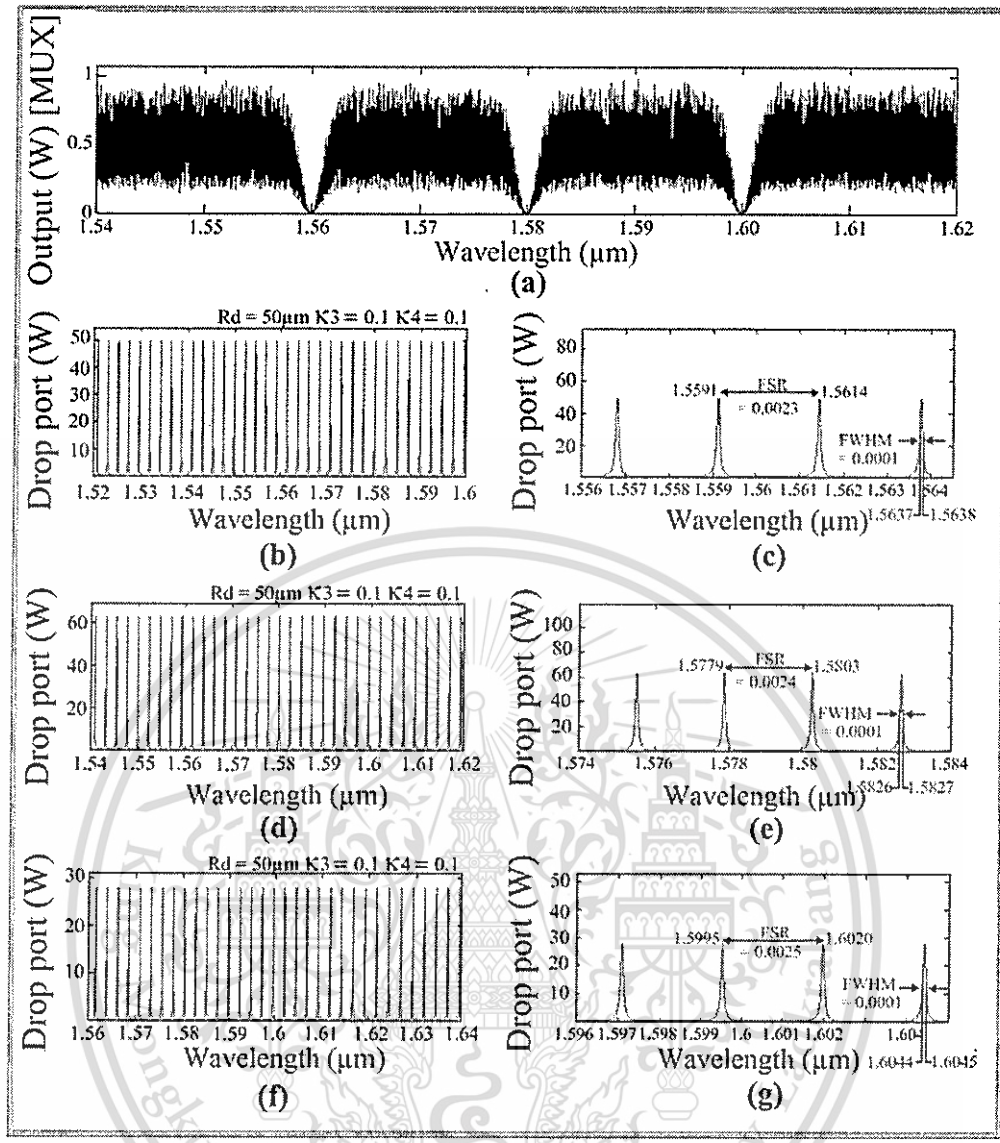

Figure 4.4 Simulation result of the dark-soliton array when the dark-soliton input wavelengths are 1.56, 1.58 and 1.60 μm: (a) dark-soliton array; (b) through (g), drop-port signals.

4.2 Proposed system on receiver (RX)

In the transceiver part, we showed a way to create multiplexed dark soliton using Gaussian pulse input. In the receiver part, we will show a way to convert dark soliton to bright soliton in order that the detector on the end of receiver can detect the carrier and the data.

Figure 4.5 Proposed system on receiver (RX)

4.3 Dark – Bright soliton conversion

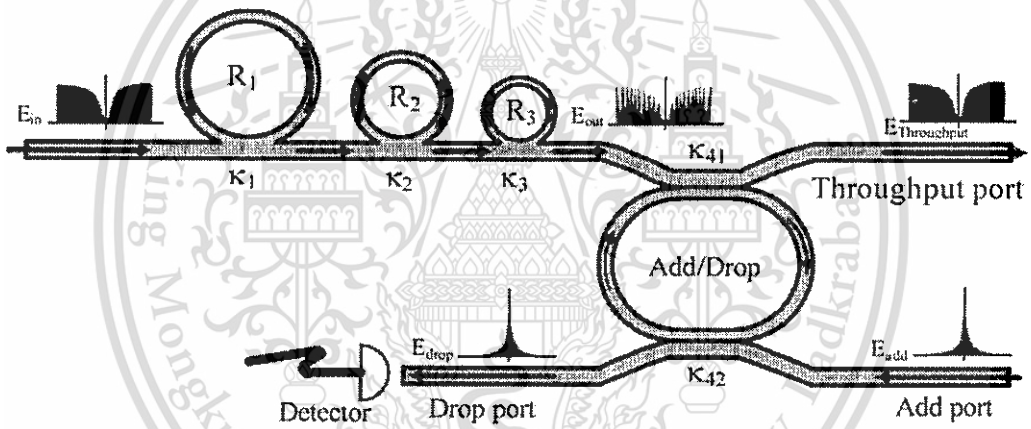

Figure 4.6 Schematic of a dark-bright soliton conversion system, where R_s is the ring radii, $\boldsymbol{K}_s$ is the coupling coefficient, and $\boldsymbol{K}_{41}$ and $\boldsymbol{K}_{42}$ are the add/drop coupling coefficients.

Dark-bright soliton control has been investigated clearly by the authors in reference [31], where one of the advantages is that the dark soliton peak signal is always low level, which can be useful for secured signal communication in the transmission link. The other is formed when the high optical field is configured as an optical tweezer or potential well, which is available for atom/molecule trapping. Optical tweezers technique has become a powerful tool for manipulation of

micrometer-sized particles in three spatial dimensions [32]. Initially, the useful static tweezer is recognized, and the dynamic tweezer is now realized in practical work. Typically, by using the continuous-wave (cw) lasers, the spatial control of atoms, beyond their trapping in stationary potentials, has been continuously gaining importance in investigations of ultra-cold gases and in the application of atomic ensembles and single atoms for cavity quantum electrodynamics (QED) and quantum information studies. Recent progress includes the trapping and control of single atoms in dynamic potentials [33, 34], the sub-micron positioning of individual atoms with standing-wave potentials [35, 36], micro-structured and dynamic traps for Bose-Einstein condensates [37, 38, 39] and, as another example, the realization of chaotic dynamics in atom-optics "billiards" [40, 41, 42] Schulz et al. [43] have shown that the transfer of trapped atoms between two optical potentials could be performed. In this chapter, we present a novel system of the optical tweezers storage using a dark-bright soliton pulse propagating within an add/drop optical filter. The multiplexing signals with different wavelengths of the dark solitons are controlled and amplified within the system. The dynamic behaviors of dark bright soliton interaction are analyzed and described. The storage signals are controlled and tuned to be an optical probe which is known as the optical tweezers. The optical tweezers storages are obtained by using the embedded nanoring resonators within the add/drop optical filter system. The controlled light pulses are added into the add port of the add/drop filter. By using the bright soliton input, the different in time of the first two dynamic wells of 1 ns is noted, while the potential well stability is seen when the Gaussian pulse is input into the add port. In application, the optical tweezers can be stored and trapped light/atom, which can be formed the dynamic tweezers and tweezers memory.

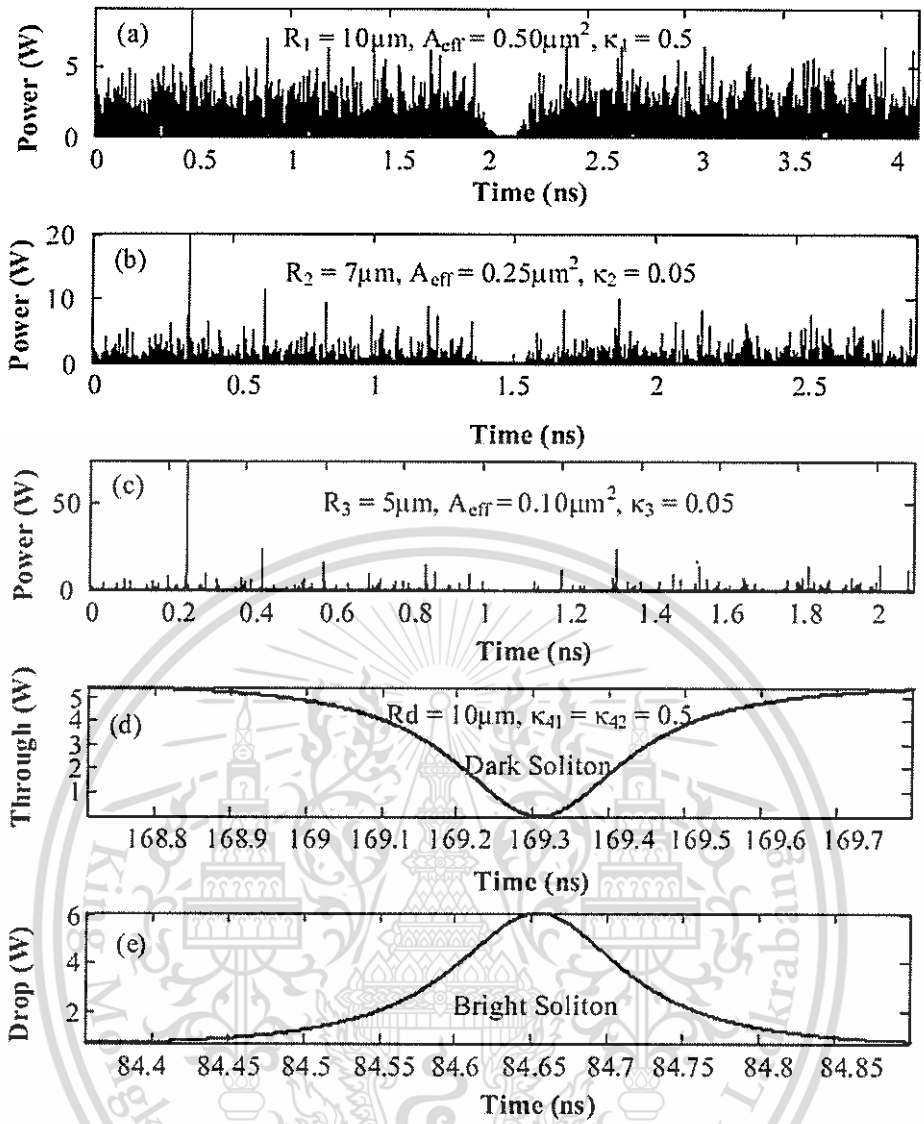

Figure 4.7 Results of the soliton signals within the ring resonator system, where (a) R_1, (b) R_2, (c) R_3, and (d) – (e) dark – bright solitons conversion at the add/drop filter. The input dark soliton power is 2W.

Experimentally, the generated dark soliton pulse, for instance, with 50ns pulse width, and a maximum power of *0.65W* is input into the dark-bright soliton conversion system, as shown in Figure 4.6 The suitable ring parameters are used, such as ring radii where R_1=*10.0*μ*m*, R_2=*7.0*μ*m*, and R_3=*5.0*μ*m*. In order to make the system associate with the practical device [19], whereas the selected parameters of the system are fixed to λ_0=*1.50*μ*m*, n_0=*3.34* (InGaAsP/InP). The effective core areas

are A_{eff}=*0.50, 0.25* and *0.10* μm^2 for a MRR and NRR, respectively. The waveguide and coupling loses are α =*0.5dBmm*$^{-1}$ and γ =*0.1*, respectively, and the coupling coefficients **K**s of the MRR are ranged from *0.05* to *0.90*. However, more parameters are used as shown in Figure 4.6 The nonlinear refractive index is n_2=*2.2*×*10*$^{-13}$ m^2/W. In this case, the waveguide loss used is *0.5 dBmm*$^{-1}$. The input dark soliton pulse is chopped (sliced) into the smaller signals, where the filtering signals within the rings R_2 and R_3 are seen. We find that the output signals from R_3 are smaller than from R_1, which is more difficult to detect when it is used in the link. In fact, the multistage ring system is proposed due to the different core effective areas of the rings in the system, where the effective areas can be transferred from *0.50* to *0.10*μm^2 with some losses. The soliton signals in R_3 is entered in the add/drop filter, where the dark-bright soliton conversion can be performed. Results obtained when a dark soliton pulse is input into a MRR and NRR system as shown in Figure 4.6 The add/drop filter is formed by using two couplers and a ring with radius (R_d) of *10*μm, the coupling constants (K_{41} and K_{42}) are the same values (*0.50*). When the add/drop filter is connected to the third ring (R_3), the dark-bright soliton conversion can be seen. The bright and dark solitons are detected by the through (throughput) and drop ports as shown in Figure 4.7 (a)-(e), respectively.

4.4 Dark-Bright Soliton Conversion in Add/Drop Filter

In operation, dark-bright soliton conversion using a ring resonator optical channel dropping filter (OCDF) is composed of two sets of coupled waveguides, as shown in Figure 4.8 The relative phase of the two output light signals after coupling into the optical coupler is $\pi/2$ before coupling into the ring and the input bus, respectively. This means that the signals coupled into the drop and through ports are acquired a phase of π with respect to the input port signal. In application, if we engineer the coupling coefficients appropriately, the field coupled into the through port on resonance would completely extinguish the resonant wavelength, and all power would be coupled into the drop port. We will show that this is possible later in this section.

$$E_{ra} = -j\kappa_1 E_i + \tau_1 E_{rd}, \tag{4.6}$$

$$E_{rb} = \exp(j\omega T/2)\exp(-\alpha L/4)E_{ra}, \tag{4.7}$$

$$E_{rc} = \tau_2 E_{rb} - j\kappa_2 E_a, \tag{4.8}$$

$$E_{rd} = \exp(j\omega T/2)\exp(-\alpha L/4)E_{rc}, \tag{4.9}$$

$$E_t = \tau_1 E_i - j\kappa_1 E_{rd}, \tag{4.10}$$

$$E_d = \tau_2 E_a - j\kappa_2 E_{rb}, \tag{4.11}$$

where E_i is the input field, E_a is the add(control) field, E_t is the through field, E_d is the drop field, $E_{ra}...E_{rd}$ are the fields in the ring at points $a...d$, κ_1 is the field coupling coefficient between the input bus and ring, κ_2 is the field coupling coefficient between the ring and output bus, L is the circumference of the ring, T is the time taken for one round trip(roundtrip time), and α is the power loss in the ring per unit length. We assume that this is the lossless coupling, i.e., $\tau_{1,2} = \sqrt{1-\kappa_{1,2}^2}$. $T = L n_{eff}/c$.

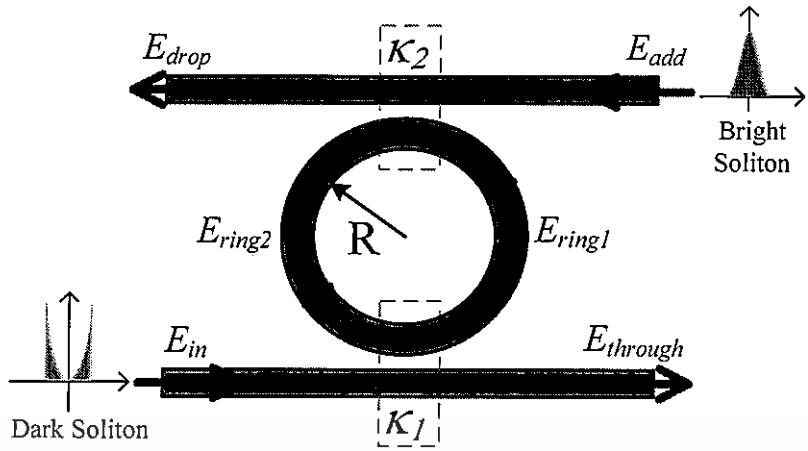

Figure 4.8 A schematic of dark-bright soliton conversion using a ring resonator optical channel dropping filter (OCDF).

The output power/intensities at the drop and through ports are given by

$$\left|E_d\right|^2 = \left|\frac{-\kappa_1\kappa_2 A_{1/2}\Phi_{1/2}}{1-\tau_1\tau_2 A\Phi}E_i + \frac{\tau_2-\tau_1 A\Phi}{1-\tau_1\tau_2 A\Phi}E_a\right|^2. \tag{4.12}$$

$$\left|E_t\right|^2 = \left|\frac{\tau_2-\tau_1 A\Phi}{1-\tau_1\tau_2 A\Phi}E_i + \frac{-\kappa_1\kappa_2 A_{1/2}\Phi_{1/2}}{1-\tau_1\tau_2 A\Phi}E_a\right|^2. \tag{4.13}$$

where $A_{1/2} = \exp(-\alpha L/4)$ (the half-round-trip amplitude), $A = A_{1/2}^2$, $\Phi_{1/2} = \exp(j\omega T/2)$ (the half-round-trip phase contribution), and $\Phi = \Phi_{1/2}^2$.

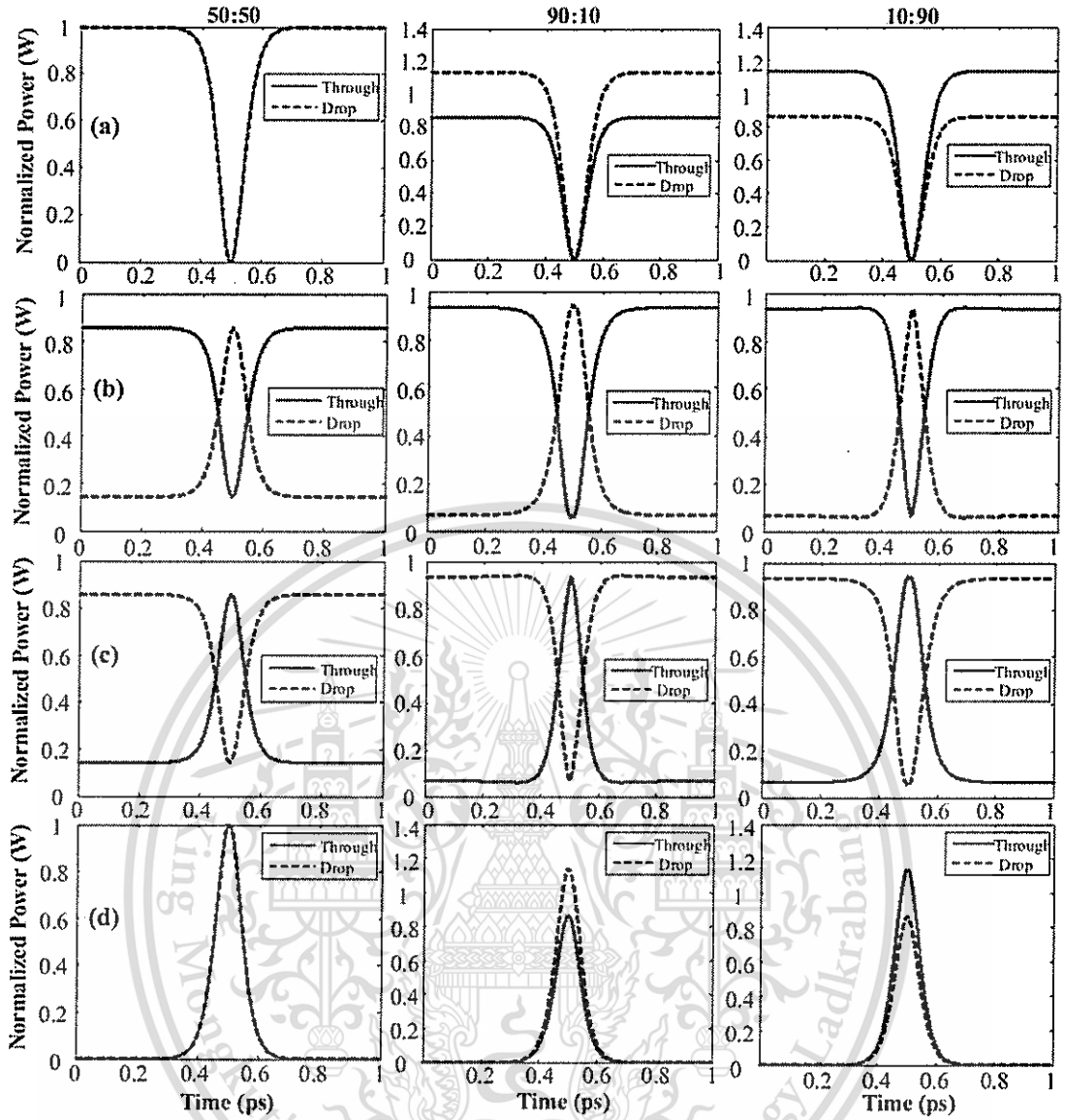

Figure 4.9 Dark-bright soliton conversion results using a ring resonator optical channel dropping filter (OCDF)

The input and control fields at the input and add ports are formed by the dark-bright optical soliton as shown in eqs (4.14) and (4.15),

$$E_{in}(t) = E_0 \tanh\left[\frac{T}{T_0}\right] \exp\left[\left(\frac{z}{2L_D}\right) - i\omega_0 t\right] \tag{4.14}$$

$$E_{in}(t) = E_0 \sec h\left[\frac{T}{T_0}\right] \exp\left[\left(\frac{z}{2L_D}\right) - i\omega_0 t\right] \quad (4.15)$$

where E_0 and z are the optical field amplitude and propagation distance, respectively. $T=t-\beta_1 z$, where β_1 and β_2 are the coefficients of the linear and second-order terms of Taylor expansion of the propagation constant. $L_D=\tau_0^2/|\beta_2|$ is the dispersion length of the soliton pulse. T_0 in equation is a soliton pulse propagation time at initial input (or soliton pulse width), where t is the soliton phase shift time, and the frequency shift of the soliton is ω_0. When the optical field is entered into the nanoring resonator as shown in Figure Figure 4.9, where the coupling coefficient ratio κ_1: κ_2 are *50:50, 90:10, 10: 90*. By using (a) dark soliton is input into input and control ports, (b) dark and bright soliton are used for input and control signals, (c) bright and dark soliton are used for input and control signals, and (d) bright soliton is used for input and control signals. The ring radii R_{ad} = *5μm*, A_{eff} = *0.25μm*^{2}, n_{eff} = *3.14*(for InGaAsP/InP), α = *5dB/mm*, γ= *0.1*, λ_0 = *1.51 μm*.

In application, the dynamic optical tweezers occurs, when we added bright soliton input at the add port with shown in Figure 4.8, the parameters of system are set the same as the previous section. The bright soliton was generated at the central wavelength λ_0 = *1.5μm*, when the bright soliton propagating into the add/drop system, the occurrence of dark-bright soliton collision in add/drop system is shown in Figure 4.10 (a)-(d) and Figure 4.11 (a) – (d).

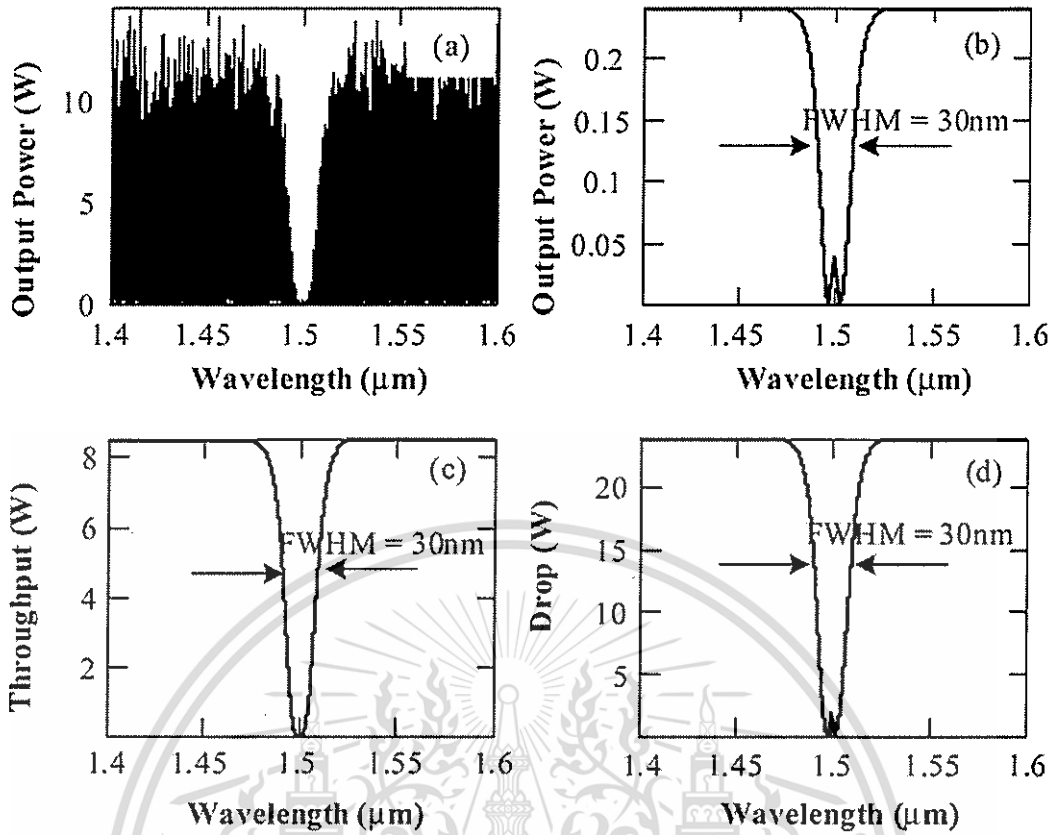

Figure 4.10 The dynamic optical tweezers output within the add/drop filter, when the bright soliton input with the central wavelength $\lambda_0 = 1.5\mu m$, where (a) add/drop signal, (b) dark – bright soliton collision, (c) optical tweezers at throughput port, and (d) optical tweezers at drop port.

The optical tweezers probe can be trapped/confined atom/light by using the appropriate probe, which can be tuned to meet the specific requirement. The stability of the dual Brillouin is shown in Figure 4.7 The dark soliton valley dept, i.e. potential well, is changed when it was modulated by the trapping energy (dark-bright solitons interaction) as shown in Figure 4.11 (a) - (d). The trapping of photon within the dark well occurs and is seen, the recovery photon can be obtained by using the dark-bright soliton conversion, which is well analyzed by Sarapat et al. [31], where the trapped photon or molecule can be released an seen separately from the dark soliton pulse, in practice, in this case the bright soliton is become alive and seen.

The more results of the dynamic dark-bright solitons conversion are shown in Figure 4.12 and Figure 4.13

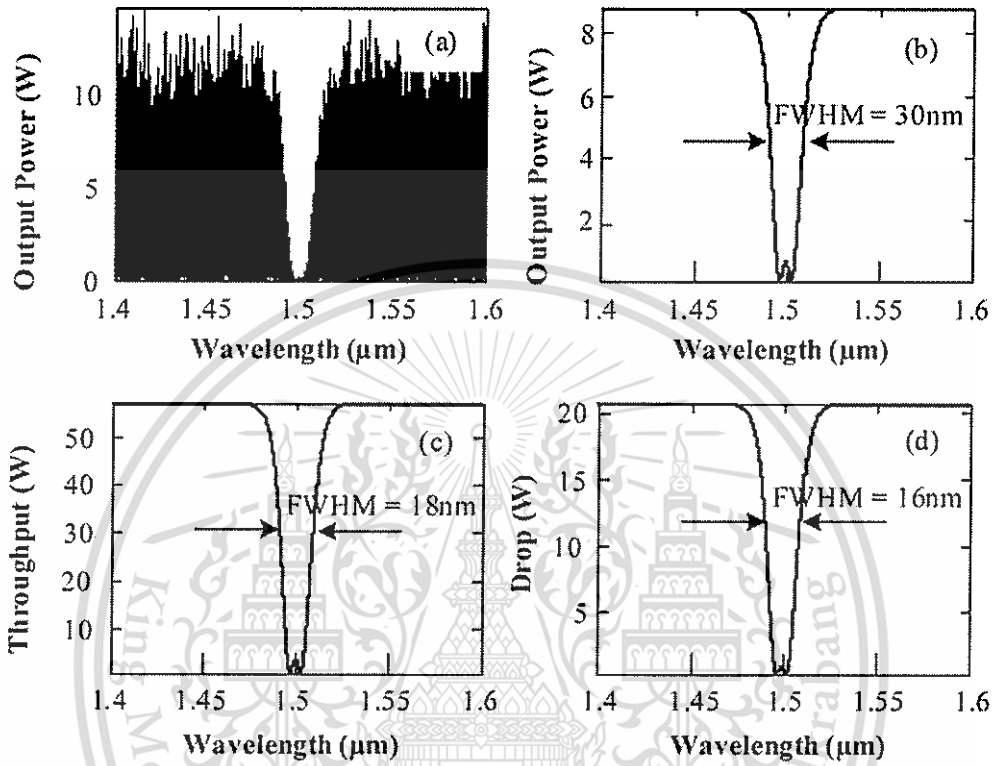

Figure 4.11 The tuned dynamic optical tweezers output within the add/drop filter, when the bright soliton input with the central wavelength λ_0 = 1.5μm, where (a) the add/drop signal, (b) dark – bright soliton collision, (c) optical tweezers at throughput port, and (d) optical tweezers at drop port.

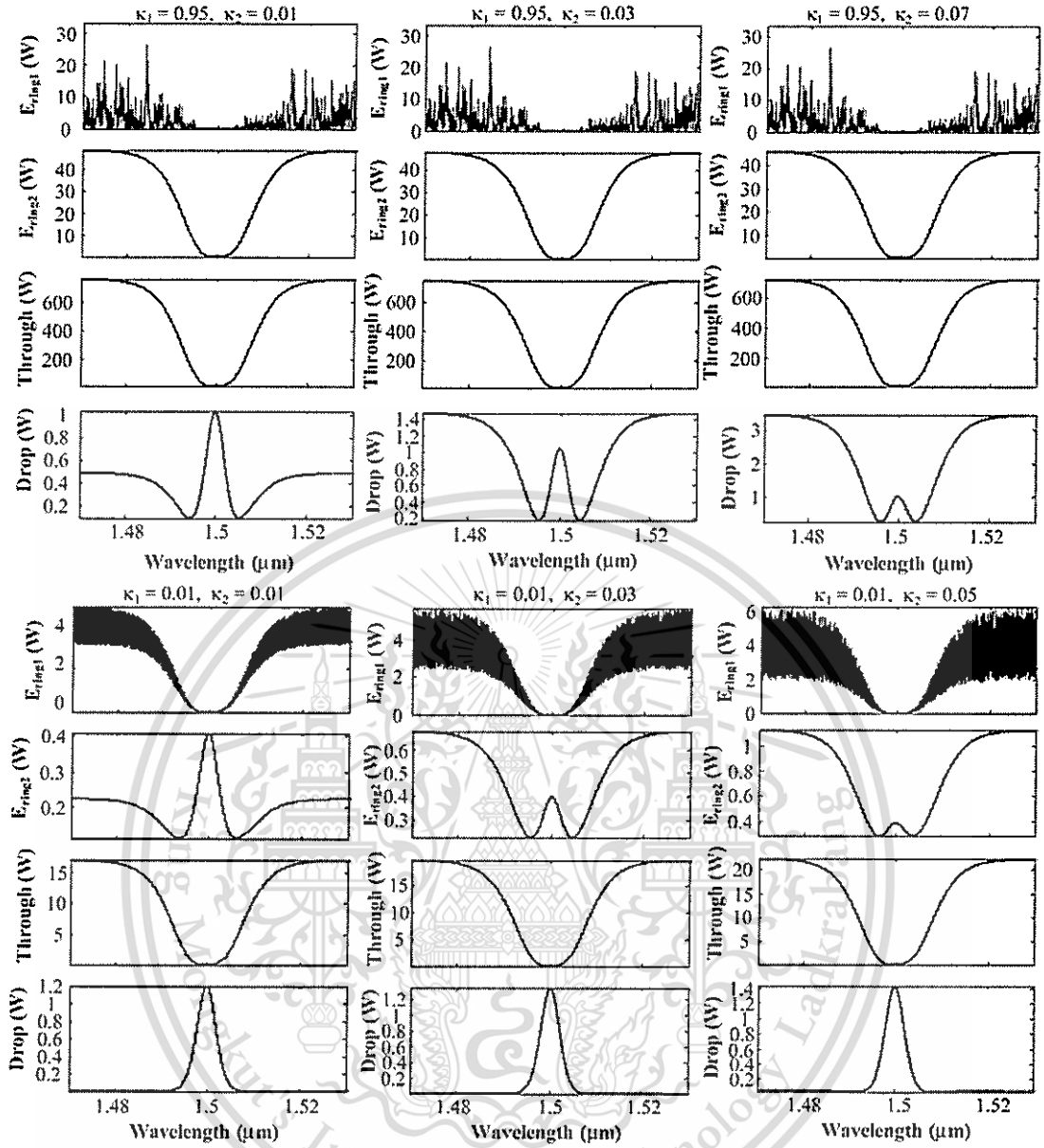

Figure 4.12 Results of the dark-bright soliton conversion, where the coupling coefficient are varied within Figure 4.8

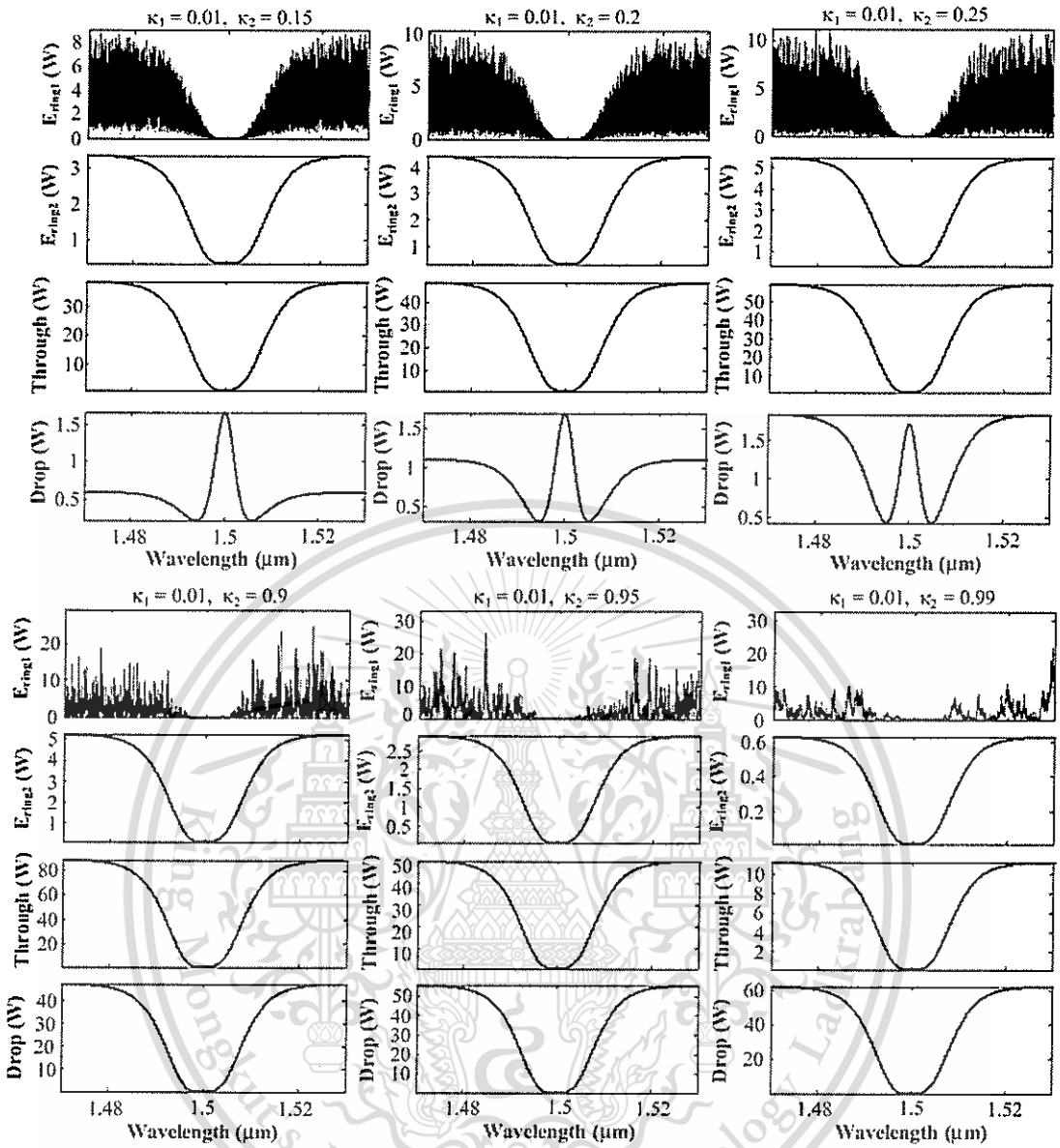

Figure 4.13 Results of the dark-bright soliton conversion, where coupling coefficients are varied within Figure 4.8

4.5 Proposed system TX & RX

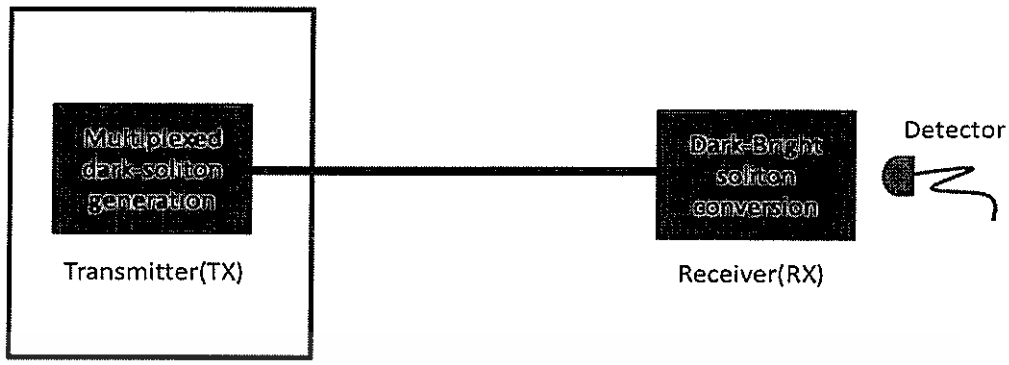

Figure 4.14 Proposed system both TX and RX

In this thesis we proposed a way to use the dark soliton instead of bright in fiber optic communication. The dark soliton has an advantage over bright that the specific center wavelength has been vanished. So, The detector of attacker that has tapped the transmission line cannot detect the carrier.

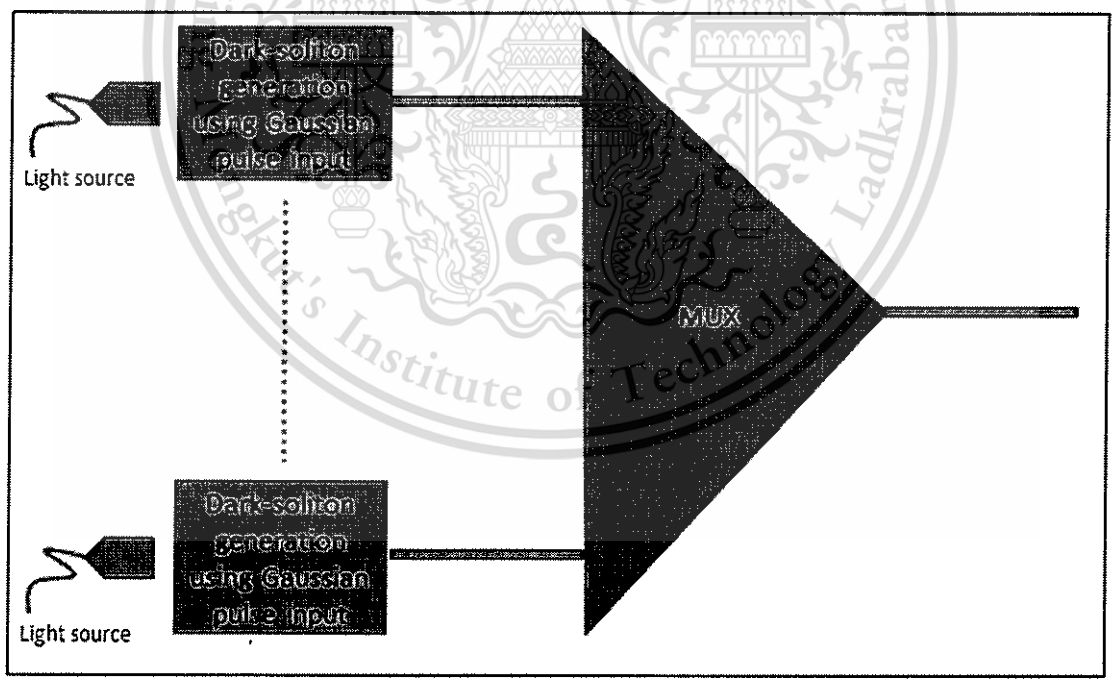

Figure 4.15 The multiplex dark soliton generation system

In order to generate multiplex dark soliton, we propose a better system which cost is reduced and the input laser diode is not needed. By using multi-ring resonator, the low cost and light weight multiplex dark soliton has been proposed.

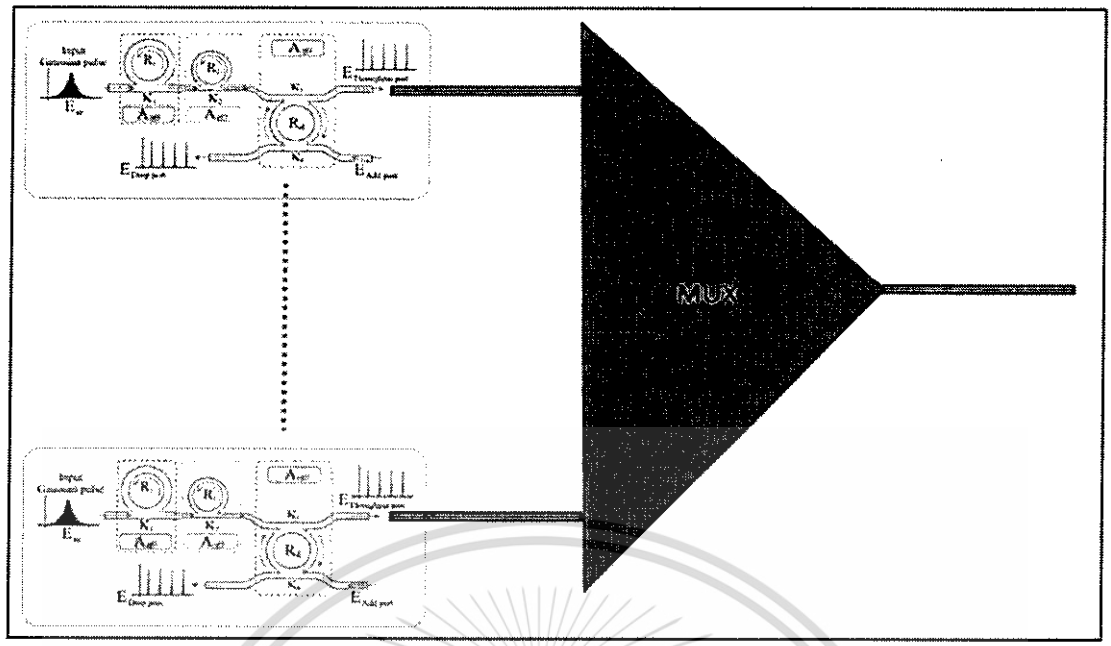

Figure 4.16 Multiplex dark-soliton generation system using multi-ring resonator

When we combined all the parts of the propose system, we will have a system look liked this.

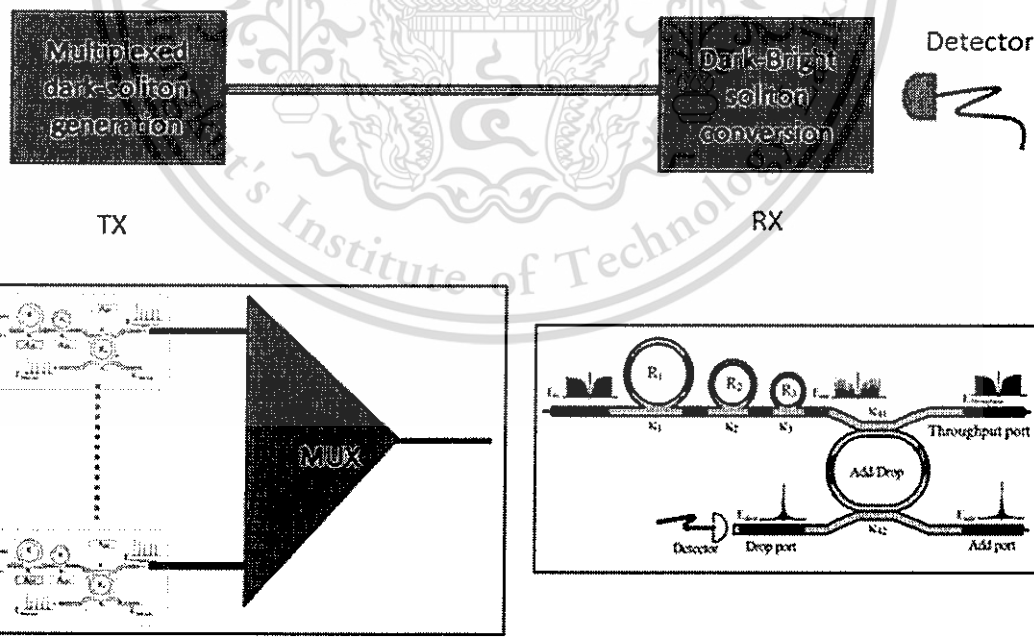

Figure 4.17 Overall of the proposed system

4.6 Insertion loss & Cross talk

In operation, because this router is made up of add-drop filters its performance depends on that of add-drop filters. At the time of writing, the micro- and Nano waveguides are gaining prominence. Filters offer good stability and isolation between channels at moderate cost.

The add-drop filters' capability will limit the size of network. The maximum of nodes of a network depend on the maximum number of add-drop filter channels. The popular dense wavelength division multiplexing (DWDM) component with many channels has been achieved in both theoretical and laboratory works [44, 45]. Thus in future is should be possible to build multivariable routers with many ports. At present, absolutely secure communication is not as popular as the internet, but this proposed system may be able to cover a big city.

Secondly, the insertion loss will reduce the efficient transmission distance, since signals will pass through an add-drop filter when they pass the router. The insertion loss of popular device is 5 dB. According to the performance of present point-to- point transmission system, we can build a network over 50 km at least. That will still meet the requirement of a big city. With the progress of DWDM technology, the insertion loss will be less than 1 dB in future [46], and then the multivariable network will cover more than 100 km with high capacity.

The third problem is crosstalk, which will be considered here in terms of channel separability. For a network, crosstalk will produce bit errors, so it must be made as low as possible. We think it can be estimated as follows: The insertion loss (IL) and crosstalk (FC) are

$$IL = 10 \times \log (P_{in}/P_{out}), \tag{4.16}$$

$$FC_j(\lambda_i) = 10 \times \log[P_j (\lambda_i)/P_i(\lambda_i)]. \tag{4.17}$$

Here P_{in} and P_{out} are input and output of solitons, $P_j(\lambda_i)$ is the output of solitons with wavelength λ_i exported from port j. and $P_i(\lambda_i)$ is the output of solitons with wavelength λ_i exported from port i. Since $P_i(\lambda_i)$ in Eq. (7) equal to P_{out} in Eq. (4.16), we have

$$P_{out}/P_{in} = 10^{-IL/10}, \tag{4.18}$$

$$[P_j(\lambda_i)/P_{in}]=[P_j(\lambda_i)/P_{out}]\times[P_{out}/P_{in}]= 10^{[FCj(\lambda i)-IL]/10}. \tag{4.19}$$

We first assume that the total input of photons from any user is the same when they enter the router. Since one soliton will pass through two add-drop filters when it passes a router, the radio of crosstalk to correct the signals is

$$P_j(\lambda_i)/P_{in}]^2/[P_{out}/P_{in}]^2 = 10^{2\times FCj(\lambda i)/10}. \tag{4.20}$$

Now we consider the situation that the inputs of photons are not the same. The worst case is that input photons that produce correct signals pass through a device that has X-dB insertion loss before passing through the router, but those solitons that produce crosstalk do not. The ratio in Eq. (4.20) then become $10^{[X+2\times FCj(\lambda i)]/10}$. If there are many inputs that produce crosstalk, the ratio must be $\sum_{j=1}^{N-1} 10^{\frac{[X+2\times FCj(\lambda_i)]}{10}}$ where $j \neq i$; here N is the amount of channels. For popular product we have N = 40; $FC_j(\lambda_i) < -25$dB (when $j = i \pm 1$), $FC_j(\lambda_i) < -30$dB (when $j \neq i \pm 1$), and $X < 10$. The ratio is less than 0.056%. So the errors brought about by crosstalk are less than other affects and can be ignored. With further development of DWDM technology, crosstalk will be still smaller and the performance of the router will improve. In that case, we should easily be able to build a multivariable network operating over 50 km with 40 users.

We proposed system for dark-soliton array generation using multiplexed dark-soliton pulses. The dark-solitons are input into the series microring resonators, where they are multiplexed, and signals filtered within an add-drop ring system can be generated and can be used to obtain large channel capacity in a secure communication link.

In principle, a dark soliton is one whose amplitude vanishes during propagation in a transmission line, which gives it an advantage over a bright soliton. The main difference between bright solitons and dark solitons is that detection of dark solitons is extremely difficult, which makes them suitable for communication security applications. Moreover, stable dark solitons can be generated; they have been reported by Hanim et al. and confirmed by Sama.

Finally, the use of dark solitons to provide large channel capacity within a wavelength router has been analyzed. A FSR of 2.5 nm and an amplified power of 30 W can be achieved for a dark soliton with wavelength 1.60 μm, respectively. Thus, the channel spacing of the communication signals within a wavelength router can be provided by using a suitable FSR, which can be determined by using crosstalk effect analysis. One example has shown that a multivariable network over 50 km with 40 users can be achieved.

CHAPTER 5

CONCLUSION

In this chapter, we showed the conclusion of the main idea of this thesis in the way to increase the security of the optical communication. Then, we showed the future work of the next step of this thesis, in order to get more easily control the dark-bright soliton conversion and increase the bandwidth of the communication link.

5.1 Conclusion

We have shown that the dark soliton can be used in optical communication in order to increase the security of the link. The sender sent the signal in the form of dark soliton, lack of center frequency carrier. The only designator receiver with the circuit of dark-bright soliton conversion can convert the dark soliton back into the bright one, then the detector can detector the signal and get the information. Furthermore, to increase the bandwidth of communication, the multiplexed dark soliton has been use. More center frequency means more channel of communication.

In conclusion, we summarized the mainly idea of this thesis were.

1. To ensure the security of the signal in optical fiber and prevent the middle man attack to trap the fiber, dark soliton technique has been proposed.
2. To maximize the using and bandwidth of communication link, multiplexed (dark) soliton has been proposed.

5.2 Future work

In the previous part of this thesis, we demonstrate the security improvement in optical communication with dark soliton's technique using add/drop filters. In this

section we propose a better way to use PANDA ring resonator to convert bright-dark soliton.

5.2.1 PANDA Ring resonator

In this part, we have derived and presented the dynamic behavior of dark-bright soliton collision within the modified add/drop filter, which it is known as PANDA ring resonator. By using the dark-bright soliton conversion control, the obtained outputs of the dynamic states can be used to form the random binary codes, which can be available for communication security application. Results obtained have shown that the random binary codes can be formed by using the polarized light components. The retrieved (decoded) codes can be obtained by using the dark-bright soliton conversion signals.

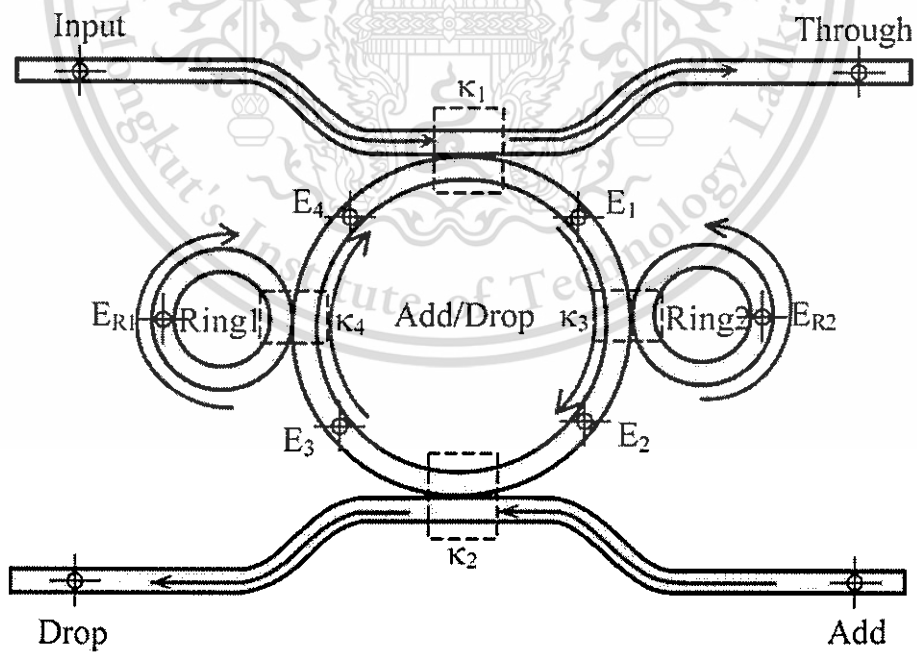

Figure 5.1 A schematic of single-PANDA ring resonator

5.2.1.1 Theory and Modeling

The proposed system consists of an add/drop filter and double nanoring resonators known as a **PANDA** ring resonator as shown in Figure 5.1 and Figure 5.2 To perform the dark-bright soliton conversion, dark and bright solitons are input into the add/drop optical filter system. the input optical field (E_{i1}) and the control port optical field (E_{con}) of the dark-bright solitons pulses are given by [29]

$$E_{i1}(t) = A\tanh\left[\frac{T}{T_0}\right]\exp\left[\left(\frac{x}{2L_D}\right) - i\phi(t)\right], \tag{5.1}$$

$$E_{con}(t) = A\,\mathrm{sech}\left[\frac{T}{T_0}\right]\exp\left[\left(\frac{x}{2L_D}\right) - i\phi(t)\right], \tag{5.2}$$

in which A and z are the optical field amplitude and propagation distance, respectively. $\phi(t) = \phi_0 + \phi_{NL} = \phi_0 + \frac{2\pi n_2 L}{A_{eff}\lambda}|E_0(t)|^2$ is the random phase term related to the temporal coherence function of the input light, ϕ_0 is the linear phase shift, ϕ_{NL} is the nonlinear phase shift, n_2 is the nonlinear refractive index of InGaAsP/InP waveguide. The effective mode core area of the device is given by A_{eff}, $L = 2\pi R_{ad}$, R_{ad} is the radius of device, λ is the input wavelength light field and $E_0(t)$ is the circulated field within nanoring coupled to the right and left add/drop optical filter system as shown in Figure 5.1 T is a soliton pulse propagation time in a frame moving at the group velocity, $T=t-\beta_1 z$, where β_1 and β_2 are the coefficients of the linear and second-order terms of Taylor expansion of the propagation constant. $L_D = T_0^2/|\beta_2|$ is the dispersion length of the soliton pulse. T_0 in equation is a soliton pulse propagation time at initial input (or soliton pulse width), where t is the soliton phase shift time, and the frequency shift of the soliton is ω_0. This solution describes a pulse that

keeps its temporal width invariance as it propagates, and is thus called a temporal soliton. When a soliton peak intensity $\left(\left|\beta_2/\Gamma T_0^2\right|\right)$ is given, T_0 is known. For the soliton pulse in the microring device, a balance should be achieved between the dispersion length (L_D) and the nonlinear length ($L_{NL}=1/\Gamma\phi_{NL}$). $\Gamma=n_2k_n$, is the length scale over which dispersive or nonlinear effects makes the beam become wider or narrower. For a soliton pulse, there is a balance between dispersion and nonlinear lengths, hence $L_D = L_{NL}$.

When light propagates within the nonlinear medium, the refractive index (n) of light within the medium is given by

$$n = n_0 + n_2 I = n_0 + \frac{n_2}{A_{eff}} P, \tag{5.3}$$

with n_0 and n_2 as the linear and nonlinear refractive indexes, respectively. I and P are the optical intensity and the power, respectively. The effective mode core area of the device is given by A_{eff}. For the add/drop optical filter design, the effective mode core areas range from 0.50 to 0.10 μm^2. Parameters were obtained by using the related practical material parameters (InGaAsP/InP) [47, 48, 30]. When a dark soliton pulse is input and propagated within a add/drop optical filter as shown in Figure 5.1, the resonant output is formed

Figure 5.1, consists of add/drop optical multiplexing used for generated random binary coded light pulse and add/drop optical filter device for decoded binary code signal. The resonator output field, E_{t1} and E_1 consists of the transmitted and circulated components within the add/drop optical multiplexing system, which can perform the driven force to photon/molecule/atom.

When the input light pulse passes through the first coupling device of the add/drop optical multiplexing system, the transmitted and circulated components can be written as

$$E_{t1} = \sqrt{1-\gamma_1}\left[\sqrt{1-\kappa_1}E_{i1} + j\sqrt{\kappa_1}E_4\right] \tag{5.4}$$

$$E_1 = \sqrt{1-\gamma_1}\left[\sqrt{1-\kappa_1}E_4 + j\sqrt{\kappa_1}E_{i1}\right] \tag{5.5}$$

$$E_2 = E_{R2}e^{-\frac{\alpha}{2}\frac{L}{2}-jk_n\frac{L}{2}} \tag{5.6}$$

where κ_1 and γ_1 are the intensity coupling coefficient and the fractional coupler intensity loss of the add/drop optical filter, respectively. α is the attenuation coefficient, $k_n = 2\pi/\lambda$ is the wave propagation number, λ is the input wavelength light field and $L = 2\pi R_{ad}$, R_{ad} is the radius of add/drop device.

For the second coupler of the add/drop optical multiplexing system,

$$E_{t2} = \sqrt{1-\gamma_2}\left[\sqrt{1-\kappa_2}E_{i2} + j\sqrt{\kappa_2}E_2\right] \tag{5.7}$$

$$E_3 = \sqrt{1-\gamma_2}\left[\sqrt{1-\kappa_2}E_2 + j\sqrt{\kappa_2}E_{i2}\right] \tag{5.8}$$

$$E_4 = E_{R1}e^{-\frac{\alpha}{2}\frac{L}{2}-jk_n\frac{L}{2}} \tag{5.9}$$

where κ_2 is the intensity coupling coefficient, γ_2 is the fractional coupler intensity loss. The circulated light fields, E_{R1} and E_{R2} are the light field circulated components of the nanoring radii, R_1 and R_2 which coupled into the left and right sides of the add/drop optical multiplexing system, respectively. The light field transmitted and circulated components in the right nanoring, R_2, are given by

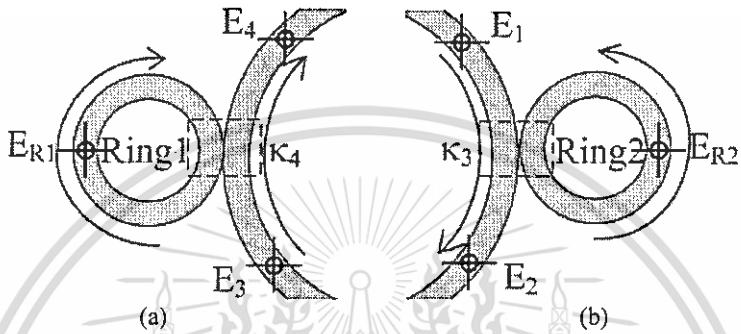

Figure 5.2 A schematic of PANDA ring, where (a) the left nanoring and (b) the right nanoring.

$$E_{R2} = \sqrt{1-\gamma_3}\left[\sqrt{1-\kappa_3}E_1 + j\sqrt{\kappa_3}E_{r2}\right] \tag{5.10}$$

$$E_{r1} = \sqrt{1-\gamma_3}\left[\sqrt{1-\kappa_3}E_{r2} + j\sqrt{\kappa_3}E_1\right] \tag{5.11}$$

$$E_{r2} = E_{r1}e^{-\frac{\alpha}{2}L_2 - jk_nL_2} \tag{5.12}$$

where κ_3 and γ_3 are the intensity coupling coefficient and the fractional coupler intensity loss of the right nanoring, respectively. α is the attenuation coefficient, $k_n = 2\pi/\lambda$ is the wave propagation number, λ is the input wavelength light field and $L_2 = 2\pi R_2$, R_2 is the radius of right nanoring.

From Eq. (5.10) - (5.12), the circulated roundtrip light fields of the right nanoring radii, R_2, are given in Eq. (5.13) and (5.15), respectively.

$$E_{r1} = \frac{j\sqrt{1-\gamma_3}\sqrt{\kappa_3}E_1}{1-\sqrt{1-\gamma_3}\sqrt{1-\kappa_3}e^{-\frac{\alpha}{2}L_2 - jk_nL_2}} \tag{5.13}$$

$$E_{r2} = \frac{j\sqrt{1-\gamma_3}\sqrt{\kappa_3}E_1 e^{-\frac{\alpha}{2}L_2 - jk_nL_2}}{1-\sqrt{1-\gamma_3}\sqrt{1-\kappa_3}e^{-\frac{\alpha}{2}L_2 - jk_nL_2}} \tag{5.14}$$

Thus, the output circulated light field, E_{R2}, for the right nanoring is given by

$$E_{R2} = E_1\left\{\frac{\sqrt{(1-\gamma_3)(1-\kappa_3)} - (1-\gamma_3)e^{-\frac{\alpha}{2}L_2 - jk_nL_2}}{1-\sqrt{(1-\gamma_3)(1-\kappa_3)}e^{-\frac{\alpha}{2}L_2 - jk_nL_2}}\right\}. \tag{5.15}$$

Similarly, the output circulated light field, E_{R1}, for the left nanoring at the left side of the add/drop optical multiplexing system is given by

$$E_{R2} = E_1 \left\{ \frac{\sqrt{(1-\gamma_3)(1-\kappa_3)} - (1-\gamma_3)e^{-\frac{\alpha}{2}L_2 - jk_n L_2}}{1-\sqrt{(1-\gamma_3)(1-\kappa_3)}e^{-\frac{\alpha}{2}L_2 - jk_n L_2}} \right\}. \quad (5.16)$$

where κ_4 is the intensity coupling coefficient, γ_4 is the fractional coupler intensity loss, α is the attenuation coefficient, $k_n = 2\pi/\lambda$ is the wave propagation number, λ is the input wavelength light field and $L_1 = 2\pi R_1$, R_1 is the radius of left nanoring.

From Eq. (5.4) - (5.16), the circulated light fields, E_1, E_3 and E_4 are defined by given $x_1 = (1-\gamma_1)^{1/2}$, $x_2 = (1-\gamma_2)^{1/2}$, $y_1 = (1-\kappa_1)^{1/2}$, and $y_2 = (1-\kappa_2)^{1/2}$.

$$E_1 = \frac{jx_1\sqrt{\kappa_1}E_{i1} + jx_1x_2y_1\sqrt{\kappa_2}E_{R1}E_{i2}e^{-\frac{\alpha L}{4\,4} - jk_n\frac{L}{4}}}{1 - x_1x_2y_1y_2E_{R2}E_{R1}e^{-\frac{\alpha}{2}L - jk_nL}} \quad (5.17)$$

$$E_3 = x_2y_2E_{R2}E_1e^{-\frac{\alpha L}{4\,2} - jk_n\frac{L}{2}} + jx_2\sqrt{\kappa_2}E_{i2} \quad (5.18)$$

$$E_4 = x_2y_2E_{R2}E_{R1}E_1e^{-\frac{\alpha}{2}L - jk_nL} + jx_2\sqrt{\kappa_2}E_{R1}E_{i2}e^{-\frac{\alpha L}{4\,4} - jk_n\frac{L}{4}} \quad (5.19)$$

Thus, from Eq. (5.4), (5.6), (5.17) - (5.19), the output optical field of the through port (E_{t1}) is expressed by

$$E_{t1} = x_1 y_1 E_{i1} + \left(j x_1 x_2 y_2 \sqrt{\kappa_1} E_{R2} E_{R1} E_1 - x_1 x_2 \sqrt{\kappa_1 \kappa_2} E_{R1} E_{i2} \right) e^{-\frac{\alpha L}{4\,4} - j k_n \frac{L}{4}} \quad (5.20)$$

The power output of the through port (P_{t1}) is written by

$$P_{t1} = \left(E_{t1}\right) \cdot \left(E_{t1}\right)^* = \left| x_1 y_1 E_{i1} + \left(j x_1 x_2 y_2 \sqrt{\kappa_1} E_{R2} E_{R1} E_1 - x_1 x_2 \sqrt{\kappa_1 \kappa_2} E_{R1} E_{i2} \right) e^{-\frac{\alpha L}{4\,4} - j k_n \frac{L}{4}} \right| \quad (5.21)$$

Similarly, from Eq. (5.6), (5.7), (5.17) - (5.19), the output optical field of the drop port (E_{t2}) is given by

$$E_{t2} = x_2 y_2 E_{i2} + j x_2 \sqrt{\kappa_2} E_{R2} E_1 e^{-\frac{\alpha L}{4\,4} - j k_n \frac{L}{4}} \quad (5.22)$$

The power output of the drop port (P_{t2}) is expressed by

$$P_{t2} = \left(E_{t2}\right) \cdot \left(E_{t2}\right)^* = \left| x_2 y_2 E_{i2} + j x_2 \sqrt{\kappa_2} E_{R2} E_1 e^{-\frac{\alpha L}{4\,4} - j k_n \frac{L}{4}} \right|^2 . \quad (5.23)$$

In order to retrieve the required signals, we propose to use the add/drop optical multiplexing device with the appropriate parameters. This is given in the following details. The optical circuits of a PANDA ring resonator for the through port and drop port can be given by Eq. (5.21) and (5.23), respectively. The chaotic noise cancellation can be managed by using the specific parameters of the add/drop multiplexing device. The required signals can be retrieved by the specific users. κ_1 and κ_2 are the coupling coefficients of the add/drop filters, $k_n = 2\pi/\lambda$ is the wave propagation number for in a vacuum, and the waveguide (ring resonator) loss is α = 5×10^{-5} dBmm^{-1}. The fractional coupler intensity loss is γ = 0.01. In the case of the add/drop multiplexing device, the nonlinear refractive index is neglected. Figure 5.3

A schematic of single-PANDA ring with a 10 x 12μm2 size, which is drawn by using the OptiFDTD commercial software shows the schematic diagram of single-PANDA ring by using OptiFDTD commercial software. The dynamic pulse train is generated in z-direction of InGaAsP/InP waveguide with n_0 = 3.34 by using OptiFDTD. As shown in Figure 5.4 Dynamic pulse in z-direction of PANDA ring size 10 x 12 μm2 by using OptiFDTD, where (a) z = 0, (b) z = 0.88μm, (c) z = 1.62μm, (d) z = 2.74μm, (e) z = 3.30μm, (f) z = 3.44μm, (g) z = 5.72μm, (h) z = 8.10μm, and (i) z = 9.06μm, (j) z = 10.7 μm, (k) z = 10.0μm, and (l) z = 11.0μm., (a) z = 0, (b) z = 0.88μm, (c) z = 1.62μm, (d) z = 2.74μm, (e) z = 3.30μm, (f) z = 3.44μm, (g) z = 5.72μm, (h) z = 8.10μm, and (i) z = 9.06μm, (j) z = 10.7 μm, (k) z = 10.0μm, and (l) z = 11.0μm. The results are obtained by the through (Th) and drop (Dr) ports as shown in Figure 5.5 The simulation results obtained at through port (Th) and drop port (Dr). We we found that the output power at the drop port is higher than the through port, which means that the required and the transmitted signals are obtained, in which the delay signals within left and right nanoring are seen as shown in Figure 5.6 The simulation results generated at ring1 (MRR1) and ring2 (MRR2).

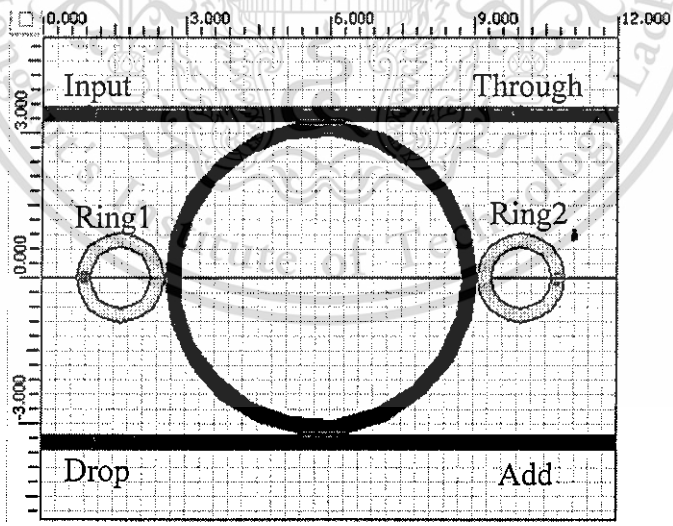

Figure 5.3 A schematic of single-PANDA ring with a 10 x 12μm2 size, which is drawn by using the OptiFDTD commercial software

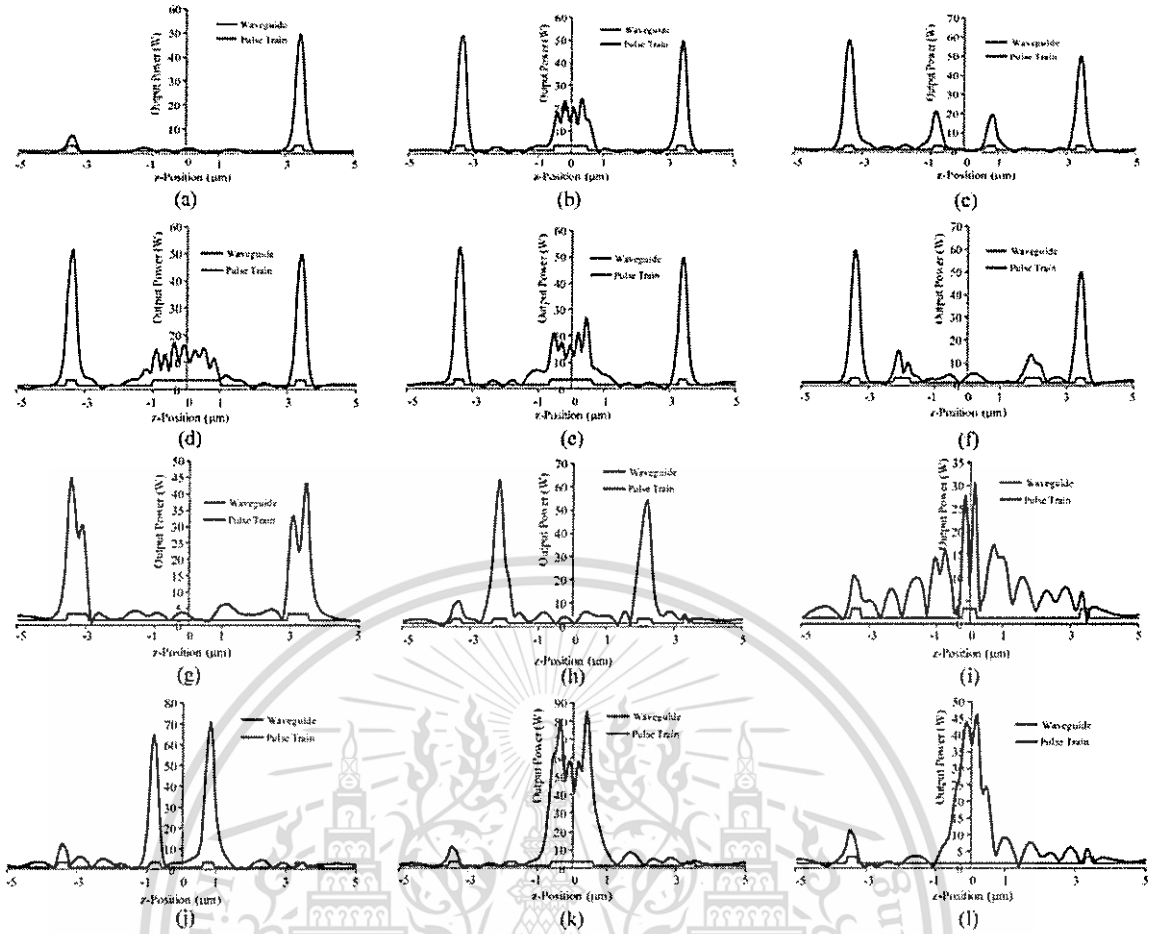

Figure 5.4 Dynamic pulse in z-direction of PANDA ring size 10 x 12 μm2 by using OptiFDTD, where (a) z = 0, (b) z = 0.88μm, (c) z = 1.62μm, (d) z = 2.74μm, (e) z = 3.30μm, (f) z = 3.44μm, (g) z = 5.72μm, (h) z = 8.10μm, and (i) z = 9.06μm, (j) z = 10.7 μm, (k) z = 10.0μm, and (l) z = 11.0μm.

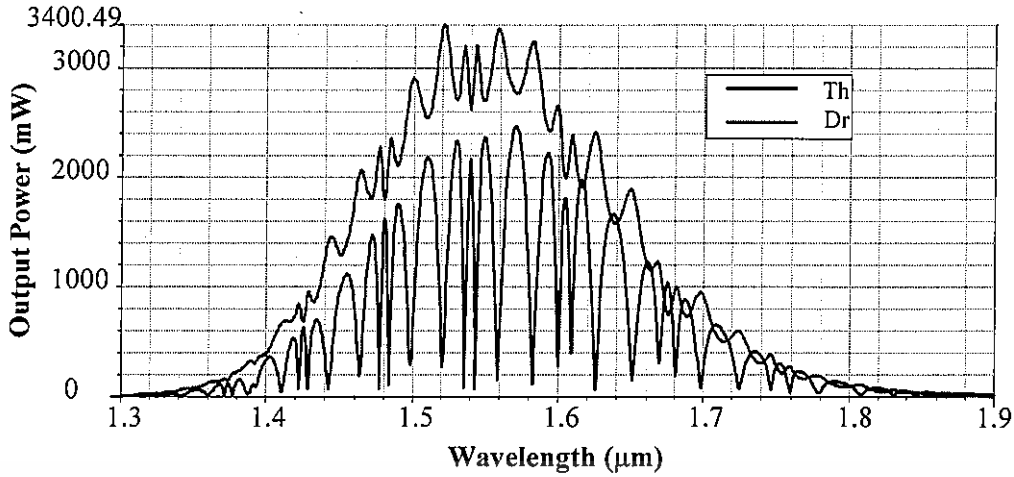

Figure 5.5 The simulation results obtained at through port (Th) and drop port (Dr).

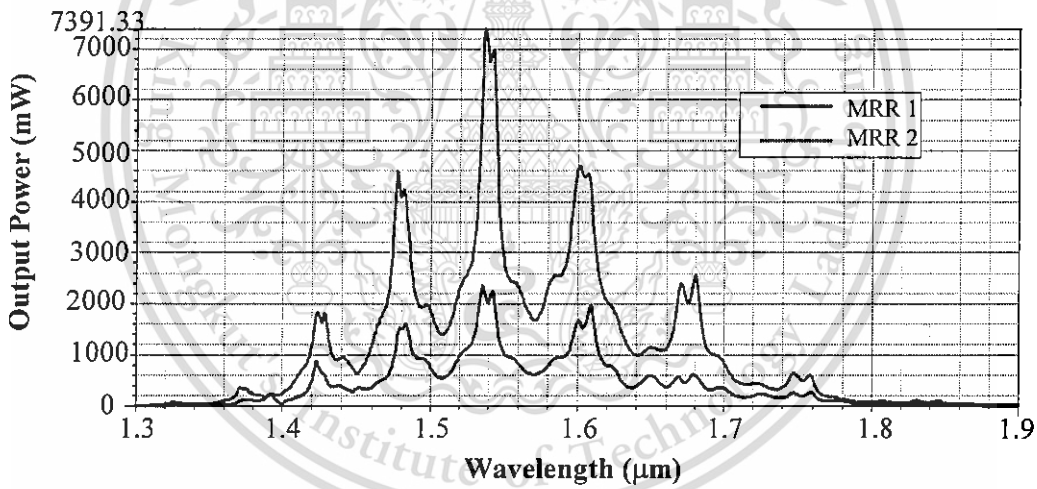

Figure 5.6 The simulation results generated at ring1 (MRR1) and ring2 (MRR2)

REFERENCES

[1] Hecht and J. Hecht, "Half a century of laser weapons," OPN, vol. 20, no. 2, pp. 14-21, 2009.

[2] G. P. Agarwal, Nonlinear Fiber optics, Newyork: Academic Press, 2007.

[3] Y. Kokubun, Y. Hatakeyama, M. Ogata, S. Suzuki and N. Zaizen, "Fabrication technologies for vertically coupled microring resonator with multilevel crossing busline and ultracompact-ring radius," IEEE J. Sel. Top Quantum Electron, vol. 11, pp. 4-10, 2005.

[4] P. Yupapin and W. Sunwancharoen, "Chaotic signal generation and cancellation using a micro ring resonator incorporating and optical add/drop multiplexer," Opt. Commun, vol. 280, no. 2, pp. 343-350, 2007.

[5] Yupapin, P. Yupapin, P. Saeung and C. Li, "Characteristics of complementary ring-resonator add/drop filters modeling by graphical approach," Opt. Commun., vol. 272, pp. 81-86, 2007.

[6] R. W. Eason and A. Miller, Nonlinear optics in signal processing, London: Champan & Hall, 1993.

[7] M. N. Islam, Fiber switching devices and systems, New york: Cambridge university press, 1992.

[8] P. Yupapin, P. Phiphithirankarn and S. Suchat, "A Quantum CODEC Design via an Optical Add/Drop Multiplexer in a Fiber Optic Network," Far East Journal of Electronics and Communications, vol. 1, pp. 259-267, 2007.

[9] E. A. J. Marcatili, "Bends in Optical Dielectric Guides," Bell. Syst. Syst. Tech. J., vol. 48, pp. 2103-2132, 1969.

[10] E. A. J. Marcatili, "Dielectric Rectangular Waveguide and Directional Coupler for Integrated Optics," Bell. Syst. Tech. J., vol. 48, pp. 2071-2101, 1969.

[11] C. K. Madsen and J. H. Zhao, "A General Planar Waveguide Autoregressive Optical Filter," IEEE J. Lightwave Tech., vol. 14, no. 3, pp. 437-447, 1996.

[12] S. C. Hagness, "FDTD Microvavity Simulations: Design and Experimental Realization of Waveguide-Coupled Single-Mode Ring and Whispering-Gallery-Mode Disk Resonators," IEEE J. Lightwave tech., vol. 15, no. 11, pp. 2145-2165, 1997.

[13] D. Rafizadeh, "Waveguide-coupled AlGaAs/GaAs microcavity ring and disk resonators with high finesse and 21.6 nm free spectral range," Opt. Lett., vol. 22, no. 16, pp. 1244-1246, 1997.

[14] B. E. Little, "Ultra-Compact Si-SiO2 Microring resonator Optical Channel Dropping Filters," IEEE Photon. Techn. Lett., vol. 10, no. 4, pp. 549-551, 1998.

[15] D. J. Klunder, "Vertically and laterally waveguide-coupled cylindrical microresonators in Si3Ni4 on SiO2 technology," Appl. Phys., vol. B 73, pp. 603-608, 2001.

[16] B. Vanderhaegen, "High Q GaInAsP ring resonator filters," in ECIO, Torino, 1999.

[17] C. K. Madsen and J. H. Zhao, Optical Filter Design and Analysis: A Signal Processing Approach, New York: Wiley, 1999.

[18] D. Deng and Q. Guo, "Ince-Gaussian solitons in strongly nonlocal nonlinear media," Opt. Lett., vol. 32, pp. 3206-3208, 2007.

[19] G. Xia, Z. Wu and J. Wu, "Effect of fiber chromatic dispersion on incedent super-Gaussian pulse transmission in single-mode finers," Chinese J. Phys., vol. 41, no. 2, pp. 118-120, 2003.

[20] S. Supparpola, Y. Sun and S. A. Chiramida, "Gaussian pulse decomposition: An intuitive model of electrocardiogram waveforms," Annals of Biomedical Engineering, vol. 25, pp. 252-260, 1997.

[21] P. Wai and K. Nakkeeran, "On the uniquesness of Gaussian ansatz parameters equations:generalized projection operator method," Phys. Lett., vol. 332, no. A, pp. 239-243, 2004.

[22] P. Yupapin and W. Suwancharoen, "Chaotic signal generation and cancellation using a micro ring resonator incorporating an optical add-drop multiplexer," Opt. Commun., vol. 280, no. 2, pp. 343-350, 2007.

[23] P. Yupapin, N. Pornsuwancharoen and S. Chaiyasoonthorn, "Attosecond pulse generation using nonlinear microring resonators," Microw. and Opt. Technol. Lett., vol. 50, pp. 3108-3111, 2008.

[24] N. Pornsuwancharoen and P. Yupapin, "Generalized fast, slow, stop, and store light optically within a nanoring resonator," Microw. and Opt. Technol. Lett., vol. 51, pp. 899-902, 2009.

[25] T. Iizuka and Y. S. Kivshar, "Optical gap solitons in nonresonant quadratic media," Phys., vol. 59, no. E, pp. 7148-7151, 1999.

[26] Y. S. Kivshar and B. Luther-Davies, "Dark optical solitons:Physics and applications," Phys. Rep., vol. 298, pp. 81-197, 1998.

[27] P. Yupapin, P. Saeung and C. Li, "Characteristics of complementary ring-resonator add-drop filters modeling by using graphical approach," Opt. Commun., vol. 272, pp. 81-86, 2007.

[28] Q. Xu and M. Lipson, "All-optical logic based on siliconmicro-ring resonators," Optics Express, vol. 15, no. 3, pp. 924-929, 2007.

[29] G. P. Agarwal, Nonlinear Fiber Optics, 4 ed., New York: Academic Press, 2007.

[30] Y. Kokubun, Y. Hatakeyama, M. Ogata, S. Suzuki and N. Zaizen, "Fabrication technologies for vertically coupled microring resonator with multilevel crossing busline and ultracompact-ring radius," IEEE J. Sel. Top. Quantum Electron., vol. 11, pp. 4-10, 2005.

[31] K. Sarapat, N. Sangwara, K. Srinuanjan, P. Yupapin and P. Pornsuwancharoen, "Novel dark-bright optical solitons conversion and power amplification," Optical Engineering, vol. 48, pp. 045004-1, 2009.

[32] A. Ashkin, J. Dziedzic, J. Bjorkholm and S. Chu, "Observation of a single-beam gradient force optical trap for dielectric particles," Opt. Lett., vol. 11, pp. 288-290, 1986.

[33] S. Bergamini, B. Darqui, M. Jones, L. Jacubowiez, A. Browaeys and P. Grangier, "Holographic generation of microtrap arrays for single atoms by use of a progammable phase modulator," J. opt. Soc. Am.B, vol. 21, pp. 1889-1894, 2004.

[34] D. Yavuz, P. Kulatunga, E. Urban, T. A. Johnson, N. Proite, T. Henage, T. G. Walker and M. Saffman, "Fast ground state manipulation of neutral atoms in microscopic optical traps," Phys. Rev. Lett., vol. 96, p. 063001, 2006.

[35] D. Schrader, I. Dotsenko, M. Khudaverdyan, Y. Miroshnychenko, A. Rauschenbeutel and D. Meschede, "Neutral atom quantum resigter," Phys. Rev. Lett., vol. 93, p. 450501, 2004.

[36] J. A. Sauer, K. M. Fortier, M. S. Chang, C. D. Hamley and M. S. Capman, "Submicrometer position control of single trapped neutral atoms," Phys. Rev., vol. A69, p. 051804, 2004.

[37] T. P. Meyrath, F. Schreck, J. L. Hanssen, C. S. Chuu and M. G. Raizen, "Bose-Einstein condensate in a box," Phys. Rev. A, vol. 71, p. 041604, 2005.

[38] V. Boyer, R. M. Godun, G. Smirne, D. Cassettari, C. M. Chandrashekar, A. B. Deb, Z. J. Laczik and C. J. Foot, "Dynamic manipulation of bose-Einstein condensates with a spatial light modulator," Phys. Rev. A, vol. 73, p. 031402, 2006.

[39] A. V. Capentier, J. Belmonte-Neitai, H. Michinel and V. M. Perez-Garcia, "Laser tweezers for atomic solitons," J. of Mod. Opt., vol. 55, no. 17, pp. 2819-2829, 2008.

[40] V. Milner, L. Hanssen, W. C. Campbell and M. G. Raizen, "Optical billiards for atoms," Phys. Rev. Lett., vol. 86, pp. 1514-1516, 2001.

[41] N. Friedman, A. Kaplan, D. Carasso and N. Davidsoc, "Observation of chaotic and regular dynamics in atom-optics billiards," Phys. Rev. Lett., vol. 86, pp. 1518-1520, 2001.

[42] M. Li and J. Arlt, "Trapping multiple particels in single optical tweezers," Opt. Commun, vol. 281, pp. 135-140, 2008.

[43] M. Schulz, H. Crepaz, F. Schmidt-Kaler, J. Eschner and R. Blatt, "Transfer of trapped atoms between two optical tweezer potentials," J. of Mod. Opt., vol. 54, no. 11, pp. 1619-1626, 2007.

[44] Takada, "Field demonstration of over 1000-channel DWDM transmission with supercontinuum multi-carrier source," Electron. Lett., vol. 38, pp. 572-573, 2002.

[45] Sarapat, "A novel storage and tunable light source generated by a soliton pulse in a micro ring resonator system for super dense wavelength division multiplexing use," Microw. and Opt. Technol. Lett., vol. 51, no. 12, pp. 2948-2952, 2009.

[46] M. K. Smit, "Progress in AWG design and technology," in IEEE/LEOS Workshop on Fiber and Optical Passive Components, Mondello, 2005.

[47] F. M. Lee, C. L. Tsai, C. W. Hu, F. Y. Cheng, M. C. Wu and C. C. Lin, "High-reliable and high-speed 1.3 um complex-coupled distributed feedback buried-heterostructure laser diodes with Fe-doped InGaAsP/InP hybrid grating layers grown by MOCVD," IEEE Trans. on Elect. Devices, vol. 55, no. 2, pp. 540-546, 2008.

[48] S. Tomofuji, S. Matsuo, T. Kakitsuka and K. Kitywama, "Dynamic swithcing characteristics of InGaAsP/InP multimode interference optical waveguide switch," Opt. Express, vol. 17, no. 26, pp. 23380-23388, 2009.

[49] M. Ballav and A. R. Chowdhury, "On a study of diffraction and dispersion managed soliton in a cylindrical media," Progress In Electromagnetics Research, no. PIER 63(2006), pp. 33-50, 2006.

[50] S. Konar and A. Biswas, "Soliton-soliton interaction with power law nonlinearity," Progress In Electromagnetics Research, no. PIER 54(2005), pp. 95-108, 2005.

[51] R. Gangwar, S. P. Singh and N. Singh, "Soliton based optical communication," Progress In Electromagnetics Research, no. PIER 74(2007), pp. 157-166, 2007.

LIST OF PUBLICATIONS

1. **C. Vongchumyen**, S. Mitatha, J. Ali and P.P. Yupapin, "**Dark Soliton Array Generation: Theory and Experiment**", Microwave and Optical technology Letters, Volume 52, Issue 11, November 2010, Pages 2397-2400.

2. **C. Vongchumyen**, K. Kulsirirat, S. Mitatha and P.P. Yupapin, "**Dark-soliton multiplexing system for high-capacity and -security communication within a wavelength router**", Optical Engineering, Volume 49, Issue 05, May 2010
   [Errata : Volume 50, Issue 05, May 2011]

3. **C. Vongchumyen**, S. Mitatha and P.P. Yupapin, "**An Atom/Molecule/DNA Probing and Transportation using Dynamic Optical Tweezers via a Wavelength Router**", Optik – International Journal for Light and Electron Optics, Volume 122, Issue 6, March 2011, Pages 520-523

Dark Soliton Array Generation: Theory and Experiment

C. Vongchumyen, S. Mitatha, J. Ali and P.P. Yupapin

Microwave and Optical technology Letters,

Volume 52, Issue 11, November 2010, Pages 2397-2400

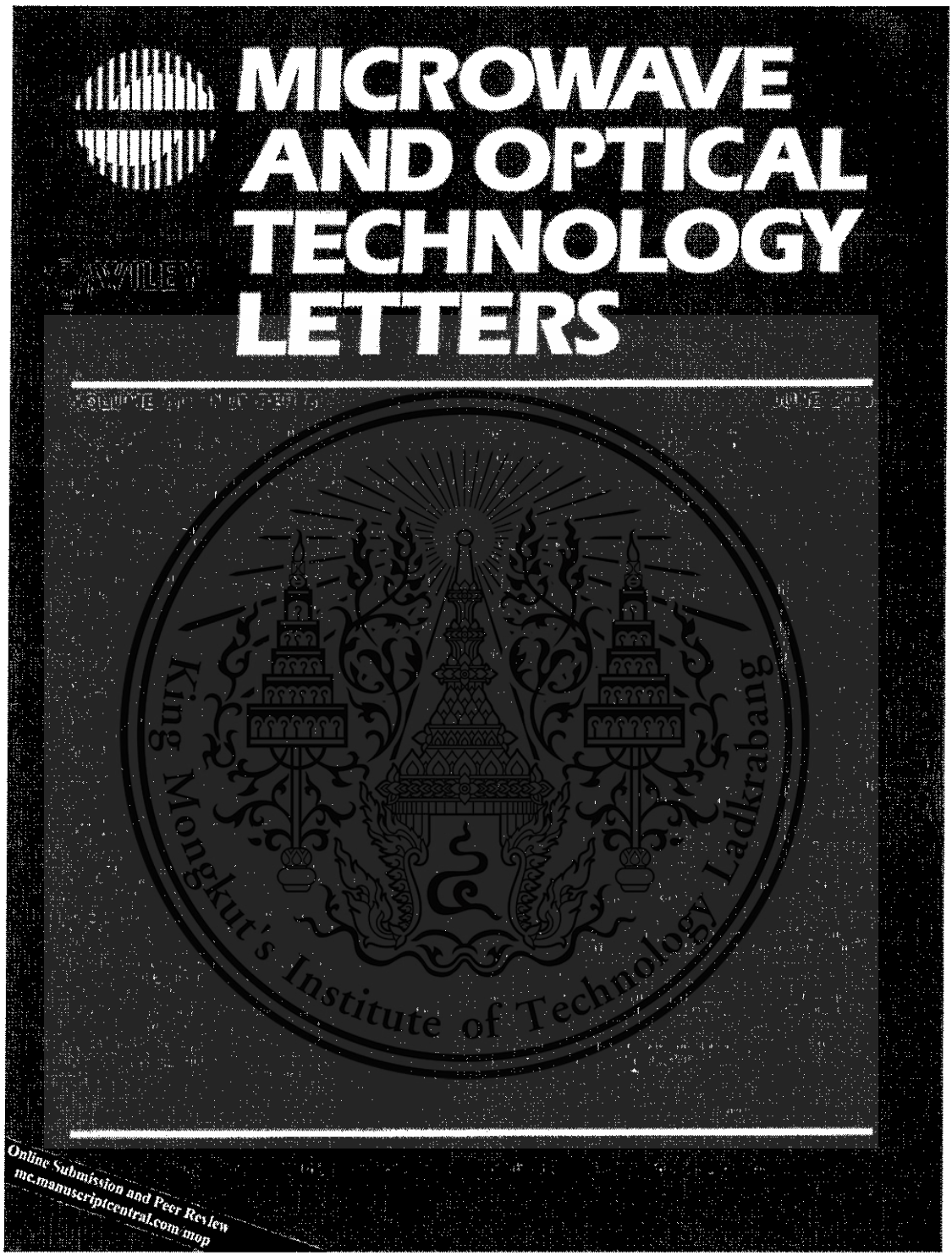

UMTS, IMT2000, Wibro, WiMAX2350, and WLAN2400 bands, the antenna gain is varied from 1.6 to 3.8 dBi, and the simulated radiation efficiency is above 75% in the most of frequency band.

4. CONCLUSIONS

We designed and successfully implemented a planar monopole antenna with a meander structure, L-shaped slots in the ground plane and tapered feeding line to cover eight communication bands: GSM900, DCS1800, PCS1900, UMTS, IMT-2000, Wibro, WiMAX2350, and WLAN2400. A dual-frequency operation with broad impedance bandwidth is achieved. We observed a good agreement between simulated and measured results, as well as the relatively good radiation characteristics. The proposed antenna has wide and potential applications as an internal multiband antenna for wireless communication terminals.

REFERENCES

1. IEEE P802.16e/D10, Draft IEEE Standard for Local and Metropolitan Area Networks Part 16: Amendment for Physical and Medium Access Control Layers for Combined Fixed and Mobile Operation in Licensed Bands, August 2005.
2. W.L. Schroeder, A.A. Vila, and C. Thorne, Extremely small, wideband mobile phone antennas by inductive chassis mode coupling, 9th European Conference on Wireless Technology, 2006, pp. 407–410.
3. P.L. Teng, H.T. Chen, and K.L. Wong, Multi-frequency planar monopole antenna for GSM/DCS/PCS/WLAN operation, Microwave Opt Technol Lett 36 (2003), 350–352.
4. K.L. Wong, G.Y. Lee, and T.W. Chiou, A low-profile planar monopole antenna for multiband operation of mobile handsets, IEEE Trans Antennas Propag 51 (2003), 121–125.
5. C.T. Lee, K.L. Wong, and Y.C. Lin, Wideband monopole antenna for DTV/GSM operation in the mobile phone, Microwave Opt Technol Lett 50 (2008), 801–806.
6. R.A. Bhatti, Y.-T. Im, N. N. Anh, and S.-O. Park, Multiband internal monopole antenna for mobile phones, Microwave Opt Technol Lett 51 (2008), 739–742.
7. M.F. Abedin and M. Ali, Modifying the ground plane and its effect on planar inverted-F antennas (PIFAs) for mobile phone handsets, IEEE Antennas Wireless Propag Lett 2 (2003), 226–229.
8. R. Hossa, A. Byndas, and M.E. Bialkowski, Improvement of compact terminal antenna performance by incorporating open-ends slots in ground plane, IEEE Microwave Wireless Compon Lett 14 (2004), 283–285.
9. T.K. Nguyen, B. Kim, H. Choo, and I. Park, Multiband Dual Spiral Stripline-Loaded Monopole Antenna, IEEE Antennas Wireless Propag Lett 8 (2009), 57–59.
10. R. Feick, H. Carrasco, M. Olmos, and H.D. Hristov, PIFA input bandwidth enhancement by changing feed plate silhouette, Electron Lett 40 (2004), 921–922.

DARK SOLITON ARRAY GENERATION: THEORY AND EXPERIMENT

C. Vongchumyen,[1] S. Mitatha,[1] J. Ali,[2] and P. P. Yupapin[3]

[1] Hybrid Computing Research Laboratory, Faculty of Engineering, King Mongkut's Institute of Technology Ladkrabang, Bangkok 10520, Thailand

[2] Institute of Advanced Photonics Science, ESciNano Research Alliance, Universiti Teknologi Malaysia (UTM), 81310 Johor Bahru, Malaysia

[3] Advanced Research Center for Photonics, Faculty of Science, King Mongkut's Institute of Technology Ladkrabang, Bangkok 10520, Thailand; Corresponding author: kypreech@kmitl.ac.th

Received 23 January 2010

ABSTRACT: *We present the fascinating results of dark soliton pulse array generation using the multilight sources via an optical multiplexer. The dark soliton array with different center wavelengths can be generated. The experimental setup was operated by using the brillouin-enhanced fiber laser scheme, whereas the experimental results of the dark soliton array are generated and achieved. In application, the dark soliton array can be used to form the molecules/atom trapping array, which can be used to form the molecules/atoms memory array for molecular computer and communication. Moreover, the transmission molecules/atoms can be secured by using the dark-bright soliton conversion behaviors. Results obtained have shown that the free spectrum range and the amplified power of 2.1 nm and 20 W of the bright soliton after dark-bright soliton conversion with wavelength center at 1.50 μm can be achieved, respectively.* © 2010 Wiley Periodicals, Inc. Microwave Opt Technol Lett 52:2397–2400, 2010; View this article online at wileyonlinelibrary.com. DOI 10.1002/mop.25514

Key words: *dark soliton array; multidark solitons; dark-bright soliton conversion; molecular transportation*

1. INTRODUCTION

Soliton communication has been a successful system for long distance optical communication link, whereas the required minimum repeater is the advantage, which becomes the key advantage of the required system performance. However, in practice, soliton collision and dispersion management is required to solve the problem of soliton–soliton interaction [1–3]. Generally, there are two types of soliton known as bright and dark solitons [4], where the soliton behaviors and applications are well analyzed and described by Agarwal [5]. In principle, the detection of dark soliton is extremely difficult. To date, several articles have investigated the dark soliton behaviors [6–10] and one of them shows an interesting result that the dark soliton can be converted into a bright soliton and finally detected. This means that the dark soliton penalty can be used as a communication security so that it can be retrieved by the dark-bright soliton conversion [11, 12]. A soliton pulse has been used to produce fast switching [13] localized within a nanowaveguide [14, 15] and it was reported that they have designed a system, which consists of micro- and nanoring resonators. Therefore, in this article, we present the results of dark solitons generated by using the multilight sources/tunable source to form the multidark soliton multiplexing system, where the multiplexed solitons can be transmitted into the link via an optical multiplexer (MUX). The dark soliton array, that is, wavelength division multiplexing of dark soliton is formed, which may be used to form the multiwavelength soliton bands for high capacity molecules/atoms trapping and transportation [16]. Results obtained have shown that slight difference of soliton center wavelengths can be generated and used for multichannels applications. By using the dark-bright conversion, the multibright solitons can be obtained, which means that the large number of molecules/atoms can be kept in the secured communication link, that is, a wavelength router, which is also available for molecular communication and large memory applications.

2. DARK SOLITON ARRAY GENERATION AND CONVERSION

To describe the multiplexed dark soliton pulses, a stationary dark soliton pulse that is introduced into the nonlinear microring resonator system as shown in Figure 1. Each of input optical fields (E_{in}) of the dark soliton pulses input is given by [5]

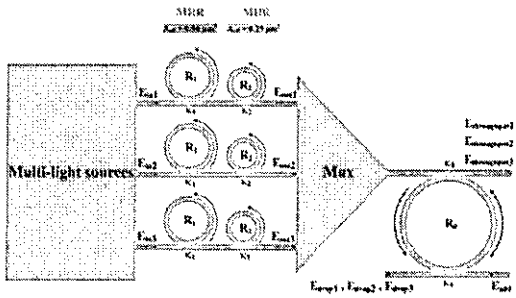

Figure 1 Schematic of generation trapping tool system, where E_{in}: soliton inputs, R_x: ring radii, κ_x: coupling coefficients, MUX: optical multiplexer, R_d: add/drop radius. [Color figure can be viewed in the online issue, which is available at wileyonlinelibrary.com]

$$E_{in}(t) = A\tanh\left[\frac{T}{T_0}\right]\exp\left[\left(\frac{z}{2L_D}\right) - i\omega_0 t\right] \quad (1)$$

Where A and z are the optical field amplitude and propagation distance, respectively. T is a soliton pulse propagation time in a frame moving at the group velocity, $T = t - \beta_1^* z$, where β_1 and β_2 are the coefficients of the linear and second-order terms of Taylor expansion of the propagation constant. $L_D = T_0^2/|\beta_2|$ is the dispersion length of the soliton pulse. T_0 in equation is a soliton pulse propagation time at initial input (or soliton pulse width), where t is the soliton phase shift time, and the frequency shift of the soliton is ω_0. This solution describes a pulse that keeps its temporal width invariance as it propagates, and thus is called a temporal soliton. When a soliton peak intensity ($|\beta_2|\Gamma \times T_0^2|$) is given, then T_0 is known. For the soliton pulse in the microring device, a balance should be achieved between the dispersion length (L_D) and the nonlinear length ($L_{NL} = 1/\Gamma\phi_{NL}$), where $\Gamma = n_2{}^*k_0$, is the length scale over which dispersive or nonlinear effects makes the beam become wider or narrower. For a soliton pulse, there is a balance between dispersion and nonlinear lengths, hence $L_D = L_{NL}$.

When light propagates within the nonlinear material (medium), the refractive index (n) of light within the medium is given by

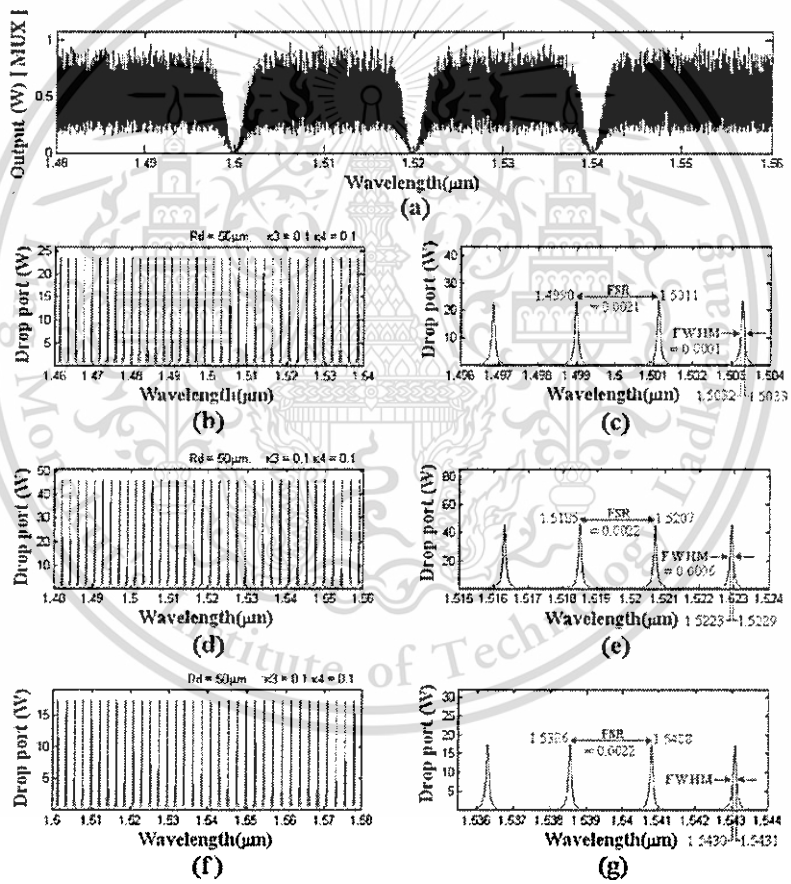

Figure 2 Simulation result of the dark soliton array when the dark soliton input wavelengths are 1.50, 1.52, and 1.54 μm, where (a) dark soliton array, (b) and (c), (d) and (e), (f) and (g) are the drop port signals, respectively. [Color figure can be viewed in the online issue, which is available at wileyonlinelibrary.com]

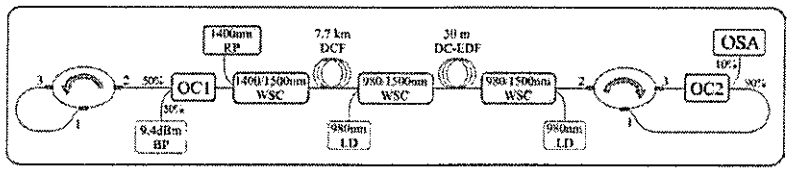

Figure 3 Experimental setup for forward pumping, where OSA: optical spectrum analyzer, OCs: optical circulators, BP: Brillouin pumping, RP: Raman pumping, WSC: wavelength division multiplexing, DCF: dispersion compensated fiber, LDs: laser diodes, DC-EDF: depressed cladding erbium-doped fiber. [Color figure can be viewed in the online issue, which is available at wileyonlinelibrary.com]

$$n = n_0 + n_2 I = n_0 + \frac{n_2}{A_{\text{eff}}} P \tag{2}$$

where n_0 and n_2 are the linear and nonlinear refractive indexes, respectively. I and P are the optical intensity and optical power, respectively. The effective mode core area of the device is given by A_{eff}. For the series microring resonator (MRRs), the effective mode core areas range from 0.50 to 0.10 μm^2 [17]. When a soliton pulse is input and propagated within a MRR, as shown in Figure 1, which consists of a series MRRs. The resonant output is formed, thus, the normalized output of the light field is the ratio between the output and input fields [$E_{\text{out}}(t)$ and $E_{\text{in}}(t)$] in each roundtrip, which is given by [18]

$$\left|\frac{E_{\text{out}}(t)}{E_{\text{in}}(t)}\right|^2 = (1-\gamma)\left[1 - \frac{(1-(1-\gamma)x^2)\kappa}{(1-x\sqrt{1-\gamma}\sqrt{1-\kappa})^2 + 4x\sqrt{1-\gamma}\sqrt{1-\kappa}\sin^2(\frac{\phi}{2})}\right] \tag{3}$$

The close form of Eq. (3) indicates that a ring resonator in this particular case is very similar to a Fabry–Perot cavity, which has an input and output mirror with a field reflectivity, $(1 - \kappa)$, and a fully reflecting mirror. κ is the coupling coefficient, and $x = \exp(-\alpha L/2)$ represents a roundtrip loss coefficient. $\phi_0 = k\text{Ln}_0$ and $\phi_{\text{NL}} = k\text{Ln}_2|E_{\text{in}}|^2$ are the linear and nonlinear phase shifts, $k = 2\pi/\lambda$ is the wave propagation number in a vacuum, where L and α are waveguide length and linear absorption coefficient, respectively. In this work, the iterative method is introduced to obtain the results as shown in Eq. (3), and similarly, when the output field is connected and input into the other ring resonators.

The input optical field as shown in Eq. (1), that is, a dark soliton pulse, is input into a nonlinear series microring resonator. By using the appropriate parameters, we propose to use the add/drop device with the appropriate parameters. This is given in details as followings. The optical outputs of a ring resonator add/drop filter can be given by the Eqs. (4) and (5), respectively [19].

$$\left|\frac{E_t}{E_{\text{in}}}\right|^2 = \frac{(1-\kappa_1) - 2\sqrt{1-\kappa_1}\sqrt{1-\kappa_2}e^{-\frac{\alpha L}{2}}\cos(k_n L) + (1-\kappa_2)e^{-\alpha L}}{1+(1-\kappa_1)(1-\kappa_2)e^{-\alpha L} - 2\sqrt{1-\kappa_1}\sqrt{1-\kappa_2}e^{-\frac{\alpha L}{2}}\cos(k_n L)} \tag{4}$$

and

$$\left|\frac{E_d}{E_{\text{in}}}\right|^2 = \frac{\kappa_1\kappa_2 e^{-\frac{\alpha L}{2}}}{1+(1-\kappa_1)(1-\kappa_2)e^{-\alpha L} - 2\sqrt{1-\kappa_1}\sqrt{1-\kappa_2}e^{-\frac{\alpha L}{2}}\cos(k_n L)} \tag{5}$$

where E_t and E_d represent the optical fields of the throughput and drop ports, respectively. $\beta = kn_{\text{eff}}$ is the propagation constant, n_{eff} is the effective refractive index of the waveguide, and the circumference of the ring is $L = 2\pi R$, with R as the radius of the ring. In the following, new parameters is used for simplification with $\phi = \pi L$ as the phase constant. The chaotic noise cancellation can be managed by using the specific parameters of the add/drop device, and the required signals can be retrieved by the specific users. κ_1 and κ_2 are the coupling coefficient of the add/drop filters, $k_n = 2\pi/\lambda$ is the wave propagation number for in a vacuum, and where the waveguide (ring resonator) loss is $\alpha = 0.5$ dB mm^{-1}. The fractional coupler intensity loss is $\gamma = 0.1$. In the case of the add/drop device, the nonlinear refractive index is neglected.

In simulation, the generated dark soliton pulse, for instance, with 50-ns pulse width, and a maximum power of 0.5 W is input into each of ring resonator systems with different center wavelengths, as shown in Figure 1. The suitable ring parameters are used, such as ring radii and ring coupling coefficients, where $R_1 = 15.0$ μm and $R_2 = 10.0$ μm. To make the system associate with the practical device [17], $n_0 = 3.34$ (InGaAsP/InP). The effective core areas are $A_{\text{eff}} = 0.50$ and 0.25 μm^2 for MRRs. The waveguide and coupling loses are $\alpha = 0.5$ dB mm^{-1} and $\gamma = 0.1$, respectively, and the coupling coefficients κ, of the MRRs are ranged from 0.03 to 0.1. The nonlinear refractive index is $n_2 = 2.2 \times 10^{-13}$ m^2/W. In this case, the waveguide loss used is 0.5 dB mm^{-1}. However, more parameters are used as shown in Figure 1. The input dark soliton pulse is chopped (sliced) into the smaller signals R_1, R_2, and the filtering signals within add/drop ring R_d are seen. We find that the output signals from R_2 is larger than from R_1 because of the different core effective areas of the rings in the system, however, the effective areas can be transferred from 0.50 and 0.25 μm^2 with some losses. The soliton signals in R_d is entered in the add/drop filter, where the dark soliton conversion can be performed by using Eqs. (4) and (5). In application, the different dark soliton wavelength is input into the series microring resonators system, whereas the parameters of system are set the same. For instance, the dark solitons are input into the system at the center wavelengths $\lambda_1 = 1.5$, $\lambda_2 = 1.52$, and $\lambda_3 = 1.54$ μm, respectively. When a dark soliton propagates into the MRRs system, the occurrence of dark soliton collision (modulation) in MUX system and the filtering signals within add/drop ring (R_d) is as shown in Figure 2. The dark soliton generated by multilight sources at the center wavelength $\lambda_1 = 1.5$ μm. Simulation results obtained have shown that the band of bright solitons is seen, whereas there is no signal at $\lambda_1 = 1.50$ μm. The free spectrum range (FSR) and the amplified power of 2.1 nm and 20 W of the dark soliton are obtained, where in this case, the spectral width (Full width at half maximum, FWHM) of 0.1 nm is achieved.

3. EXPERIMENTAL RESULTS

Figure 3 shows the experimental setup for multiwavelength brillouin-enhanced fiber laser in the forward pumping configuration, which can be used to performed the dark soliton array by using nonlinear fiber optic setup system. The setup consists of a Brillouin

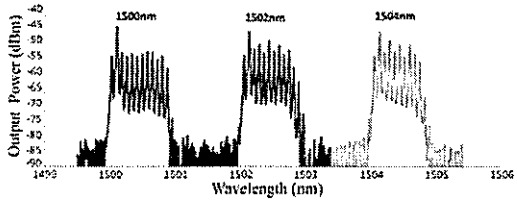

Figure 4 Tunable multiple-Brillouin lasing at different wavelengths of Brillouin pumping. [Color figure can be viewed in the online issue, which is available at wileyonlinelibrary.com]

pump (BP) with a 9.4 dBm output power, a Raman pump with a 296 mW output power that pumps the 7.7 km dispersion compensated fiber and two laser diodes (LD) with an output power of 48 mW and 121 mW, respectively. These LD's was bidirectionally pumped into a 30-m length depressed cladding fiber with a spooling diameter of 7 cm. A linear resonator consists of two optical circulators (OC), where both ends of the setup were used. These two OC also created a double pass configuration inside the cavity. Three wavelength division MUXs (WSC) were used to combine the different wavelength inside the cavity. A 3-dB OC1 couples the signal from the BP into the cavity. A 90:10 output coupler that is replaced at different locations as shown in Figure 3 will tap 10% of this signal. This signal is directly observed using an optical spectrum analyzer with a resolution of 0.02 nm.

Figure 4 shows the tunable multiple-Brillouin lasing at different settings of wavelengths at BP. Note that this multiwavelength Brillouin lasing are obtained from the experimental setup in Figure 3. The power setting of the BP is kept constant at 9.4 dBm but the wavelength of the signal is varied at 1500, 1502, and 1504 nm. From the spectrum obtained, 13, 12, and 11 peaks are obtained at 1500, 1502, and 1504 nm, respectively. The lasing peaks at 1500 nm are more stable and fluctuates less when compared with 1502 nm and 1504 nm lasing. Due to the less numbers of fluctuations of the lasing spectrum and the highest number of peaks obtained at 1500 nm, the multi-Brillouin lasing at this wavelength is chosen for close scrutiny. Figure 5 shows the stability and evolution of the lasing spectrum of the dark-bright soliton conversion pulses. It can be seen that the same spectrum is almost reproducible. The time interval between two spectra is 60 s. The generation of multi-Brillouin lasing is much dependent on the pumping power that interacts with the acoustic wave.

4. DISCUSSION AND CONCLUSIONS

We propose a novel system of the dark soliton array generation using the multiplexed dark soliton pulse. The multidark solitons are input into the series microring resonators, where the multiplexed and the filtering signals within add/drop ring system can be generated and obtained, which can be used to perform the large channel capacity in the secure communication link. The use of dark solitons to form the large channel capacity within the wavelength router is analyzed. The FSR and the amplified power of 2.1 nm and 20 W of the dark soliton with wavelength at 1.50 μm can be achieved, respectively. The experimental results have shown that the dark soliton array can be generated. The dark-bright soliton conversion is also formed, which is in good agreement with theoretical simulation results, however, the slightly different of center wavelengths of both results are noted.

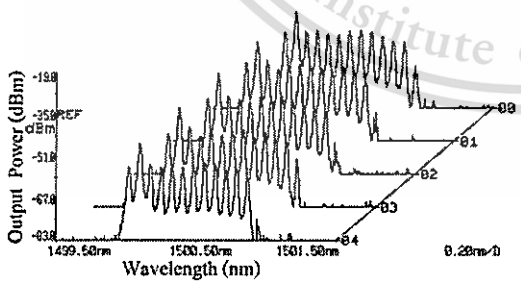

Figure 5 Shows the multidark-bright soliton train at 1500 nm from 0 to 4.0 ns

REFERENCES

1. M. Ballav and A.R. Chowdhury, On a study of diffraction and dispersion managed soliton in a cylindrical media, Prog Electromagn Res PIER 63 (2006), 33–50.
2. S. Konar and A. Biswas, Soliton-soliton interaction with power law nonlinearity, Prog Electromagn Res PIER 54 (2005), 95–108.
3. R. Gangwar, S.P. Singh, and N. Singh, Soliton based optical communication, Prog Electromagn Res PIER 74 (2007), 157–166.
4. F.G. Gharakhili, M. Shahabadi, and M. Hakkak, Bright and dark soliton generation in a left-handed nonlinear transmission line with series nonlinear capacitors, Prog Electromagn Res PIER 96 (2009), 237–249.
5. G.P. Agarwal, Nonlinear fiber optics, 4th ed., Academic Press, New York, 2007.
6. Y.S. Kivshar and B. Luther-Davies, Dark optical solitons: Physics and applications, Phys Rep 298 (1998), 81–197.
7. W. Zhao and E. Bourkoff, Propagation properties of dark solitons, Opt Lett 14 (1989), 703–705.
8. I.V. Barashenkov, Stability criterion for dark soliton, Phys Rev Lett 77 (1996), 1193–1195.
9. D.N. Christodoulides, T. H. Coskun, M. Mitchell, Z. Chen, and M. Segev, Theory of incoherent dark solitons, Phys Rev Lett 80 (1998), 5113–5115.
10. A.D. Kim, W.L. Kath, and C.G. Goedde, Stabilizing dark solitons by periodic phase-sensitive amplification, Opt Lett 21 (1996), 465–467.
11. K. Sarapat, N. Sangwara, K. Srinuanjan, P.P. Yupapin, and N. Pornsuwancharoen, Novel dark-bright optical soliton conversion system and power amplification, Opt Eng 48 (2009), 045004.
12. B.A. Malomed, A. Mostofi, and P.L. Chu, Transformation of a dark soliton into a bright pulse, J Opt Soc Am B 17 (2000), 507–513.
13. P.P. Yupapin, N. Pornsuwanchroen, and S. Chaiyasoonthorn, Attosecond pulse generation using nonlinear microring resonators, Microwave Opt Technol Lett 50 (2008), 3108–3110.
14. P.P. Yupapin and N. Pornsuwanchroen, Proposed nonlinear microring resonator arrangement for stopping and storing light, IEEE Photon Technol Lett 21 (2009), 404–406.
15. S. Mithata, N. Pornsuwancharoen, and P.P. Yupapin, A simultaneous short wave and millimeter wave generation using a soliton pulse within a nano-waveguide, IEEE Photon Technol Lett 21 (2009), 932–934.
16. S.F. Hanim, J. Ali, and P.P. Yupapin, Dark soliton generation using dual Brillouin fiber laser in a fiber optic ring resonator, Microwave Opt Technol Lett, in press.
17. Y. Kokubun, Y. Hatakeyama, M. Ogata, S. Suzuki, and N. Zaizen, Fabrication technologies for vertically coupled microring resonator with multilevel crossing busline and ultracompact-ring radius, IEEE J Sel Top Quantum Electron 11 (2005), 4–10.
18. P.P. Yupapin and W. Suwancharoen, Chaotic signal generation and cancellation using a micro ring resonator incorporating an optical add/drop multiplexer, Opt Commun 280 (2007), 343–350.
19. P.P. Yupapin, P. Saeung, and C. Li, Characteristics of complementary ring-resonator add/drop filters modeling by using graphical approach, Opt Commun 272 (2007), 81–86.

Dark-soliton multiplexing system for high-capacity and -security communication within a wavelength router

C. Vongchumyen, K. Kulsirirat, S. Mitatha and P.P. Yupapin

Optical Engineering

Volume 49, Issue 05, May 2010

[Errata : Volume 50, Issue 05, May 2011]

Vol. 55 • No. 8 | August 2016
ISSN 0091-3286

Optical Engineering

SPIE.

Optical Engineering 50(5), 059802 (May 2011)

Errata: Dark-soliton multiplexing system for high-capacity and -security communication within a wavelength router

Charoen Vongchumyen
King Mongkut's Institute of Technology Ladkrabang
Faculty of Engineering
Hybrid Computing Research Laboratory
Chalongkrung Road
Ladkrabang, Bangkok 10520, Thailand

Kathawut Kulsirirat
King Mongkut's Institute of Technology Ladkrabang
Faculty of Science
Advanced Photonics Research Center
Chalongkrung Road
Ladkrabang, Bangkok 10520, Thailand

Somsak Mitatha
King Mongkut's Institute of Technology Ladkrabang
Faculty of Engineering
Hybrid Computing Research Laboratory
Chalongkrung Road
Ladkrabang, Bangkok 10520, Thailand

Preecha P. Yupapin
King Mongkut's Institute of Technology Ladkrabang
Faculty of Science
Advanced Photonics Research Center
Chalongkrung Road
Ladkrabang, Bangkok 10520, Thailand
E-mail: kypreech@kmitl.ac.th

[DOI: 10.1117/1.3592833]

This article [*Opt. Eng.* 49, 055002 (2010)] was originally published on 11 May 2010 with errors in the author affiliations. The correct affiliations appear above. The article was corrected online on 4 May 2011.

Optical Engineering 49(5), 055002 (May 2010)

Dark-soliton multiplexing system for high-capacity and -security communication within a wavelength router

Charoen Vongchumyen
King Mongkut's Institute of Technology Ladkrabang
Faculty of Science
Advanced Research Center for Photonics
Chalongkrung Road
Ladkrabang, Bangkok 10520, Thailand

Kathawut Kulsirirat
King Mongkut's Institute of Technology Ladkrabang
Faculty of Engineering
Hybrid Computing Research Laboratory
Chalongkrung Road
Ladkrabang, Bangkok 10520, Thailand

Somsak Mitatha
King Mongkut's Institute of Technology Ladkrabang
Faculty of Science
Advanced Research Center for Photonics
Chalongkrung Road
Ladkrabang, Bangkok 10520, Thailand

Preecha P. Yupapin
King Mongkut's Institute of Technology Ladkrabang
Faculty of Engineering
Hybrid Computing Research Laboratory
Chalongkrung Road
Ladkrabang, Bangkok 10520, Thailand
E-mail: kypreech@kmitl.ac.th

Abstract. We propose a novel system for generating multiplexed dark-soliton pulses using multiple light sources via an optical multiplexer, whereby dark solitons with different center wavelengths can be generated. The multiplexed signals can be transmitted into the communication link and filtered by using an optical add-drop filter. By using suitable simulation parameters, we have shown that dark solitons with different center wavelengths can in fact be obtained. In application, the communication capacity can be increased by using the multiplexed dark solitons; moreover, the transmission signals can be secured by utilizing the behavior of dark solitons. A free spectrum range (FSR) 2.5 nm and an amplified power of 30 W of dark solitons with wavelength 1.60 μm can be achieved. Channel spacing of the communication signals within a wavelength router can be provided by using a suitable FSR, which can be managed by using crosstalk effect analysis. [DOI: 10.1117/1.3425658]

Subject terms: wavelength router; dark-soliton array; multiplexed dark solitons; communication security.

Paper 100049R received Jan. 24, 2010; revised manuscript received Mar. 9, 2010; accepted for publication Mar. 9, 2010; published online May 11, 2010.

1 Introduction

Soliton communication has been a successful system for long-distance optical communication links, where minimization of the required number of repeaters is a key to system performance. In practice, however, the problems of soliton-soliton interaction, soliton collision, and dispersion management have to be solved.[1–3] Generally, there are two types of soliton, known as bright and dark solitons,[4] whose behavior and applications are well analyzed and described by Agarwal.[5] In principle, the detection of dark solitons is extremely difficult. To date, several papers have investigated their behavior,[6–10] and one of them shows the interesting result that a dark soliton can be converted into a bright soliton and finally detected. This means that the undetectability of dark solitons can be used for communication security, the information being retrieved by dark-bright soliton conversion.[11,12] Recently, a soliton pulse has been used to produce fast switching[13] within a nanowaveguide,[14,15] and Mithata et al.[15] reported that they have designed a system that consists of micro- and nano-ring resonators.

Since then, the application of dark solitons has become promising in that a transmitted dark soliton can be converted into a bright soliton after passing through a specific add-drop filter,[11] which means that signals can be transmitted in the form of dark solitons, which are difficult to detect, whereas the end user who connects to the link via the add-drop filter can obtain the signals. Although dark-soliton applications have been widely investigated,[16–19] the search for new techniques with wider applications continues.

In this paper, we propose the use of multiple dark solitons generated by using multiple light sources and/or tunable sources to form a dark-soliton multiplexing system, where the multiplexed solitons can be transmitted into the link via an optical multiplexer (MUX). A dark-soliton array is formed through wavelength division multiplexing

0091-3286/2010/$25.00

(WDM) of dark solitons, and may be used to form the multiwavelength soliton bands for high-capacity communication. Simulation results have shown that slightly different soliton center wavelengths can be generated and used for multichannel applications. By using the dark-bright conversion, multiple bright solitons can be obtained, which means that a large number of channels can be kept in a secured communication link, which is thus available for communication security with high capacity over long distances.

2 Generation of Multiplexed Dark Solitons

To create a system by which multiplexed dark soliton pulses can be used to generate a dark-soliton array, stationary dark soliton pulses are introduced into the microring resonator system shown in Fig. 1. Each of input optical fields (E_{in}) of the dark soliton pulses is given by[5]

$$E_{in}(t) = A \tanh\left(\frac{T}{T_0}\right)\exp\left[\left(\frac{z}{2L_D}\right) - i\omega_0 t\right], \tag{1}$$

where A and z are the optical field amplitude and propagation distance, respectively; T is the soliton pulse propagation time in a frame moving at the group velocity, $T=t-\beta_1 z$, where β_1 and β_2 are the coefficients of the linear and second-order terms of the Taylor expansion of the propagation constant; $L_D=T_0^2/|\beta_2|$ is the dispersion length of the soliton pulse; T_0 is the soliton pulse propagation time at initial input (the soliton pulse width); t is the soliton phase-shift time; and the frequency shift of the soliton is ω_0. This solution describes a pulse that keeps its temporal width invariant as it propagates, and thus is called a temporal soliton. When the soliton peak intensity ($|\beta_2/\Gamma T_0^2|$) is given, then T_0 is known. For the soliton pulse in the microring device, a balance should be achieved between the dispersion length (L_D) and the nonlinearity length ($L_{NL}=1/\Gamma\phi_{NL}$), where $\Gamma=n_2k_0$ is the length scale over which dispersive or nonlinear effects make the beam become wider or narrower. For a soliton pulse, there is a balance between dispersion and nonlinear lengths; hence $L_D=L_{NL}$.

When light propagates within the nonlinear material (medium), the refractive index (n) of light within the medium is given by

$$n = n_0 + n_2 I = n_0 + \frac{n_2}{A_{eff}}P, \tag{2}$$

where n_0 and n_2 are the linear and nonlinear refractive indices, respectively, and I and P are the optical intensity and optical power, respectively. The effective mode core area of the device is given by A_{eff}. For the series of microring resonators (MRRs), the effective mode core areas range from 0.50 to 0.10 μm^2.[20] When a soliton pulse is input and propagated within a MRR (as shown in Fig. 1, which consists of a series of MRRs), a resonant output is formed. Thus, the normalized output light field is the ratio between the output and input fields [$E_{out}(t)$ and $E_{in}(t)$] in each round trip, which is given by[21]

$$\left|\frac{E_{out}(t)}{E_{in}(t)}\right|^2 = (1-\gamma)\left\{1 - \frac{[1-(1-\gamma)x^2]\kappa}{[1-x(1-\gamma)^{1/2}(1-\kappa)^{1/2}]^2 + 4x(1-\gamma)^{1/2}(1-\kappa)^{1/2}\sin^2(\phi/2)}\right\}, \tag{3}$$

The closed form of Eq. (3) indicates that a ring resonator in this particular case is very similar to a Fabry-Perot cavity, which has an input and output mirror with a field reflectivity $1-\kappa$, and a fully reflecting mirror. Here κ is the coupling coefficient, $x=\exp(-\alpha L/2)$ represents a round-trip loss coefficient, $\phi_0=kLn_0$ and $\phi_{NL}=kLn_2|E_{in}|^2$ are the linear and nonlinear phase shifts, and $k=2\pi/\lambda$ is the wave propagation number in a vacuum, where L and α are the waveguide length and linear absorption coefficient, respectively. In this work, an iterative method is introduced to obtain the results shown in Eq. (3), and similarly when the output field is connected and input into the other ring resonators.

The input optical field as shown in Eq. (1), i.e., a dark-soliton pulse, is input into a nonlinear series microring resonator. We propose to use an add-drop device with the appropriate parameters. This is given in detail as follows. The optical outputs of a ring-resonator add-drop filter are given by[22]

$$\left|\frac{E_t}{E_{in}}\right|^2 = \frac{(1-\kappa_1) - 2(1-\kappa_1)^{1/2}(1-\kappa_2)^{1/2}\exp[-(\alpha/2)L]\cos k_n L + (1-\kappa_2)e^{-\alpha L}}{1 + (1-\kappa_1)(1-\kappa_2)e^{-\alpha L} - 2(1-\kappa_1)^{1/2}(1-\kappa_2)^{1/2}\exp[-(\alpha/2)L]\cos k_n L} \tag{4}$$

and

$$\left|\frac{E_d}{E_{in}}\right|^2 = \frac{\kappa_1\kappa_2\exp[-(\alpha/2)L]}{1 + (1-\kappa_1)(1-\kappa_2)e^{-\alpha L} - 2(1-\kappa_1)^{1/2}(1-\kappa_2)^{1/2}\exp[-(\alpha/2)L]\cos k_n L}, \tag{5}$$

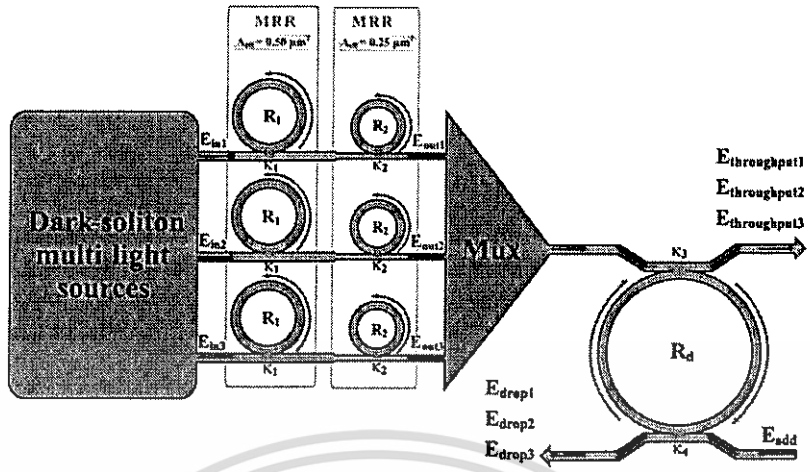

Fig. 1 Schematic of generation trapping tool system: E_{in3}, soliton inputs; R_s, ring radii; κ_s, coupling coefficients; MUX, optical multiplexer; R_d, add-drop radius.

where E_t and E_d represent the optical fields of the throughput and drop ports, respectively, $\beta=kn_{eff}$ is the propagation constant, n_{eff} is the effective refractive index of the waveguide, and the circumference of the ring is $L=2\pi R$, with R the radius of the ring. In the following, new parameters are used for simplification, with $\phi=\beta L$ as the phase constant. The chaotic noise cancellation can be managed by using the specific parameters of the add-drop device, and the required

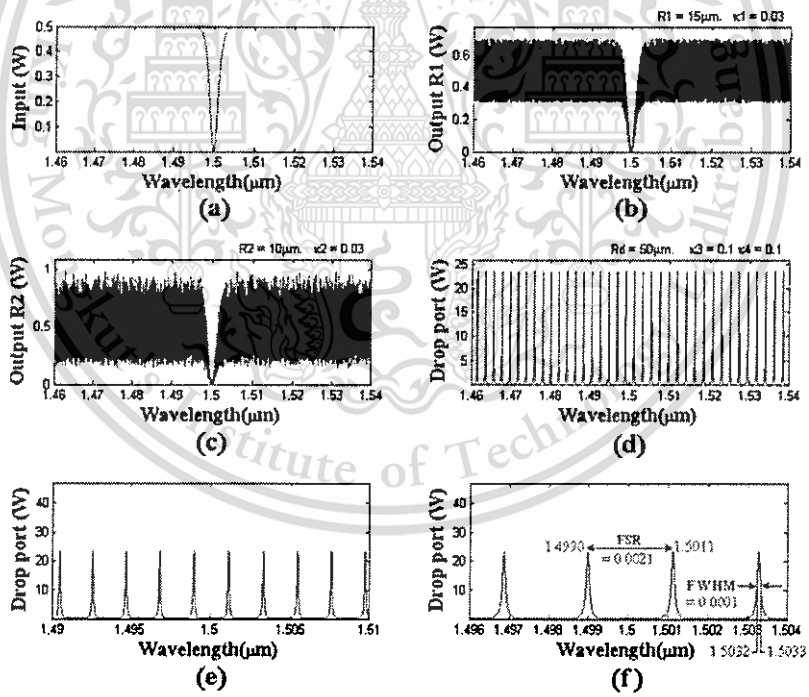

Fig. 2 Simulation results for dark solitons within the series microring resonators when the dark-soliton input wavelength is 1.5 μm: (a) dark-soliton input; (b), (c), dark solitons in rings R_1 and R_2; (d), (e), (f), drop-port signals.

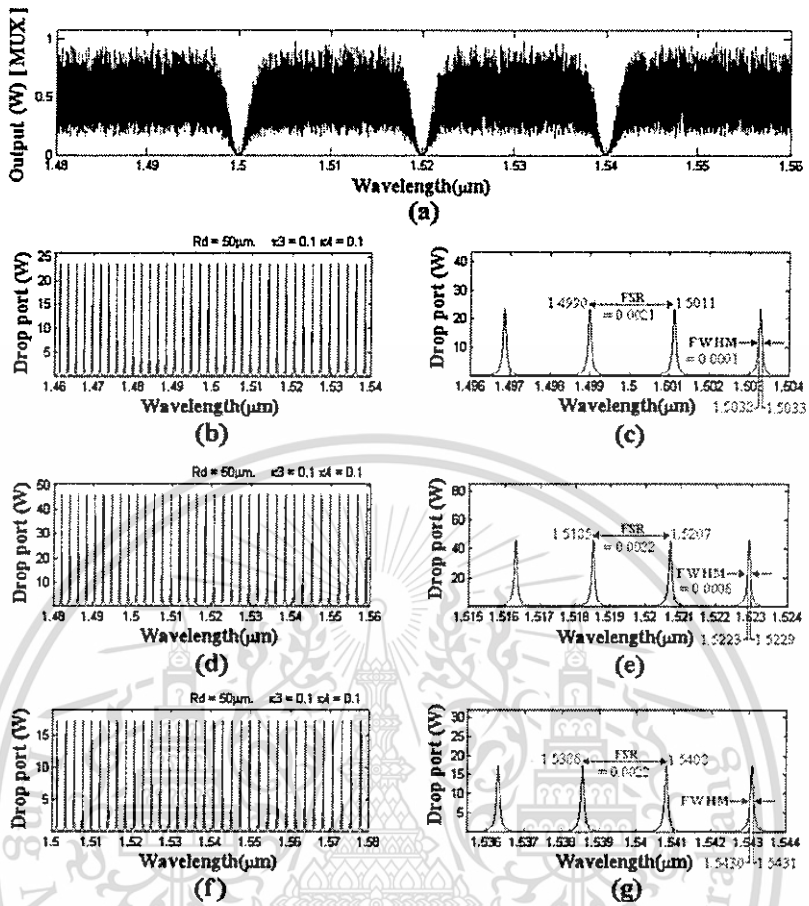

Fig. 3 Simulation result on the dark-soliton array when the dark-soliton input wavelengths are 1.5, 1.52, and 1.54 μm: (a) dark-soliton array; (b) through (g), drop-port signals.

signals can be retrieved by the specific users. In Eqs. (4) and (5). κ_1 and κ_2 are the coupling coefficients of the add-drop filters, $k_n = 2\pi/\lambda$ is the wave propagation number in a vacuum, and the waveguide (ring resonator) loss is $\alpha = 0.5$ dB mm^{-1}. The fractional coupler intensity loss is $\gamma = 0.1$. In the case of the add-drop device, the nonlinear refractive index is neglected.

In simulation, the generated dark-soliton pulse, for instance, with 50-ns pulse width and a maximum power of 0.5 W, is input into each of ring resonator systems with different center wavelengths, as shown in Fig. 1. Suitable ring parameters are used, such as the ring radii ($R_1 = 15.0$ μm and $R_2 = 10.0$ μm) and ring coupling coefficients. In order to make the system correspond to a practical device,[20] we set $n_0 = 3.34$ (for InGaAsP/InP). The effective core areas are $A_{eff} = 0.50$ and 0.25 μm^2 for the MRRs. The waveguide and coupling loses are $\alpha = 0.5$ dB mm^{-1} and $\gamma = 0.1$, respectively, and the coupling coefficients κ_s of the MRRs range from 0.03 to 0.1. The nonlinear refractive index is $n_2 = 2.2 \times 10^{-13}$ m^2/W. In this case, the waveguide loss used is 0.5 dB mm^{-1}. Other parameters used are shown in Fig. 1. The input dark-soliton pulse is chopped (sliced) into the smaller signals R_1, R_2, and the filtering signals within the add-drop ring R_d are seen. We find that the output signal from R_2 is larger than from R_1, due to the different effective core areas (0.50 and 0.25 μm^2) of the rings in the system; however, the effective areas can be changed with some losses. The soliton signals in R_d are fed to the add-drop filter, where the dark-soliton conversion can be performed according to Eqs. (4) and (5).

In application, the different dark-soliton wavelengths are input into the series microring resonator system, whereas the parameters of the system are set the same. For instance, dark solitons are input into the system at the center wavelengths $\lambda_1 = 1.5$ μm, $\lambda_2 = 1.52$ μm, and $\lambda_3 = 1.54$ μm. When a dark soliton propagates into the MRR system, the occurrence of dark-soliton collision (modulation) in the multiplexer system and the filtering signals within an add-drop ring (R_d) is as shown in Fig. 1. The dark solitons are gen-

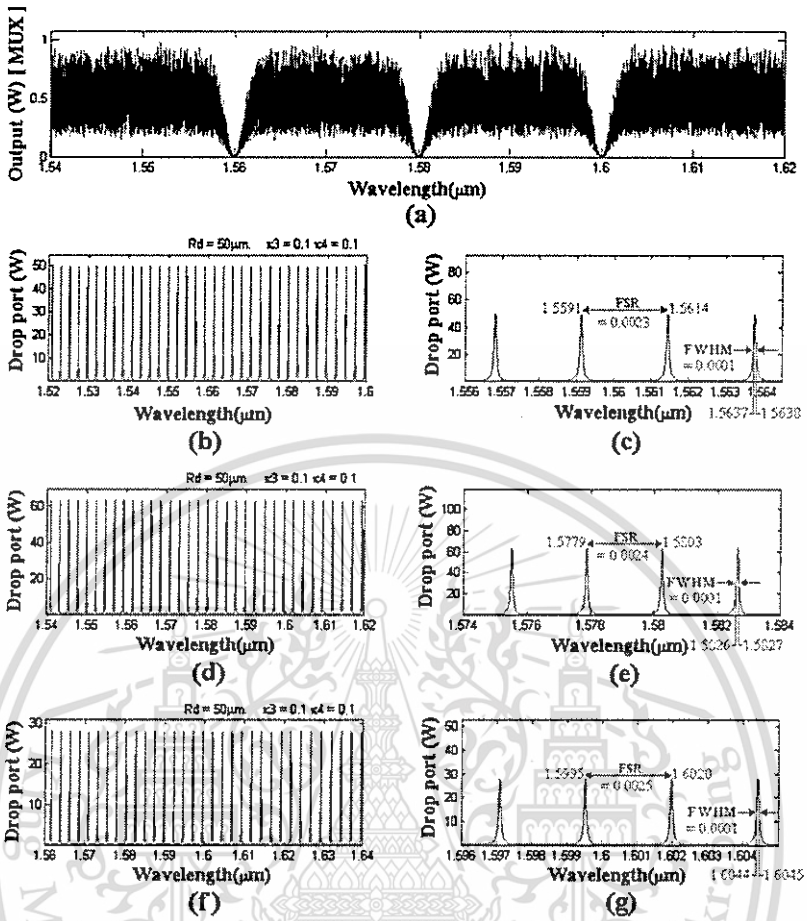

Fig. 4 Simulation result on the dark-soliton array when the dark-soliton input wavelengths are 1.56, 1.58, and 1.60 μm: (a) dark-soliton array; (b) through (g), drop port signals, respectively.

erated by multiple light sources at the center wavelength $\lambda_1 = 1.5$ μm; the filtered signals are as shown in Fig. 2.

Simulation results have shown that a band of bright solitons is seen, whereas there is no signal at $\lambda_1 = 1.5$ μm. A free spectrum range (FSR) of 2.1 nm and an amplified power of and 20 W for the dark solitons are obtained, where in this case a spectral width (full width at half maximum, FWHM) of 0.1 nm is achieved. In Fig. 3, the dark-soliton array generated by multiple light sources at the center wavelengths $\lambda_1 = 1.5$ μm, $\lambda_2 = 1.52$ μm, and $\lambda_3 = 1.54$ μm and the corresponding filtered signals are shown. Similarly, the dark-soliton array generated by multiple light sources at the center wavelengths $\lambda_1 = 1.56$ μm, $\lambda_2 = 1.58$ μm, and $\lambda_3 = 1.60$ μm and the corresponding filtered signals are as shown in Fig. 4, where the optical-ring radii used are 15 and 10 μm, and $R_d = 50$ μm.

3 Multiplexed Dark Solitons in a Wavelength Router

In operation, because this router is made up of add-drop filters as shown in Fig. 5, its performance depends on that of the add-drop filters. At the time of writing, micro- and nanowaveguides are gaining prominence. Filters offer good stability and isolation between channels at moderate cost.

The add-drop filters' capability will limit the size of the network. The maximum number of nodes of a network depends on the maximum number of add-drop filter channels. The popular dense wavelength division multiplexing (DWDM) component with many channels has been achieved in both theoretical and laboratory works.[23,24] Thus in future it should be possible to build multivariable routers with many ports. At present, absolutely secure communication is not as popular as the internet, but this proposed system may be able to cover a big city.

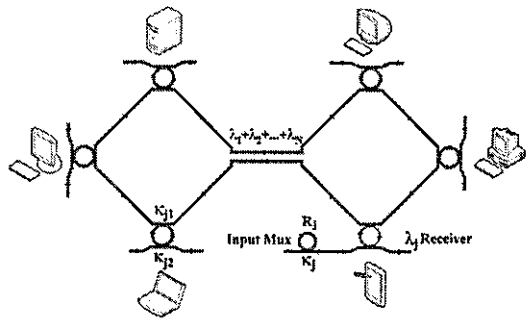

Fig. 5 A schematic multiwavelength router, where R_i, R_j are the ring radii, κ_{j1}, κ_{j2} are the coupling coefficients, and λ_i are the dark-soliton wavelengths.

Secondly, the insertion loss will reduce the efficient transmission distance, since signals will pass through an add-drop filter when they pass the router. The insertion loss of popular devices is 5 dB. According to the performance of present point-to-point transmission systems, we can build a network over 50 km at least. That will still meet the requirements of a big city. With the progress of DWDM technology, the insertion loss will be less than 1 dB in future,[25] and then the multivariable network will cover more than 100 km with high capacity.

The third problem is crosstalk, which is considered here in terms of channel separability. For a network, crosstalk will produce bit errors, so it must be made as low as possible. We think it can be estimated as follows: The insertion loss (IL) and crosstalk (FC) are

$$\mathrm{IL} = 10 \times \log(P_{\mathrm{in}}/P_{\mathrm{out}}), \tag{6}$$

$$\mathrm{FC}_j(\lambda_i) = 10 \times \log\left[\frac{P_j(\lambda_i)}{P_i(\lambda_i)}\right]. \tag{7}$$

Here P_{in} and P_{out} are the input and output of solitons, $P_j(\lambda_i)$ is the output of solitons with wavelength λ_i exported from port j, and $P_i(\lambda_i)$ is the output of solitons with wavelength λ_i exported from port i. Since $P_i(\lambda_i)$ in Eq. (7) is equal to P_{out} in Eq. (6), we have

$$P_{\mathrm{out}}/P_{\mathrm{in}} = 10^{-\mathrm{IL}/10}, \tag{8}$$

$$\frac{P_j(\lambda_i)}{P_{\mathrm{in}}} = \frac{P_j(\lambda_i)}{P_{\mathrm{out}}} \times \frac{P_{\mathrm{out}}}{P_{\mathrm{in}}} = 10^{[\mathrm{FC}_j(\lambda_i)-\mathrm{IL}]/10}. \tag{9}$$

We first assume that the total input of photons from any user is the same when they enter the router. Since one soliton will pass through two add-drop filters when it passes a router, the ratio of crosstalk to correct signals is

$$\frac{[P_j(\lambda_i)/P_{\mathrm{in}}]^2}{(P_{\mathrm{out}}/P_{\mathrm{in}})^2} = 10^{2\times\mathrm{FC}_j(\lambda_i)/10}. \tag{10}$$

Now we consider the situation that the inputs of photons are not the same. The worst case is that input photons that produce correct signals pass through a device that has X-dB insertion loss before passing through the router, but those solitons that produce crosstalk do not. The ratio in Eq. (10) then becomes $10^{[X+2\times\mathrm{FC}_j(\lambda_i)]/10}$. If there are many inputs that produce crosstalk, the ratio must be $\sum_{j=1}^{N-1} 10^{[X+2\times\mathrm{FC}_j(\lambda_i)]/10}$ where $j \neq i$; here N is the number of channels. For popular products we have $N=40$; $\mathrm{FC}_j(\lambda_i) < -25$ dB (when $j=i\pm1$), $\mathrm{FC}_j(\lambda_i) < -30$ dB (when $j \neq i\pm1$), and $X < 10$. The ratio is less than 0.056%. So the errors brought about by crosstalk are less than other effects and can be ignored. With further development of DWDM technology, crosstalk will be still smaller and the performance of the router will improve. In that case, we should easily be able to build a multivariable network operating over 50 km with 40 users.

4 Conclusion

We propose a novel system for dark-soliton array generation using multiplexed dark-soliton pulses. The dark solitons are input into the series microring resonators, where they are multiplexed, and signals filtered within an add-drop ring system can be generated and can be used to obtain large channel capacity in a secure communication link.

In principle, a dark soliton is one whose amplitude vanishes during propagation in a transmission line,[11,16] which gives it an advantage over a bright soliton. The main difference between bright solitons and dark solitons is that detection of dark solitons is extremely difficult, which makes them suitable for communication security applications. Moreover, stable dark solitons can be generated; they have been reported by Hanim et al.[17] and confirmed by Sama.[26]

Finally, the use of dark solitons to provide large channel capacity within a wavelength router has been analyzed. A FSR of 2.5 nm and an amplified power of 30 W can be achieved for a dark soliton with wavelength 1.60 μm, respectively. Thus, the channel spacing of the communication signals within a wavelength router can be provided by using a suitable FSR, which can be determined by using crosstalk effect analysis. One example has shown that a multivariable network over 50 km with 40 users can be achieved.

Acknowledgments

This research project has been supported by the Advanced Research Center for Photonics (ARCP), Faculty of Science, King Mongkut's Institute of Technology Ladkrabang, Bangkok 10520, Thailand

References

1. M. Ballav and A. R. Chowdhury, "On a study of diffraction and dispersion managed soliton in a cylindrical media," *Prog. Electromagn. Res.* PIER 63, 33–50 (2006).
2. S. Konar and A. Biswas, "Soliton-soliton interaction with power law nonlinearity," *Prog. Electromagn. Res.* PIER 54, 95–108 (2005).
3. R. Gangwar, S. P. Singh, and N. Singh, "Soliton based optical communication," *Prog. Electromagn. Res.* PIER 74, 157–166 (2007).
4. F. G. Gharakhili, M. Shahabadi, and M. Hakkak, "Bright and dark soliton generation in a left-handed nonlinear transmission line with series nonlinear capacitors," *Prog. Electromagn. Res.* PIER 96, 237–249 (2009).
5. G. P. Agarwal, *Nonlinear Fiber Optics*, 4th ed., Academic Press, New York (2007).
6. Y. S. Kivshar and B. Luther-Davies, "Dark optical solitons: physics and applications," *Phys. Rep.* 298, 81–197 (1998).
7. W. Zhao and E. Bourkoff, "Propagation properties of dark solitons,"

Opt. Lett. **14**, 703–705 (1989).
8. I. V. Barashenkov, "Stability criterion for dark soliton," *Phys. Rev. Lett.* **77**, 1193–1195 (1996).
9. D. N. Christodoulides, T. H. Coskun, M. Mitchell, Z. Chen, and M. Segev, "Theory of incoherent dark solitons," *Phys. Rev. Lett.* **80**, 5113–5115 (1998).
10. A. D. Kim, W. L. Kath, and C. G. Goedde, "Stabilizing dark solitons by periodic phase-sensitive amplification," *Opt. Lett.* **21**, 465–467 (1996).
11. K. Sarapat, N. Sangwara, K. Srinuanjan, P. P. Yupapin, and N. Pornsuwancharoen, "Novel dark-bright optical soliton conversion system and power amplification," *Opt. Eng.* **48**, 045004 (2009).
12. B. A. Malomed, A. Mostofi, and P. L. Chu, "Transformation of a dark soliton into a bright pulse," *J. Opt. Soc. Am. B* **17**, 507–513 (2000).
13. P. P. Yupapin, N. Pornsuwancharoen, and S. Chaiyasoonthorn, "Attosecond pulse generation using nonlinear microring resonators," *Microwave Opt. Technol. Lett.* **50**, 3108–3110 (2008).
14. P. P. Yupapin and N. Pornsuwancharoen, "Proposed nonlinear microring resonator arrangement for stopping and storing light," *IEEE Photon. Technol. Lett.* **21**(6), 404–406 (2009).
15. S. Mitthata, N. Pornsuwancharoen, and P. P. Yupapin, "A simultaneous short wave and millimeter wave generation using a soliton pulse within a nano-waveguide," *IEEE Photon. Technol. Lett.* **21**(13), 932–934 (2009).
16. S. Mitatha, "Dark soliton behaviors within the nonlinear micro and nanoring resonators and applications," *Prog. Electromagn. Res.* **PIER 99**, 383–404 (2009).
17. S. F. Hanim, J. Ali, and P. P. Yupapin, "Dark soliton generation using dual Brillouin fiber laser in a fiber optic ring resonator," *Microwave Opt. Technol. Lett.* **52**(4), 881–883 (2010).
18. A. M. Weiner, J. P. Heritage, R. J. Hawkins, R. N. Thurston, E. M. Kirschner, D. E. Leaird, and W. J. Tomlinson, "Experimental observation of the fundamental dark soliton in optical fibers," *Phys. Rev. Lett.* **61**(21), 2445–2448 (1988).
19. C. Finot, J. M. Dudley, and G. Millot, "Generation of dark solitons by interaction between similaritons in Raman fiber amplifiers," *Opt. Fiber Technol.* **12**, 217–226 (2006).
20. Y. Kokubun, Y. Hatakeyama, M. Ogata, S. Suzuki, and N. Zaizen, "Fabrication technologies for vertically coupled microring resonator with multilevel crossing busline and ultracompact-ring radius," *IEEE J. Sel. Top. Quantum Electron.* **11**, 4–10 (2005).
21. P. P. Yupapin and W. Suwancharoen, "Chaotic signal generation and cancellation using a micro ring resonator incorporating an optical add/drop multiplexer," *Opt. Commun.* **280**(2), 343–350 (2007).
22. P. P. Yupapin, P. Saeung, and C. Li, "Characteristics of complementary ring-resonator add/drop filters modeling by using graphical approach," *Opt. Commun.* **272**, 81–86 (2007).
23. K. Takada, M. Abe, T. Shibata, and K. Okamoto, "Field demonstration of over 1000-channel DWDM transmission with supercontinuum multi-carrier source," *Electron. Lett.* **38**, 572–573 (2002).
24. K. Sarapat, J. Ali, and P. P. Yupapin, "A novel storage and tunable light source generated by a soliton pulse in a micro ring resonator system for super dense wavelength division multiplexing use," *Microwave Opt. Technol. Lett.* **51**(12), 2948–2952 (2009).
25. M. K. Smit, "Progress in AWG design and technology," in *Proc. WFOPC 2005: 4th IEEE/LEOS Workshop on Fiber and Optical Passive Components*, p. 26 (2005).
26. A. K. Sarma, "Dark soliton switching in an NLDC in the presence of higher-order perturbative effects," *Opt. Laser Technol.* **41**(3), 247–250 (2009).

Charoen Vongchumyen is a doctorial student in computer engineering at King Mongkut's Institute of Technology Ladkrabang (KMITL), Bangkok, Thailand. He is a lecturer in computer engineering at KMITL and a member of the Hybrid Computing Research Laboratory (HCRL). His research interests are in the fields of microprocessor and microcomputer design and verification, embedded system design and development, nonlinear optical communication, and hybrid computing systems.

Kathawut Kulsirirat received his BEd and MSc in physics and applied physics from Rajanagarindra Rajabhat University, Chachoengsao, Thailand, and King Mongkut's Institute of Technology, Bangkok, Thailand, in 2006 and 2009, respectively. He is currently a PhD student in applied physics in the Faculty of Science, King Mongkut's Institute of Technology Ladkrabang, Bangkok, Thailand. His research interests are in the fields of soliton communication, DWDM, optical communication and network, hybrid computing systems, and mathematical modeling.

Somsak Mitatha received his BInd degree in technology television, MEng degree in electrical engineering, and DEng degree in electrical engineering from King Mongkut's Institute of Technology Ladkrabang (KMITL), Bangkok, Thailand, in 1987, 1995, and 2008, respectively. He is a member of the Department of Computer Engineering, where he is currently an associate professor in computer engineering. He has authored or coauthored of 20 ISI journal papers. His research interests are in computer hardware design, pattern recognition, embedded systems, nonlinear optical communication, and computer networks and security.

Preecha P. Yupapin received his PhD in electrical engineering from City University of London, United Kingdom, in 1993. He is a professor of applied physics in the Department of Applied Physics, Faculty of Science, King Mongkut's Institute of Technology Ladkrabang (KMITL), Bangkok, Thailand. He has authored or coauthored 200 ISI journal papers and 9 books. His research interests are in optical sensors, nanophotonics, linear and nonlinear optical communication, ad hoc networks, security cameras, nanoengineering, quantum information, and networks. Professor Yupapin is a member of the Thai Institute of Physics (TIP) and SPIE, and was a president of the Optical Society of America, Thailand Chapter (OSA-Thailand) in 2002.

An Atom/Molecule/DNA Probing and Transportation using Dynamic Optical Tweezers via a Wavelength Router

C. Vongchumyen, S. Mitatha and P.P. Yupapin

Optik – International Journal for Light and Electron Optics

Volume 122, Issue 6, March 2011, Pages 520-523

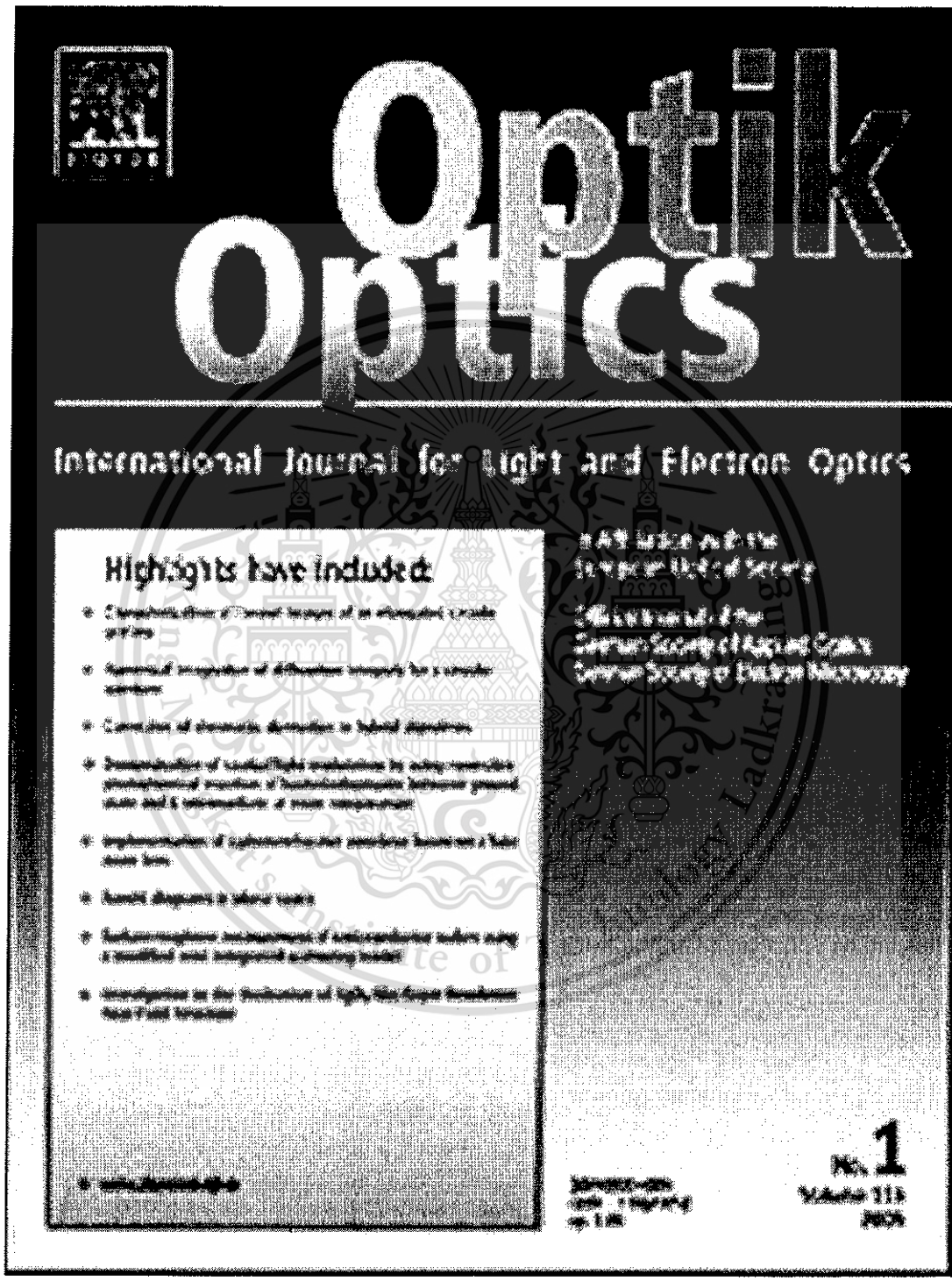

Optik 122 (2011) 520–523

Contents lists available at ScienceDirect

Optik

journal homepage: www.elsevier.de/ijleo

An atom/molecule/DNA probing and transportation using dynamic optical tweezers via a wavelength router

C. Vongchumyen[a], M. Tasakorn[b], S. Mitatha[a], P.P. Yupapin[b,*]

[a] Hybrid Computing Research Center, Faculty of Engineering, King Mongkut's Institute of Technology Ladkrabang, Bangkok 10520, Thailand
[b] Advanced Research Center for Photonics, Faculty of Science, King Mongkut's Institute of Technology Ladkrabang, Bangkok 10520, Thailand

ARTICLE INFO

Article history:
Received 14 June 2009
Accepted 2 March 2010

Keywords:
Dynamic tweezers
Atom transportation
DNA transportation
Wavelength router

ABSTRACT

A dark soliton pulse beam that has potential applications in the probing and transport of atoms or molecules as an optical tweezers is demonstrated. The trapped pulse beam is formed in the gap between a BP signal at 1500.00 nm and Stokes signal at 1500.09 nm, which has peak powers of ~12 dBm. The generated beam is seen to be stable with no fluctuations over a test period of 10 min, which is important to ensure that the transported atom/molecule is not lost in the link media, therefore, the dynamic optical tweezers are now plausible. The theoretical background of the trapped atom/molecule is also analyzed and described in details. The atomic/molecular network via a wavelength router is also described.

1. Introduction

Optical tweezers are a powerful tool for use in the three-dimensional rotation of and translation (location manipulation) of nano-structures such as micro- and nano-particles as well as living micro-organisms [1]. Many research works have been concentrated on the static tweezers [2–6], which it cannot move. The benefit offered by optical tweezers is the ability to interact with nano-scaled objects in a non-invasive manner, i.e. there is no physical contact with the sample, thus preserving many important characteristics of the sample, such as the manipulation of a cell with no harm to the cell. Optical tweezers are now widely used and they are particularly powerful in the field of microbiology [7–9] to study cell–cell interactions, manipulate organelles without breaking the cell membrane and to measure adhesion forces between cells. In this paper we describe a new concept of developing an optical tweezers source using a dark soliton pulse. The developed tweezers have many potential applications in electron, ion, atom and molecule probing and manipulation as well as DNA probing and transportation. Furthermore, the soliton pulse generator is a simple and compact design, making it more commercially viable. In this paper, we present the theoretical background in the physical model concept, where potential well can be formed by the barrier of optical filed. The change in potential value, i.e. gradient of potential can produce force that can be used to confine/trap atoms/molecule. Furthermore, the change in potential well is still stable in some conditions, which mean that the dynamic optical tweezers are plausible, therefore, the transportation of atoms/molecules in the optical network via a dark soliton being realized in the near future.

2. Trapping forces

The optical forces generated by a milliwatt of visible light are more than enough to overwhelm the random thermal forces which drive the dynamics of microparticles. The goal in creating an optical tweezers is to direct the optical forces from a single laser beam to trap a particle in all three dimensions. While quite general formulations of this problem have been developed [10–13] a simplified discussion suffices to motivate the design of optical tweezers arrays. We consider the forces exerted by monochromatic light of wave-number k on a dielectric sphere of radius a in the Rayleigh limit, where $a \times 2p/k$. The total optical force, F, is the sum of two contributions which is given by [14]

$$\mathbf{F} = \mathbf{F}_{\nabla} + \mathbf{F}_{s} \tag{1}$$

where the first of which arises from gradients in the light's intensity and the second of which is due to scattering of light by the particle. The gradient force on a particle of dielectric constant ε immersed in a medium of dielectric constant ε_0 and subjected to an optical field with Poynting vector S, where

$$F_{\nabla} = 2\pi a^3 \frac{\sqrt{\varepsilon_0}}{c}\left(\frac{\varepsilon - \varepsilon_0}{\varepsilon + 2\varepsilon_0}\right)\nabla|S| \tag{2}$$

* Corresponding author at: Advanced Research Center for Photonics, Faculty of Science, King Mongkut's Institute of Technology Ladkrabang, Applied Physics Department, Bangkok 10520, Thailand Fax: +66 2 3264354.
E-mail address: kyprreech@kmitl.ac.th (P.P. Yupapin).

0030-4026/$ – see front matter © 2010 Elsevier GmbH. All rights reserved.
doi:10.1016/j.ijleo.2010.03.017

It tends to draw the particle toward the region of the highest intensity. The scattering force is expressed by

$$F_s = \frac{8}{3}\pi(ka)^4 a^2 \frac{\sqrt{\varepsilon_0}}{c}\left(\frac{\varepsilon-\varepsilon_0}{\varepsilon+2\varepsilon_0}\right)^2 S \tag{3}$$

It drives the particle along the direction of propagation of the light. When dark soliton pulse is generated in the fiber optic system, the optical field (E_{in}) of the dark soliton pulse is given by an Eq. (4) as [15]:

$$E_{in}(t) = A\tanh\left[\frac{T}{T_0}\right]\exp\left[\left(\frac{z}{2L_D}\right) - i\omega_0 t\right] \tag{4}$$

where A and z are the optical field amplitude and propagation distance, respectively. T is a soliton pulse propagation time in a frame moving at the group velocity, $T = t - \beta_1 \times z$, where β_1 and β_2 are the coefficients of the linear and the second order terms of Taylor expansion of the propagation constant. $L_D = T_0^2/|\beta_2|$ is the dispersion length of the soliton pulse. T_0 in equation is a soliton pulse propagation time at initial input. Where t is the soliton phase shift time, and the frequency shift of the soliton is ω_0. This solution describes a pulse that keeps its temporal width invariance as it propagates, and thus is called a temporal soliton. When a soliton peak intensity ($|\beta_2/\Gamma T_0^2|$) is given, then T_0 is known. For the soliton pulse in the micro ring device, a balance should be achieved between the dispersion length (L_D) and the nonlinear length ($L_{NL} = 1/\Gamma\phi_{NL}$), where $\Gamma = n_2 \times k_0$ is the length scale over which dispersive or nonlinear effects make the beam becomes wider or narrower. For a soliton pulse, there is a balance between dispersion and nonlinear lengths, hence $L_D = L_{NL}$.

3. Trapping stability

We propose the trapping stability of an atom/molecule using the trapping photon within a potential well that generates within the fiber grating, where two photon components being trapped within the well. Firstly, wave propagation in optical fibers is analyzed by solving Maxwell's equation with appropriate boundary conditions. In the presence of Kerr nonlinearity, using the coupled-mode theory, the nonlinear coupled-mode equation is defined under the absence of material and waveguide dispersive effects. The dispersion arising from the periodic structure dominates near Bragg resonance conditions and it is valid only for wavelengths near to the Bragg wavelength. By substituting the stationary solution into the coupled-mode equation and by assuming $E(z,t) = e(z)e^{-i\hat{\delta}ct/\bar{n}}$, we obtain

$$i\frac{de_f}{dz} + \hat{\delta}e_f + \kappa e_b + (\Gamma_s|e_f|^2 + 2\Gamma_x|e_b|^2)e_f = 0$$

$$\text{and} \quad -i\frac{de_b}{dz} + \hat{\delta}e_b + \kappa e_f + (\Gamma_s|e_b|^2 + 2\Gamma_x|e_f|^2)e_b = 0, \tag{5}$$

Eq. (5) represents the time-independent light transmission through the gratings structure where e_f and e_b are the forward and backward propagating modes [16]. In order to explain the formation of Bragg soliton, consider the Stokes parameter since it provides useful information about the total energy and energy difference between the forward and backward propagating modes. In this study, we consider the following Stokes parameter [17]:

$$A_0 = |e_f|^2 + |e_b|^2, \quad A_1 = e_f e_b^* + e_f^* e_b, \quad \text{and} \quad A_2 = i(e_f e_b^* - e_f^* e_b),$$

$$A_3 = |e_f|^2 - |e_b|^2 \tag{6}$$

with the constraint $A_0^2 = A_1^2 + A_2^2 + A_3^2 + A_4^2$ where we introduce $A_4 = g(e)$ defined as the unknown function. In the FBG theory, the nonlinear coupled-mode (NLCM) equation requires that the total power $P_0 = A_3 = |e_f|^2 - |e_b|^2$ inside the grating is constant along the grating structures. Rewriting the NLCM equations in terms of Stokes parameter gives

$$\frac{dA_0}{dz} = -2\kappa A_2, \quad \frac{dA_1}{dz} = 2\hat{\delta}A_2 + 3\Gamma A_0 A_2,$$

$$\frac{dA_2}{dz} = -2\hat{\delta}A_1 - 2\kappa A_0 - 3\Gamma A_0 A_1, \quad \frac{dA_3}{dz} = 0, \quad \frac{dA_4}{dz} = g'(e), \tag{7}$$

In Eq. (7), we drop the distinction between the self-phase modulation and cross effect modulation effects and hence it becomes $3\Gamma = 2\Gamma_x + \Gamma_s$. It can be clearly shown that the total power, P_0 ($=A_3$) inside the grating is found to be conserved along the grating structure [18]. In the construction of the anharmonic oscillator type equation, it is necessary to use the conserved quantity, and it is obtained in the form $\hat{\delta}A_0 + (3/4)\Gamma A_0^2 + \kappa A_1 = C$, where C is the constant of integration and $\hat{\delta}$ is the detuning parameter. Using Eq. (7), we obtain

$$\frac{d^2A_0}{dz^2} - \alpha A_0 + \beta A_0^2 + \gamma A_0^3 + \theta A_0^4 = 4\hat{\delta}C \tag{8}$$

where $\alpha = 2[2\hat{\delta}^2 - 2\kappa^2 - 3\Gamma C]$, $\beta = 9\Gamma\hat{\delta}$, $\gamma = (9/4)\Gamma^2$ and $\theta = f(\theta)$. To simplify Eq. (8), it is assumed the parameters of α, β and γ is independent with respect to parameter θ. Eq. (8) contains all the physical parameter of the NLCM equation.

In order to describe the motion of a particle moving with the classic anharmonic potential, we have the solution as follows:

$$V(A_0) = -\alpha\frac{A_0^2}{2} + \beta\frac{A_0^3}{3} + \gamma\frac{A_0^4}{4} + \theta\frac{A_0^5}{5} \tag{9}$$

It represents the potential energy distribution in Fiber Bragg Grating structures. Where $\hat{\delta}$ is the potential energy distribution in the FBG structure [19].

Fig. 1 depicts the motion of photon in a dynamic potential well when nonlinear parameters are taken into account as shown by Eq. (9) for a potential well with $\alpha = 0.9$, $\beta = 0.3$, $\theta = 0.09$ and γ is varied from 0.3 to 0.9. The photon is trapped by the α parameter which is depicted by V. When α is too large, the potential well produces an increase in A_0 and has a wider double well. The γ parameter is represented by X. When γ is large, the potential well produces an increase in A_0. Suppose that the power source is imposed on the FBG and the initial power is used to generate the particles. It shows that the double well potential well is not symmetrical and the potential energy decreases within a certain region indicated by Y. The other effect is the disturbance of the potential energy shown by Z where the photon cannot be trapped symmetrically, and it is not equilibrium. Ultimately because of instability, it will lead to losses.

In terms of parametric function, we can describe it as follows. The change in α will affect the dip of the potential well. If α is

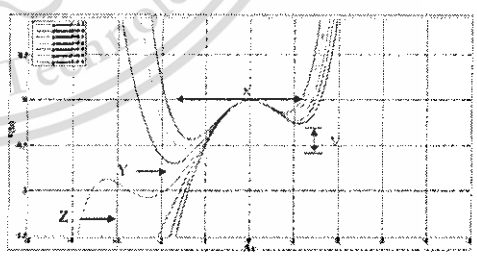

Fig. 1. The motion of photon in potential well for $\alpha = 0.9$, $\beta = 0.3$, $\theta = 0.09$ and γ is varies from 0.3 to 0.9.

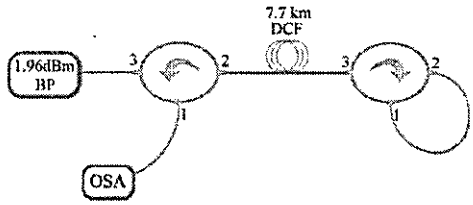

Fig. 2. Experimental setup.

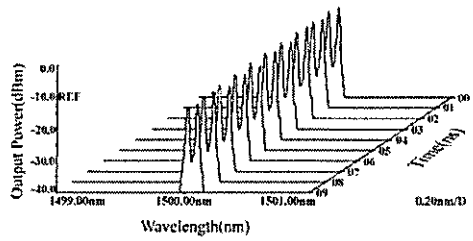

Fig. 4. Soliton propagation over time (similar a potential well, which can be seen clearly in a 3D).

approximately too small, the shape of the potential well turns into a single potential well. The occurrence of β effect on the motion of photon affects the negative region which means $A_0 < 0$. The effect of γ shows that the width of the potential well decreases if we increased the value of γ. Therefore if we increased the value of γ, we can be assumed that the photon is localized and can be trapped. The addition of another nonlinear factor θ affects the profile of potential well rapidly. We could say that if we include the existence of θ, the shape of potential well becomes chaotic. The photon does not only move in certain region that is known as potential well.

4. Trapping and transportation mechanism

The experimental setup is shown in Fig. 2. The dark soliton generator consists of a fiber laser based on a nonlinear gain medium that is placed in a linear cavity. The nonlinear gain medium is a 7.7 km Dispersion Compensating Fiber (DCF) which is pumped by a 1500 nm Brillouin Pump (BP) at 1.96 dBm. An Optical Circulator (OC) is used at one end of the setup to act as a fiber based mirror, with Port 3 connected to Port 1 while Port 2 is connected to the rest of the experimental setup. Another OC is also used in the experimental setup to guide the incoming and outgoing signals. An Optical Spectrum Analyzer (OSA) with a resolution of 0.07 nm is used to analyze the output of the proposed setup. The operation of the experimental setup is also follows; the BP generates a 1500 nm signal at 1.96 dBm, where it enters Port 1 of the first OC. The signal then travels onward to the DCF, where the nonlinear interactions will provide the first Stokes wavelength. The BP and Stokes then travel onwards to the second OC where they are reflected back to the DCF and again to Port 2 of the first OC, where they will now exit via Port 3 which is connected to the OSA.

Fig. 3 shows the generated dark soliton pulse. As can be seen in the figure, the proposed setup is able to generate two wavelength peaks at the BP at approximately 1500 nm and also at the first Stokes at approximately 1500.09 nm. Both the BP peak and the first Stokes peak have a power of approximately −12 dBm, this represents the darks soliton and the trap pulse which is formed by gaps of the two intensities. The trap pulse can be employed for trapping an atom or molecule, much akin to a pair of tweezers (the atom/molecule size would ideally be the same as the gap, which is approximately 0.09 nm). The dark soliton can also be converted into

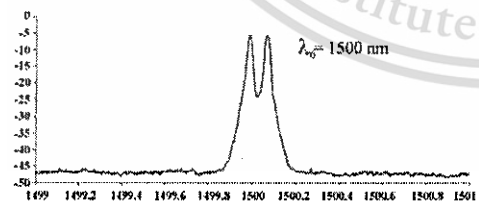

Fig. 3. Generated dark soliton pulse.

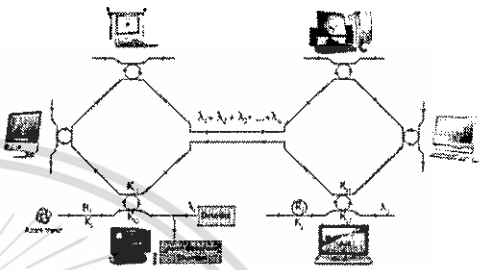

Fig. 5. A schematic of atomic/molecular router and network system, where R_i and R_j; ring radii and κ_{ik} and κ_{jk} are the coupling coefficients.

a light soliton by adding an add/drop filter. The same mechanism also allows for the recovery of the transported medium such as the atom or molecule being transported as well as the light pulse. Fig. 4 shows the pulse train of the trap pulse over a time of 10 min. From Fig. 3, the soliton propagation over time can be obtained. As can be seen in the figure, the soliton pulse maintains its shape through the time of testing with no observable fluctuation in the power or wavelength. This is critical as any slight fluctuation will cause the beam to lose its hold over the transported atom or molecule, effectively dropping it.

5. Atom/molecule transmission and transportation via wavelength router

From the above reasons, the transmission of atoms/molecules from dark soliton pulses via a wavelength router is plausible, which can be described by the following reasons: (i) a dark soliton pulse can propagate into the optical device/media, (ii) atom/molecule being trapped by tweezers force during the movement, the atom/molecule recovery can be realized using the optical detection scheme, where the dark–bright conversion technique is also available [20]. From Fig. 5, the transmission atoms/molecules can be formed by the dark soliton pulse, the atoms/molecules recovery can be taken by using the add/drop filter. However, the separation of atoms/molecules from light pulse is required to have the specific environment, which becomes the interesting research area, where light with the specific wavelength (λ_i) is detected by a detector, while the required molecule is absorbed by the specific environment.

6. Conclusion

In this paper we have demonstrated a dark soliton pulse beam that has potential applications in the probing and transport of

atoms or molecules as an optical tweezers. The pulse beam consists of a BP signal at 1500.00 nm and Stokes signal at 1500.09 nm, in which the gap formed between the two intensities of −12 dBm forms the trap pulse for the optical tweezers. The generated beam is also highly stable and shows no fluctuations over a test period of 10 min, thus showing that the beam can be used as a probe or transporter without the risk of losing the medium being probed or transported. The theoretical background of the trapped atom/molecule is analyzed, where it is shown that the dynamic optical tweezers for atoms/molecules transportation may be realized. The atomic/molecular network is also described.

References

[1] K. Svoboda, S.M. Block, Biological applications of optical forces, Annu. Rev. Biophys. Biomol. Struct. 23 (1994) 247–283.
[2] S.M. Block, Making light work with optical tweezers, Nature 360 (1992) 493–495.
[3] R.M. Simmons, J.T. Finer, S. Chu, J.A. Spudich, Quantitative measurements of force and displacement using an optical trap, Biophys. J. 70 (4) (1996) 1813–1822.
[4] I.M. Peters, B.G. de Grooth, J.M. Schins, C.G. Figdor, J. Greve, Three dimensional single-particle tracking with nanometer resolution, Rev. Sci. Instrum. 69 (7) (1998) 2762–2766.
[5] M.J. Lang, C.L. Asbury, J.W. Shaevitz, S.M. Block, An automated two-dimensional optical force clamp for single molecule studies, Biophys. J. 83 (1) (2002) 491–501.
[6] J. Pine, G. Chow, Moving live dissociated neurons with an optical tweezer, IEEE Trans. Biomed. Eng. 56 (4) (2009) 1184–1188.
[7] A. Ashkin, J.M. Dziedzic, T. Yamane, Optical trapping and manipulation of single cells using infrared laser beams, Nature 330 (1987) 769–771.
[8] K. Svoboda, S.M. Block, Biological applications of optical forces, Annu. Rev. Biophys. Biomol. Struct. 23 (1994) 247–285.
[9] J. Conia, B.S. Edwards, S. Voelkel, The micro-robotic laboratory: optical trapping and scissing for the biologist, J. Clin. Lab. Anal. 11 (1997) 26–38.
[10] G. Gouesbet, B. Maheu, G. Gréhan, Light scattering from a sphere arbitrarily located in a Gaussian beam, using a Bromwich formulation, J. Opt. Soc. Am. A 5 (1988) 1427–1443.
[11] A. Ashkin, Forces of a single-beam gradient laser trap on a dielectric sphere in the ray optics regime, Biophys. J. 61 (1992) 569–582.
[12] K.F. Ren, G. Gréhan, G. Gouesbet, Prediction of reverse radiation pressure by generalized Lorenz-Mie theory, Appl. Opt. 35 (1996) 2702–2710.
[13] O. Farsund, B.U. Felderhof, Force, torque, and absorbed energy for a body of arbitrary shape and constitution in an electromagnetic, Physica A 227 (1996) 108–130.
[14] Y. Harada, T. Asakura, Radiation forces on a dielectric sphere in the Rayleigh scattering regime, Opt. Commun. 124 (1996) 529–541.
[15] G.P. Agrawal, Nonlinear Fiber Optics, 4th edition, Academic Press, New York, 2007.
[16] Y.S. Kivshar, G.P. Agrawal, Optical Soliton: From Fibers to Photonics Crystal, Academic Press, New York, 2003.
[17] E. Collet, Polarized Light-concept and Applications, Marcel-Decker, New York, 1989.
[18] K. Senthilnathan, K. Porsezian, Symmetry-breaking instability in gap soliton, Opt. Commun. 227 (2003) 295–299.
[19] D.L. Mills, S.E. Trullinger, Gap solitons in nonlinear periodic structures, Phys. Rev. B 36 (1987) 947–952.
[20] N. Sangwara, K. Sarapat, K. Srinuanjan, P.P. Yupapin, A novel dark-bright optical solitons conversion system and power amplification, Opt. Eng. 48 (4) (2009) 045004.

BIOGRAPHY

Name	Mr. Charoen Vongchumyen
Date of birth	27 September 1974 Lamphun
Address	301/183 Chalongkrung 7 , Rungarun 2 village, Lumplatew, Ladkrabang, Bangkok Thailand 10520
Education	- Bachelor of Engineering in Computer Engineering from King Mongkut's Institute of Technology Ladkrabang in 1998 - Master of Engineering in Computer Engineering from King Mongkut's Institute of Technology Ladkrabang in 2001
Specialist	1) Optical communication 2) Embedded system 3) Digital design
Experience	1993 Diploma summer training at Chiangmai Radio-Flight control 1994 Customer service and Technician at Northland Computer Co., LTD. 1996 – 1999 Design engineer at Embedded System Lab of Computer Engineering Department of King mongkut's Institute of technology Ladkrabang 1999 – 2002 Teacher assistant of Computer engineering depart, Faculty of engineering, King mongkut's institute of technology ladkrabang

2002 – Now Lecturer of Computer engineering depart, Faculty of engineering, King mongkut's institute of technology ladkrabang